Environment heterogeneity creates fast amplifiers of natural selection in graph-structured populations

Cecilia Fruet[1,2], Arthur Alexandre[1,2], Alia Abbara[1,2], Claude Loverdo[3], Anne-Florence Bitbol[1,2]

1 Institute of Bioengineering, School of Life Sciences, École Polytechnique Fédérale de Lausanne (EPFL), Lausanne, Switzerland
2 SIB Swiss Institute of Bioinformatics, Lausanne, Switzerland
3 Sorbonne Université, CNRS, Institut de Biologie Paris-Seine (IBPS), Laboratoire Jean Perrin (LJP), Paris, France

Abstract

Complex spatial structure, with partially isolated subpopulations, and environment heterogeneity, such as gradients in nutrients, oxygen, and drugs, both shape the evolution of natural populations. We investigate the impact of environment heterogeneity on mutant fixation in spatially structured populations with demes on the nodes of a graph. When migrations between demes are frequent, we demonstrate that environment heterogeneity can amplify natural selection and simultaneously accelerate mutant fixation and extinction, thereby fostering the quick fixation of beneficial mutants. We evidence this effect in the star graph, more strongly in the line graph, and also in a more general class of graphs. We show that for amplification to occur, mutants must have a stronger fitness advantage in demes with stronger migration outflow. In circulation graphs, where migration inflow and outflow are equal in each deme, we find that environment heterogeneity has no impact in a first approximation, but increases the fixation probability of beneficial mutants to second order. When migrations between demes are rare, we show that environment heterogeneity can also foster amplification of selection, by allowing demes with sufficient mutant advantage to become refugia for mutants.

Introduction

Natural microbial populations often possess complex spatial structures, with partially isolated subpopulations, e.g. in soil-associated or host-associated microbiota [1–5]. In addition, the environment in which natural microbial populations live is generally heterogeneous, featuring spatial variability in nutrient availability, temperature, pH, and concentrations of drugs or toxins. For instance, in soils, nutrient levels vary with depth, proximity to plant roots, and localized microbial metabolic activity [6, 7]. This variability creates microhabitats that shape microbial community composition and function [8]. Aquatic environments are heterogeneous too [9], influenced by factors such as oxygen gradients [10]. The human body also constitutes a spatially structured and heterogeneous environment for its microbiota [11]. In particular, the gut features gradients of oxygen, pH, bile salts, and antibiotic drugs when they are taken. This environment heterogeneity gives rise to heterogeneous selection pressures on microorganisms, leading to complex ecological and evolutionary dynamics [2, 12, 13]. To understand how natural microbial populations evolve, it is thus important to investigate the joint impact of spatial structure and of environment heterogeneity on population genetics.

The vast majority of theoretical studies investigating the evolution of spatially structured populations assume that the environment is homogeneous. They show interesting impacts of spatial structure on evolution, in particular on the fundamental process of mutant fixation, whereby a mutant type takes over the population. Considering well-mixed subpopulations, known as demes or patches, connected by migrations [14, 15], it was shown that the probability that a mutant fixes (i.e. takes over) in the population is not impacted by spatial structure, if migrations are sufficiently symmetric [16, 17], and demes do not get extinct [18]. Models on graphs where each node comprises one individual have

allowed to consider more complex spatial structures [19]. In this framework, known as evolutionary graph theory, it was shown that specific graphs, under specific update rules defining the dynamics, can amplify or suppress natural selection [19–23]. Amplifiers of selection increase the fixation probability of a beneficial mutant compared to a well-mixed population with the same size, and decrease the one of deleterious mutants. Meanwhile, suppressors of selection decrease the fixation probability of beneficial mutants and increase that of deleterious ones. Amplifiers of natural selection have been the subject of sustained attention [19–25], given their potential to enhance adaptation, which might be useful e.g. in directed evolution. However, they generally slow down mutant fixation [26–29], which limits their impact. Evolutionary graph theory models have been generalized by placing well-mixed demes with fixed size on graph nodes, also using specific update rules [30–34]. Recently, more general models, which do not assume strictly fixed deme sizes or update rules, were proposed by some of us [35, 36]. Under rare migrations, these models generalize the findings of evolutionary graph theory, and show that whether a graph amplifies or suppresses natural selection strongly depends on the asymmetry of migration between demes [35]. Moreover, under frequent asymmetric migrations, suppression of selection was found to be pervasive, and associated to an acceleration of mutant fixation or extinction [36].

How does environment heterogeneity across demes impact mutant fixation in spatially structured populations? In evolutionary graph theory models with one individual per node, graphs with nodes falling in two categories, corresponding to two environments, have been considered [37–42], mainly focusing on the optimal repartition of these two types of nodes to foster mutant fixation [39, 40, 42] and on their impact on evolutionary timescales [37, 41]. Here, we consider a more general model with demes on nodes on the graph, where mutant fitness advantage can be different in each deme. We shed light on the impact of environment heterogeneity on mutant fixation in spatially structured populations, by comparing heterogeneous and homogeneous environments.

We generalize the spatially structured population model introduced in Ref. [36] to heterogeneous environments, modeled via a deme-dependent mutant fitness advantage. When migrations are frequent, we show that environment heterogeneity substantially impacts mutant fixation probability, and that it can lead to amplification of selection, together with acceleration of mutant fixation and extinction. This stands in contrast with the usual tradeoff between amplification and slower dynamics. We find that this joint amplification and acceleration occurs in the star graph, and more strongly in the line graph. We determine analytically the conditions for amplification of selection in the star and in the line, using a branching process approach. We show that a key ingredient for amplification is that mutants should be strongly favored in demes with strong migration outflow. We generalize these findings to graphs with one special deme that differs from others both by mutant advantage and by migration outflow. In circulation graphs, where migration inflow and outflow are equal in each deme, we find that environment heterogeneity has no impact in a first approximation, but increases mutant fixation probability to second order. Finally, we turn to the rare migration regime, and show that environment heterogeneity can turn suppressors of selection into amplifiers in this regime too, but for a different reason: demes with sufficient mutant advantage become refugia for mutants.

Results

Including environment heterogeneity in models of spatially structured populations on graphs. The impact of spatial structure on mutant fixation has traditionally been studied assuming homogeneous environments, where the fitness difference between mutants and wild-types is the same in the whole structured population [14–19, 30–36, 43–51]. In contrast, here, we assume that each node i of a graph with D nodes may have a different environment. Thus, the mutant fitness advantage $s\delta_i$ depends on deme i, with s setting the overall scale of selection strength, and δ_i encoding environment heterogeneity.

We consider that each node harbors a well-mixed deme (i.e. subpopulation), as in Refs. [35, 36]. In these models, population regulation can be modeled either by a logistic growth rate [35] or by binomial sampling events [36]. The first case gives rise to a within-deme dynamics similar to the Moran model [35], and the second one to a model similar to structured Wright-Fisher ones, which can represent a serial transfer protocol through growth and dilution-migration steps [36]. Here, we adopt the second class of models. Each deme starts at bottleneck size K, grows exponentially for time t, and then demes undergo a dilution and migration step, returning to the deme bottleneck size K [36]. Migrations take place with a probability m_{ij} between demes i and j upon each migration-dilution

step (see Methods). SI Figure S1 provides an illustration of this model, and of the spatial structures considered.

We mainly address the regime where migrations are frequent, i.e. where the non-zero m_{ij} are of order unity. In this regime, which is the most relevant experimentally [52–56], we perform stochastic simulations, and we generalize the branching process calculations of mutant fixation probability and extinction time of Ref. [36] to heterogeneous environments, see SI Section 1. In the last section, we turn to the regime of rare migrations, where mutant fixation or extinction in a deme is much faster than migration timescales [35, 44], and we present results of analytical calculations. Throughout, we focus on the fixation of a single mutant that appears uniformly at random in the graph. This situation is biologically realistic, both for mutations associated to DNA replication errors, which are expected to occur uniformly at random upon divisions, and for mutations due to external stress, which are expected to occur uniformly at random in all cells.

Environment heterogeneity strongly impacts mutant fixation probability in a star. The star graph comprises a central node connected to $D-1$ leaf nodes by migrations (see Figure 1A, inset). It has been the focus of many studies regarding the impact of spatial structure on mutant fixation, assuming homogeneous environments. In evolutionary graph theory models with one individual per node, this graph either amplifies or suppresses natural selection depending on update rules [19–22]. With demes on each node, in the rare migration regime, whether it amplifies or suppresses natural selection depends on migration asymmetry [35]. However, for more frequent migrations, it can only suppress selection [36].

How does environment heterogeneity impact mutant fixation in the star with demes on each node? To address this question, we compare a star with an environment that can differ in each node i to a star with a homogeneous environment, where the mean mutant fitness advantage is the same, i.e. where the mutant fitness advantage is $\langle\delta\rangle s$ in each deme. In the branching process approach, we show that, to leading order in $st \ll 1$, the mutant fixation probability in the heterogeneous star only depends on selection through the mean mutant fitness effect, via $\langle\delta\rangle$, and through the relative fitness excess in the center, via $\sigma_C = (\delta_C - \langle\delta\rangle)/\langle\delta\rangle$, see SI Section 1.3 (Eq. S21). Fixation probability is also impacted by migration asymmetry $\alpha = m_I/m_O$, where m_I is the probability of incoming migrations to the center from a leaf, while m_O is the probability of outgoing migrations from the center to a leaf. When there is more migration outflow from the center than inflow to the center ($\alpha < 1$), we find that environment heterogeneity increases mutant fixation probability if the center features a larger mutant fitness advantage than the leaves ($\sigma_C > 0$). Conversely, if there is more inflow to the center than outflow ($\alpha > 1$), heterogeneity increases mutant fixation probability if the center features a smaller mutant fitness advantage than the leaves ($\sigma_C < 0$), see SI Section 2.2. This suggests that having a stronger mutant advantage in locations with more migration outflow enhances mutant fixation. Finally, if $\alpha = 1$, to first order in st, environment has no impact on fixation probability. Note that in this specific case, the star is a circulation graph, where all demes have equal total outgoing and total incoming migration flows. This special category of graphs is discussed in more detail below.

Figure 1A shows the impact of environment heterogeneity, via σ_C, on the mutant fixation probability in the star. We observe that the farther σ_C is from 0 in magnitude, the more the fixation probability deviates from the baseline of the homogeneous star. We observe that environment heterogeneity yields an increase of the fixation probability when $\sigma_C > 0$, and a decrease of it when $\sigma_C < 0$. As $\alpha < 1$ in this figure, this is fully consistent with our analytical predictions. In fact, for each value of σ_C considered, Figure 1A shows excellent agreement between our stochastic simulations and our analytical predictions.

Figure 1B further illustrates how migration asymmetry α and environmental heterogeneity, via σ_C, impact the first-order coefficient (slope) in st of the mutant fixation probability in the star. This heatmap highlights the strong impact of both migration asymmetry and environmental heterogeneity on fixation probability in the star. Notably, environmental heterogeneity can also enhance fixation probability in a star beyond that of an equivalent well-mixed population, with the same average mutant fitness advantage $\langle\delta\rangle s$. This reference fixation probability is $2\langle\delta\rangle st$ to first order [57]. Hence, the heterogeneous star can amplify natural selection. This effect is further illustrated in SI Figure S2. We find an analytical condition on σ_C for amplification to occur, see SI Section 2.3. Figure 1B shows that it matches the numerical finding for the boundary of the area where the fixation probability in the heterogeneous star exceeds that of an equivalent well-mixed population. This result is particularly

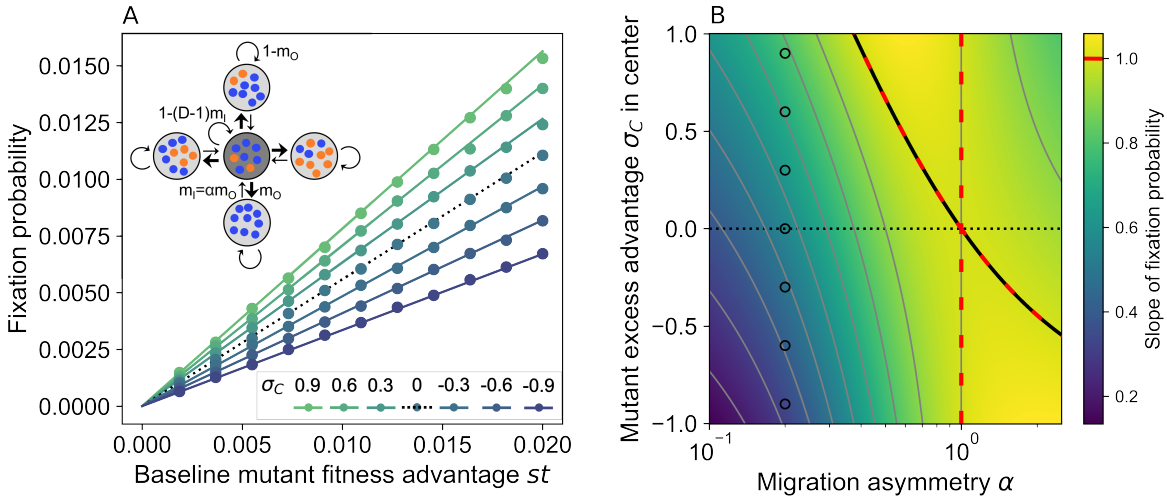

Figure 1: **Impact of environmental heterogeneity on mutant fixation in the star.** Panel A: The mutant fixation probability is shown versus the baseline mutant fitness advantage st, for different relative mutant fitness excess σ_C in the center, with migration asymmetry $\alpha = 0.2$. Markers: stochastic simulation results; lines: analytical predictions (Eq. S21). The inset shows the heterogeneous-environment star considered: $\alpha < 1$; different gray shades represent different environments. Panel B: Heatmap of the first-order coefficient (slope) in the baseline effective mutant fitness advantage st of the mutant fixation probability in a star, versus the migration asymmetry α and the relative mutant fitness excess σ_C in the center. Red dashed lines: numerically-determined limits of the region where the star amplifies selection; solid black line: analytical prediction for this limit, given by $f_{\text{star}}(\alpha, D)$ in Eq. S44. Dotted line: homogeneous environment case $\sigma_C = 0$. Markers: parameter values considered in panel A. Parameter values: in both panels, $D = 5$; $K = 1000$; $\langle\delta\rangle = 0.5$. In Panel A: $m_O = 0.6$; $\alpha = 0.2$; each marker comes from 5×10^5 stochastic simulation realizations.

striking because the star with frequent asymmetric migrations is known to suppress natural selection in a homogeneous environment [36]. Even with rare migrations, no amplification is possible in the homogeneous star with $\alpha < 1$ [35], while here, amplification exists for $\alpha < 1$, for sufficiently large σ_C. Therefore, our results demonstrate that the impact of environmental heterogeneity is strong enough to counteract this suppression, and lead to amplification of selection.

The heterogeneous line can substantially amplify and accelerate mutant fixation. Another important spatial structure is the line of demes, or linear stepping-stone model, see schematics in Figure 2. How does the line impact mutant fixation probability? In SI Section 1.3, we derive the fixation probability of a mutant in a line of demes with frequent migrations in the branching process regime, both in the homogeneous and in the heterogeneous case, see Eq. S31. Note that the line was not addressed earlier in this regime, e.g. not in Ref. [36]. In the homogeneous case, as the star and all other graphs [36], the line suppresses natural selection as soon as it has some migration asymmetry, i.e. $\alpha \neq 1$, where $\alpha = m_R/m_L$ is the ratio of migration probabilities to the right and to the left. This is explicitly shown in SI Section 3.1 and illustrated in Figure S3.

How does environment heterogeneity impact mutant fixation in the line? To address this question, we compare a line with an environment that can differ in each node i, through the mutant fitness advantage δ_is, to a homogeneous line with the same mean mutant fitness advantage $\langle\delta\rangle s$. Let us denote by $\sigma_i = (\delta_i - \langle\delta\rangle)/\langle\delta\rangle$ the relative mutant fitness excess in deme i. The fixation probability in the line with heterogeneous fitness is higher than in the homogeneous line if and only if:

$$S(\alpha) \equiv \sum_{i=1}^{D} \sigma_i \alpha^{-i} > 0\,, \tag{1}$$

see SI Section 3.2. This entails that, in a heterogeneous line with monotonically decreasing mutant fitness advantage from left to right, the mutant fixation probability is higher than in the homogeneous

line for $\alpha > 1$, see SI Section 3.2. The opposite holds for $\alpha < 1$, and there is no impact of heterogeneity for $\alpha = 1$, to first order in the baseline effective mutant fitness advantage st. Therefore, in the line, mutant spread and fixation are facilitated when the demes conferring the highest selective advantage to mutants are upstream of the overall migration flow.

We have shown that environment heterogeneity can increase fixation probability in the line. Can this result in amplification of selection? To address this question, we compare the line to a well-mixed population with the same average mutant fitness advantage, i.e. the same $\langle\delta\rangle$, or equivalently, to a clique with the same $\langle\delta\rangle$. Indeed, to first order, the fixation probability in a clique is not impacted by heterogeneity, and is the same as in a well-mixed population with the same $\langle\delta\rangle$, see SI Section 1.3. Comparing the fixation probabilities to first order, we show that a heterogeneous line has a higher fixation probability than a clique if and only if:

$$S(\alpha) > g(\alpha) \equiv \frac{(D-1)\alpha - (D+1) + (D+1)\alpha^{1-D} - (D-1)\alpha^{-D}}{\alpha^2 - 1}\,, \tag{2}$$

see SI Section 3.3.

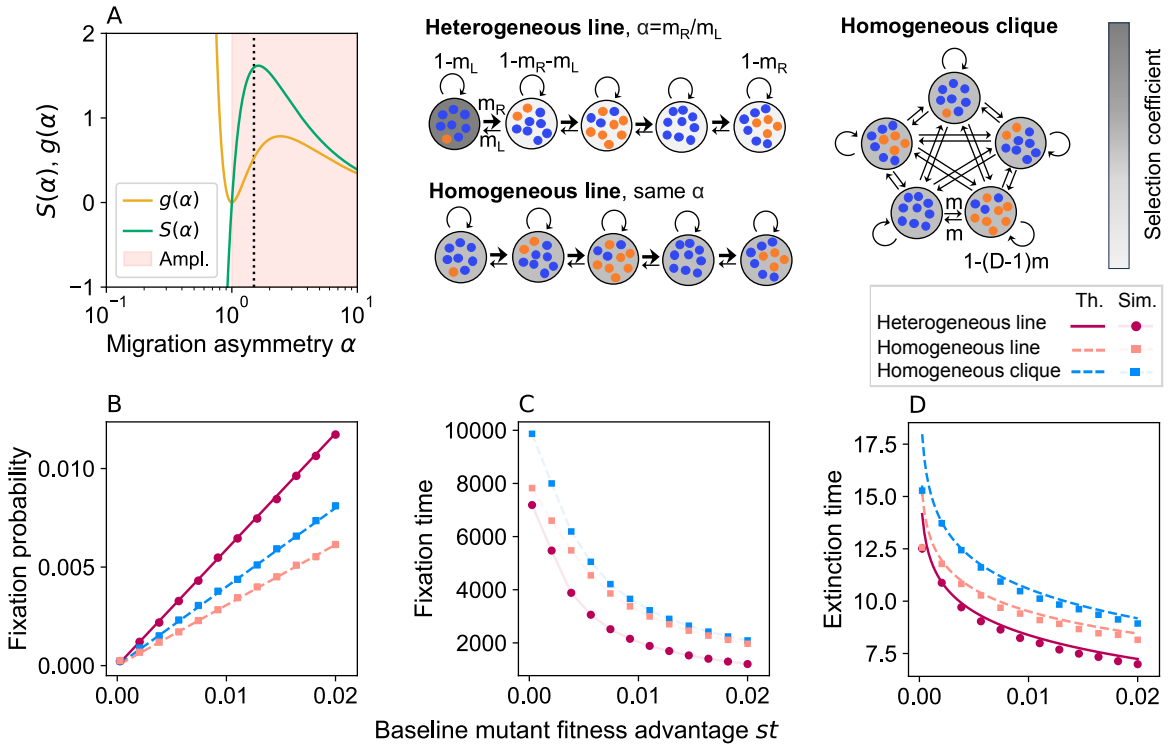

Figure 2: **Amplification of selection and accelerated dynamics in the heterogeneous line.** Panel A: Condition for amplification of natural selection in the heterogeneous line shown in the top schematic. The functions S and g, defined respectively in Eqs. 1 and 2, are plotted versus migration asymmetry α. Pink-shaded region: range of α where $S(\alpha) > g(\alpha)$, i.e. where the heterogeneous line amplifies natural selection. Dotted line: migration asymmetry ($\alpha = 1.5$) chosen in panels B-D. Panel B: Mutant fixation probability versus baseline mutant fitness advantage st, in the different spatial structures shown in the schematics (heterogeneous line with step environmental profile and $\alpha = 1.5$; homogeneous line with same α and $\langle\delta\rangle$; homogeneous clique with same $\langle\delta\rangle$). Predictions from the branching process theory ("Th."), specifically Eq. S31, and results from stochastic simulations ("Sim."), are shown. Panel C: Mutant fixation time, in number of bottlenecks, in the different structures considered, versus baseline mutant fitness advantage st. Panel D: Same as in C, but for mutant extinction time. Theoretical predictions are from Eq. S37. Parameter values for all structures: $D = 5$, $K = 1000$; for all lines: $\alpha = 1.5$, $m_L = 0.3$; for the clique: $m = 0.15$; for the line with step profile: $\delta = 1$ in the leftmost deme, $\delta = 0$ in other ones. Each marker comes from 5×10^5 stochastic simulation realizations.

Figure 2A shows S and g as a function of α for the line shown in the top schematic, which has $D = 5$ demes and features a step profile of mutant fitness advantages, with $\delta_i = 1$ for $i = 1$ and $\delta_i = 0$ for $i > 1$. For such a decreasing profile of δ_i, amplification of selection cannot exist for $\alpha < 1$ (see SI Section 3.3). We observe on Figure 2A that amplification of selection exists when $\alpha > 1$ (Eq. 2 is satisfied). Furthermore, for this particular environmental profile, $S(\alpha) > g(\alpha)$ in asymptotic behavior for large α, see SI Section 3.3. Note that for other environmental profiles, we observed that g and S cross for an $\alpha^* > 1$, and that amplification exists in a finite region from $\alpha = 1$ to $\alpha = \alpha^*$.

Figure 2B shows the mutant fixation probability in the above-described heterogeneous line with step environmental profile for $\alpha = 1.5$, and evidences a strong amplification of selection compared to a homogeneous clique with the same average fitness. This stands in contrast to the homogeneous line with the same α and $\langle\delta\rangle$, which suppresses selection, see Figure 2B, and with a heterogeneous line with an opposite environmental profile but the same α, which further suppresses selection, see SI Figure S4. Moreover, Figure 2C-D shows that the average mutant fixation and extinction times are both faster in our heterogeneous line than in the homogeneous clique with the same $\langle\delta\rangle$. Hence, the heterogeneous line is able to both amplify and accelerate fixation at the same time. Importantly, this differs from the usual behavior of amplifiers in evolutionary graph theory, which slow down fixation [26–28]. This joint amplification and acceleration is observed for diverse environmental profiles, as illustrated in SI Figure S5. The results in SI Figure S5 suggest that larger environmental contrast between demes leads to more amplification of selection and to more acceleration of mutant fixation and extinction. Note that the same effect of joint amplification and acceleration, albeit less strong, exists for the heterogeneous star, see SI Section 2.3 and SI Figure S2.

Locally increasing mutant fitness advantage and migration outflow yields amplification and acceleration of fixation. In the specific spatial structures of the star and the line, we showed that environment heterogeneity increases the fixation probability of beneficial mutants when it is such that mutants have a stronger fitness advantage in a deme that is upstream of the overall migration flow. We further found that this can lead to joint amplification and acceleration of fixation.

Do these findings hold beyond specific graphs? To address this question, we consider a graph where all nodes can be connected by migrations, but where one special deme (called deme number 1) differs from all others both by migration outflow and by environment. The prefactor of mutant fitness advantage is δ_1 in the special deme and δ_2 in other demes. We first treat the highly symmetric case in which all outgoing migration probabilities from the special deme have the same value, m_1, while all other ones have the same value, $m_2 = \alpha m_1$, where α denotes migration asymmetry, see schematic in Figure 3. When $\alpha < 1$, meaning that the special deme has a stronger migration outflow than others, the spatial structure considered amplifies natural selection if and only if:

$$\frac{\delta_2}{\delta_1} \equiv \beta < \alpha \,, \tag{3}$$

see SI Section 4.1. Hence, when the special deme sends out more individuals than others, selection is amplified if the mutant advantage is stronger enough in the special deme than in others. More precisely, this environment contrast needs to be larger than the migration contrast. In the opposite case where $\alpha > 1$, amplification occurs for $\beta > \alpha$, see SI Section 4.1. Hence, for amplification to exist in this structure, mutant advantage needs to be stronger upstream of the overall migration flow, and moreover, the environment needs to be more contrasted than the migration flows.

Figure 3A shows that our prediction in Eq. 3 is satisfied: amplification is obtained for $\beta < \alpha < 1$, and it vanishes for $\beta \geq \alpha$ with $\alpha < 1$. Moreover, Figure 3B-C shows that this amplification of selection is accompanied by acceleration of fixation and extinction. This is consistent with our findings for the star and the line, and generalizes them.

Do our findings extend to graphs without strong symmetries in their migration probabilities? To address this question, we consider a structure with a special deme, as before, but where for each deme, the migration probabilities incoming to that deme from all other ones are drawn from the same Dirichlet distribution. The parameters of this distribution are chosen such that the special (first) origin deme has a stronger expected migration outflow than others, see SI Section 4.2, but with a substantial dispersion of migration probabilities, see SI Figure S6. Figure 3D shows that, in this more general structure, substantial amplification of selection exists in the parameter region where $\beta < \alpha < 1$, i.e. under the conditions derived for the highly-symmetric structure studied above. This suggests that

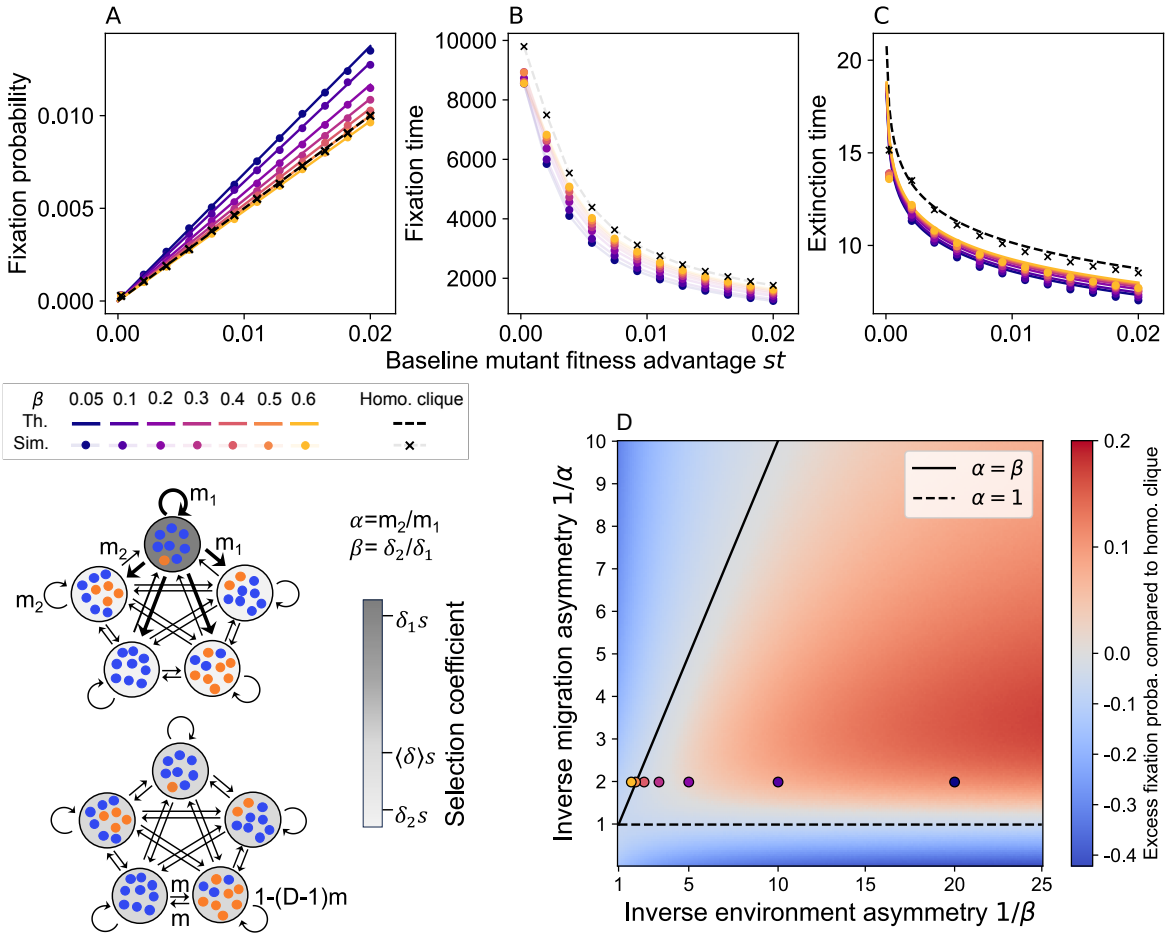

Figure 3: **Amplification of selection and accelerated dynamics in structures with a special deme in terms of mutant advantage and migration outflow.** Panel A: Mutant fixation probability versus baseline mutant fitness advantage st for population structures with one special deme, characterized by stronger migration outflow ($\alpha = m_2/m_1 = 0.5$) and greater mutant advantage than others ($\beta = \delta_2/\delta_1 < 1$), for various values of β. Results for a homogeneous clique with the same $\langle\delta\rangle$ are shown for reference. Schematics of these population structures are shown below (top: structure with a special deme; bottom: homogeneous clique). Panel B: Time to mutant fixation, in bottlenecks, versus baseline mutant fitness advantage st, for the same structures as in A. Panel C: Same as in B, but for extinction time. "Th." indicates results from the branching process theory (Eq. S65 for panel A, Eq. S37 for panel C), "Sim." results from stochastic simulations (panels A-C). Panel D: The excess fixation probability in a structure with one special deme, compared to a homogeneous clique with the same $\langle\delta\rangle$, is shown versus the inverse migration asymmetry $1/\alpha$ and the inverse environment asymmetry $1/\beta$, in the case where migration probabilities are drawn from Dirichlet distributions (no strong symmetry in migration probabilities, generalizing over the structure considered in panels A-C and in the schematics, see SI Section 4.2). The plotted values represent the difference between the first-order coefficient in st of the fixation probability (computed numerically as explained in SI Section 1.4, and averaged over many sets of migration probabilities), and the value for the homogeneous clique with the same $\langle\delta\rangle$, which is $2\langle\delta\rangle$. Solid and dashed black lines mark theoretical boundaries for amplification in the strongly symmetric structure shown in the schematics and considered in panels A-C (see Eq. 3 and main text): the solid line corresponds to $\alpha = \beta$ and the dashed line to $\alpha = 1$. Markers show the (α, β) values considered in panels A-C. Parameter values for all panels: $D = 5$, $\langle\delta\rangle = 0.25$; for panels A-C: $\alpha = 0.5$, $K = 1000$. Each value in the heatmap of panel D is obtained by averaging over 5×10^3 structures, whose migration probabilities are each time drawn independently in Dirichlet distributions.

our finding that amplification is possible when mutant advantage is stronger upstream of the overall migration flow, and the environment is more contrasted than the migration flows, is generic.

The circulation theorem extends to heterogeneous environments to first order in st, but environment heterogeneity can increase fixation probability to second order. So far, our results highlight the interplay between environment heterogeneity and overall migration asymmetries and flow in diverse spatial structures. Let us now turn to circulation graphs, a class of graphs where each node has the same total incoming and outgoing migration flow. With homogeneous environments, these structures, which possess strongly symmetric migrations, are known to exhibit the same mutant fixation probability as a well-mixed population with the same size, whatever the initial location of the mutant. A version of this result is known in population genetics models with demes on the nodes of highly-symmetric graphs [16, 17] as *Maruyama's theorem*, and it was further formalized in evolutionary graph theory models with one individual per node of a graph [19], as the *circulation theorem*. More recently, we showed that the circulation theorem extends to our model with demes on the nodes of graphs with frequent migrations, in the branching process regime [36].

How does environment heterogeneity impact mutant fixation in circulation graphs? First, as pointed out earlier, the heterogeneous clique has the same fixation probability as a well-mixed population with the same $\langle\delta\rangle$ to first order in st, namely $2\langle\delta\rangle st$. This also holds in all graphs we considered so far when $\alpha = 1$, i.e. when they reduce to circulations, as illustrated by SI Figure S7 (see SI Sections 1.3 and 4.1 for details). More generally, we show in SI Section 5.1 that the circulation theorem extends to heterogeneous environments in the branching process regime, to first order in st.

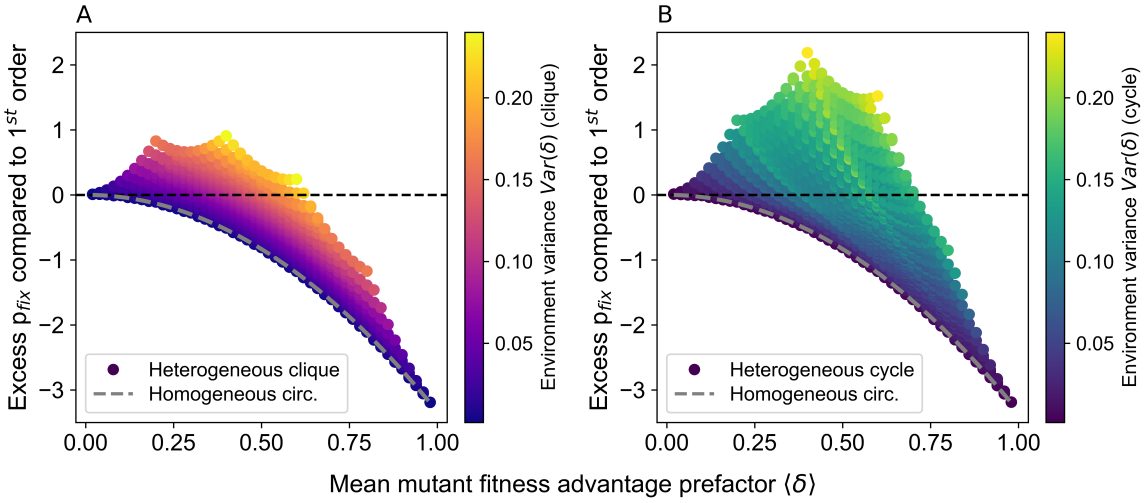

Figure 4: **Impact of environment heterogeneity on fixation probability in circulations.** As the fixation probability is the same in all circulations to first order in st, we focus on the impact of the second-order term. Specifically, we show the negative second-order coefficient in the expansion of fixation probability. This prefactor quantifies the excess fixation probability ("p_{fix}") provided by the second-order term, with respect to the first-order approximation. Panel A: This excess fixation probability (see Eq. S85) is shown versus the mean mutant fitness advantage prefactor $\langle\delta\rangle$ across the structure, for various heterogeneous cliques. Markers are colored according to the variance of the deme-specific mutant fitness advantage prefactor δ_i coefficient across demes i, a proxy for environment heterogeneity. Horizontal dashed black line: no deviation from the first-order approximation. Dashed gray line: homogeneous environment case. Panel B: Same as A, but for heterogeneous cycles with equal clockwise and anticlockwise migration probabilities (see Eq. S90). Parameters: $D = 5$, $m = 0.1$ in the clique, $m = 0.2$ in the cycle (same total of exchanges in the two structures). Numbers in $\{0, 0.1, \ldots, 0.9, 1\}$ are employed for each δ_i, and all combinations of them are considered.

Does the circulation theorem hold for heterogeneous environments beyond the first order in st? To investigate this, we calculate the second-order coefficient of the fixation probability, see SI Section 5.2. Considering the clique and a particular cycle with $D = 5$ and equal anticlockwise and clockwise mi-

grations, we show that the second-order coefficient is impacted by environment heterogeneity, can differ across individual demes in both of these structures, and can also differ between the two of them. Hence, the circulation theorem does not hold beyond first order in st for heterogeneous environments. In the clique, we find that the fixation probability averaged over all initial mutant locations is increased by environment heterogeneity, compared to that of a homogeneous clique with the same $\langle\delta\rangle$. Furthermore, the heterogeneity-specific second-order term is proportional to the environment variance $\mathrm{Var}(\delta)$ of the δ_i coefficients across demes, and increases if migration probability m decreases, see SI Section 5.2. Figure 4A shows the excess in the fixation probability compared to first order, i.e. the negative second-order coefficient. Besides being increased by environment heterogeneity, we observe that it can be positive, in which case the second order term increases the fixation probability, while for homogeneous environments, it always decreases it. The situation is similar for our particular cycle, see Figure 4B, albeit slightly more complex (see SI Section 5.2 and SI Figure S8 for details).

Heterogeneous environments can induce amplification of selection in the rare migration regime. So far, we considered frequent migrations, and focused on the branching process regime, assuming that $K \gg 1$ and $1/K \ll st \ll 1$. In this regime, we showed that environment heterogeneity can turn suppressors of selection into amplifiers. Can this also occur in the rare-migration regime, where the timescale of migrations is much slower than mutant fixation or extinction within a deme? To address this question, let us return to the star graph and to the line graph. Their mutant fixation probabilities were determined analytically for homogeneous environments in the rare migration regime, respectively in Refs. [35] and [58]. A key point under rare migrations is that a mutant that fixes always first takes over its deme of origin, before spreading to other demes, allowing a coarse-grained Markov chain description [35, 44]. Here, we generalize these calculations to heterogeneous environments. For the star, we consider the case where the center has a different environment from the leaves, associated to the mutant advantage prefactor δ_C, but the leaves all have the same environment, associated to δ_L, see SI Section 6.1. For the line, we perform a general calculation where all demes can have different environments, with a mutant advantage prefactor δ_i in deme i, see SI Section 6.2.

Figure 5 shows that the heterogeneous star in the rare migration regime can amplify natural selection, compared to a homogeneous circulation with the same mean mutant fitness, in a broad range of migration asymmetries $\alpha = m_I/m_O$. Strikingly, this includes cases where $\alpha < 1$, for which the star suppresses natural selection under rare migrations [35]. Hence, environment heterogeneity can turn suppressors of selection into amplifiers in the rare migration regime too. In Figure 5, we observe amplification of selection for weakly deleterious and weakly beneficial mutants (recall that for deleterious mutants, amplification corresponds to having a smaller fixation probability than in the well-mixed or circulation case). The results of Figure 5 are obtained with δ_C substantially larger than δ_L, i.e. when beneficial (resp. deleterious) mutants are substantially more advantaged (resp. disadvantaged) in the center than in leaves. In this case, consider st such that $1/K \ll 2\delta_C st \ll 1$ but $2\delta_L st \lesssim 1/K$. Then, if a mutant starting in the center fixes there, it should ultimately take over the whole population. Indeed, wild-type individuals migrating to the center from other leaves cannot take over again in the center, due to their substantial fitness disadvantage (their fixation probability is exponentially suppressed). This existence of a special "safe" deme for mutants sets the star apart from the homogeneous circulation with the same $\langle\delta\rangle$, and causes amplification in this regime (see SI Section 6.1 for further details, including an explanation of the suppression of selection observed for larger st). Recall that in the homogeneous star with $\alpha > 1$, amplification of selection is observed under rare migrations [35], but only when $st \lesssim 1/K$ [36]. In fact, in the rare migration regime, amplification effects are associated to the finite size of demes and only exist in that regime. Our new findings are consistent with this, and shed light on how environment heterogeneity can induce amplification in the rare migration regime.

In the case of the line, which is a suppressor of selection in the homogeneous case [58], we also find that environment heterogeneity can yield amplification of selection. This is shown in SI Figure S13, where we assume that only the leftmost deme has δ_L while the other ones have δ_R substantially smaller. A small amplification occurs in the regime where $1/K \ll 2\delta_L st \ll 1$ but $2\delta_R st \lesssim 1/K$, see SI Section 6.2. As in the star, the mutant benefits from the existence of a "safe" (leftmost) deme, where it cannot be re-invaded by wild-types. However, its location is less ideal than in the star, leading to a smaller effect. This illustrates the generality of the amplification mechanism by environment heterogeneity in

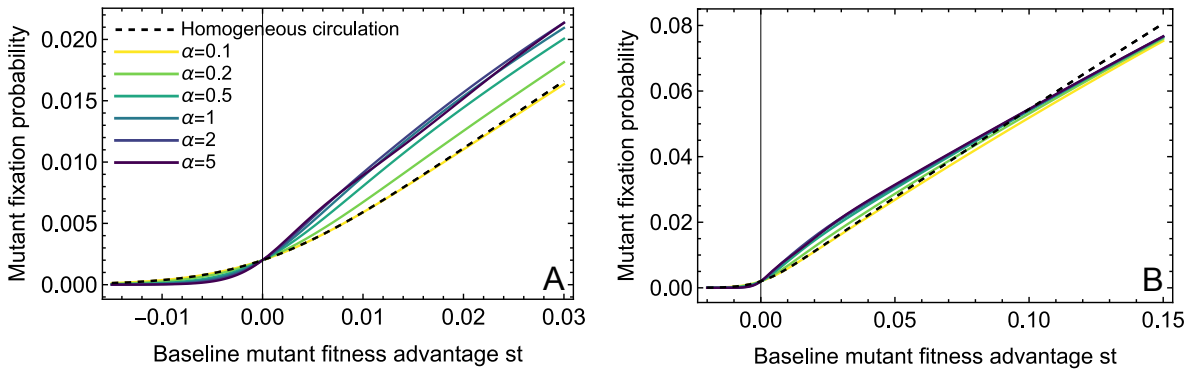

Figure 5: **Amplification in the heterogeneous star with rare migrations.** We show the mutant fixation probability, starting from one single mutant placed uniformly at random at a bottleneck (Eq. S107 using Eq. S102), in a heterogeneous star with various migration asymmetries α, and in a homogeneous circulation with the same mean mutant fitness advantage, i.e. with the same $\langle\delta\rangle$. All fixation probabilities are plotted versus the baseline effective mutant fitness advantage st. Panels A and B show different ranges of st. Parameter values: $D = 5$, $K = 100$. For the heterogeneous star, $\delta_C = 1$ and $\delta_L = 0.1$.

the rare migration regime: it relies on refugia where mutants are safe from re-invasion, and is specific to finite-sized demes and to a range of small fitness differences between mutant and wild-type individuals.

Discussion

In this work, we investigated the impact of environment heterogeneity on mutant fixation in spatially structured populations with demes on nodes of a graph. We considered two different regimes: frequent migrations and rare migrations. For frequent migrations, we demonstrated that environment heterogeneity can lead to amplification of selection, together with acceleration of mutant fixation and extinction. This result is striking for two reasons: first, without environment heterogeneity, no amplification is possible under frequent migrations [36]. Second, amplifiers of selection generally slow down fixation [26–29, 59]. We found that this simultaneous amplification and acceleration occurs in the star graph, and more strongly in the line graph. We showed that a key ingredient for amplification to occur is that mutants should be more favored in demes with stronger migration outflow. We proved that the circulation theorem remains valid to first order in heterogeneous environments: in these graphs where migrations are symmetric enough, fixation probability is the same as in an equivalent well-mixed population to first order. However, we also found that mutant fixation probability is increased by environment heterogeneity at second order in circulation graphs. Finally, in the rare migration regime, where mutant fixation or extinction in a deme is faster than migrations, we showed that environment heterogeneity can turn suppressors of selection into amplifiers.

While environment heterogeneity can foster amplification of selection both under frequent migrations and under rare migrations, the mechanisms differ between these two cases, and the regime of mutant fitness advantage where amplification is observed does too. For frequent migrations, we used a branching process analysis, which focuses on the early and highly stochastic dynamics of a mutant lineage, long before it reaches a size comparable to that of a deme. We found that in this case, regions with both stronger mutant fitness advantage and larger migration outflow allow the mutant to more successfully avoid extinction. Meanwhile, for rare migrations, fixation must occur within a deme before mutants can spread further. If mutant fitness advantage is much larger than $1/K$ in a deme, this deme essentially cannot be re-invaded by wild-type individuals if the mutant type fixes there, since wild-type fixation is extremely unlikely. Such demes with sufficient mutant advantage become refugia for mutants, compared to other demes where mutant fitness advantage is smaller and wild-types can take over again, and this enables amplification of selection. This effect is associated to the possibility that wild-types take over again in a deme, and thus requires small fitness advantages and finite deme sizes. This stands in contrast with the frequent-migration amplification effect.

Our results were obtained by extending to heterogeneous environments a general model of spatially structured populations on graphs, which does not rely on update rules [36], and is close to experimental protocols of serial transfer [52–56]. In addition, compared to studies of heterogeneous environments in evolutionary graph theory [37–42], which generally focus on two environments and their repartition across nodes, we obtained results for generic heterogeneity (where environments can differ in each deme and each be chosen in a continuum), both for frequent migrations in the branching process regime, and for rare migrations in the case of the line. Our results are thus a strong generalization over these previous studies. Moreover, we stress that while the rare migration regime can be mapped to evolutionary graph theory models with one individual per node for some migration asymmetries [35], the frequent migration regime is fundamentally different, as states where several demes comprise both mutants and wild-type individuals are then key to the mutant's fate. This frequent migration regime is particularly relevant for experimental and natural populations, while the rare migration regime leads to very long fixation times.

In the line graph, we showed that a decreasing mutant fitness advantage profile along the main flow direction can foster amplification of selection. This can have important applications to natural systems. Indeed, in the gut, which can be considered as a one-dimensional system to a first approximation, a directional hydrodynamic flow exists together with a fitness gradient due to nutrient availability [60–62]. These ingredients have been shown to impact mutant fixation [63, 64]. Considering mutants with spatially-dependent advantages would be of strong interest, as our results for a discrete line of demes suggest that their fixation could be more likely and faster.

Our results, obtained for spatially structured populations with (almost) fixed sizes, resonate with known ones for expanding populations. In particular, the presence of antibiotic concentration gradients can foster resistance evolution in expanding populations [65–68]. In these cases, expanding populations move toward zones where mutant fitness advantage is larger. It would be interesting to generalize our model to include initially empty demes where the population can grow. Another promising direction would be to include time-varying environments in demes [69, 70]. Finally, while our focus has been on the fate of a single mutation, it would be very interesting to investigate the impact of heterogeneous spatially structured populations on fitness landscape exploration [58, 71, 72], longer-term evolution [73, 74], as well as on population diversity under frequent mutations [75–77].

Models and methods

Serial dilution model on a graph with heterogeneous environment. We model a spatially structured population as a set of well-mixed demes, each sitting on one node of a connected graph with D nodes. Migration probabilities m_{ij} are defined between any pair of demes $(i, j) \in \{1, ..., D\}^2$, including $i = j$, corresponding to individuals that stay in the same deme. They differ by their exponential growth rates, which are respectively $f_W = 1$ for wild-types (taken as reference) and $f_M = 1 + s$ for mutants. Thus, s is the relative fitness advantage of mutants compared to wild-types. The population is composed of wild-types of fitness $f_W = 1$ (taken as reference) and mutants, whose fitness depends on the environment, and is denoted by $f_{M,i} = 1 + \delta_i s$ in deme i. Here, s is the baseline mutant fitness advantage, and δ_i is an environment-dependent prefactor, which is assumed to be comprised between 0 and 1, and of order unity if it is nonzero. We generalize the model introduced in Ref. [36] to heterogeneous environments. The dynamics of the population, modeling serial passage with migrations, is composed of alternations of elementary phases of growth and dilution, see SI Figure S1A. Migrations are implemented during the dilution (i.e. regulation) phases. Note that this serial dilution model with migrations is very close to a structured Wright-Fisher model [78, 79], and that results from the serial dilution model in the branching process approximation hold in structured Wright-Fisher models too [36].

Starting at a bottleneck, the elementary step of deterministic exponential growth happens simultaneously and independently in each deme for a fixed time t. It is impacted by environment heterogeneity via the mutant fitness advantage $s\delta_i$, which depends on the deme i. Let us denote the initial fraction of mutants in deme i by x_i. The fraction of mutants after growth in deme i is:

$$x_i' = \frac{x_i e^{\delta_i s t}}{1 + x_i(e^{\delta_i s t} - 1)} \,. \tag{4}$$

Note that the impact of the baseline selective advantage of mutants is encoded by the product st. We thus call st the (effective) baseline fitness advantage.

After each growth phase, a dilution (regulation) and migration phase takes place. The number of mutants going from deme i to deme j is sampled from a binomial distribution with N_i' trials, with N_i' the size of the deme after growth, and a probability of success $m_{ij}x_i'K/N_i'$. Similarly for wild types, but with a probability of success $m_{ij}(1-x_i')K/N_i'$. Each deme j thus receives on average $K\sum_{i=1}^{D} m_{ij}$ individuals, leading to a new bottleneck state. We assume that for all j, $\sum_{i=1}^{D} m_{ij} = 1$, so that all demes have the same average bottleneck size K. For each pair of demes (i, j), this phase corresponds to sampling approximately Km_{ij} bacteria from the total N_i' bacteria present in deme i, which contribute to the new bottleneck state of deme j.

Growth and dilution-migration phases are iterated, and the dynamics of the population composition can be followed through the process. We perform exact stochastic simulations of this model, using binomial sampling.

Branching process description. The state of the population is described with a multi-type branching process, where each type corresponds to mutants in each deme [36]. The branching process description assumes that all mutant lineages are independent [80]. It holds when mutants are in small numbers, e.g. at early phases starting from a single mutant, if deme sizes are large, $K \gg 1$. For mutants with substantial selective advantage $st \gg 1/K$, extinction events happen when mutants are still rare [75, 81]. Therefore, the branching process approach requires $K \gg 1$ and $st \gg 1/K$. Further assuming that all nonzero migration probabilities are of order unity, the binomial distributions used in sampling can be approximated by Poisson ones.

Under these conditions, starting from one mutant in deme i at a bottleneck, the mutant extinction probability p_i satisfies:

$$p_i = \exp\left[Kx_i'\sum_{j=1}^{D} m_{ij}(p_j - 1)\right], \tag{5}$$

for all i, where x_i' is given by Eq. 4 with $x_i = 1/K$. These equations generalize those of the homogeneous case [36], as here the mutant fraction x_i' in deme i after growth involves δ_i. To solve Eq. 5 for all i, we assume that the baseline mutant fitness advantage is small, $st \ll 1$, and perform a Taylor expansion, see SI Section 1. The fixation probability starting from one mutant in deme i at a bottleneck is then $\rho_i = 1 - p_i$. We mainly focus on the average fixation probability $\rho = \sum_{i=1}^{D} \rho_i/D$ across the structure, assuming that mutants appear uniformly at random in the structure.

The average mutant extinction time can also be obtained in the branching process regime, see SI Section 1.5.

Rare migration regime. When the timescale of migrations is much slower than mutant fixation or extinction within a deme, one can consider that each deme is always fully wild type or fully mutant as far as migration events are concerned. This allows a coarse-grained Markov chain description [35, 44], which has allowed the determination of exact fixation probabilities in the homogeneous case [35, 58]. Here, we extend this approach to the heterogeneous case, see SI Section 6.1. Contrary to the branching process results, these results hold for all values of st, including for deleterious, neutral and effectively neutral mutants. Besides, they connect to evolutionary graph theory models [35]. However, the rare migration regime is associated to slow dynamics. In contrast, the branching process calculations assume that migration probabilities are of order unity, so these two approaches cover entirely distinct regimes and provide complementary insights.

Acknowledgments

This research was partly funded by the Swiss National Science Foundation (SNSF, grant No. 315230 208196, to A.-F. B.), by the Chan-Zuckerberg Initiative (CZI, to A.-F. B.), and by the European Research Council (ERC) under the European Union's Horizon 2020 research and innovation programme (grant agreement No. 851173, to A.-F. B.). C. L. acknowledges funding by the Agence Nationale de la Recherche (grants ANR-20-CE30-0001 and ANR-21-CE45-0015, to C. L.).

Supplementary Information

Contents

1 Mutant fixation in the branching process regime **14**
- 1.1 Model . . . 14
- 1.2 Expansion of the mutant fixation probability . . . 14
- 1.3 Mutant fixation probability in strongly symmetric spatial structures . . . 16
  - 1.3.1 Clique with heterogeneous environment . . . 16
  - 1.3.2 Cycle with heterogeneous environment . . . 17
  - 1.3.3 Star with heterogeneous environment . . . 17
  - 1.3.4 Line with heterogeneous environment . . . 18
- 1.4 General determination of the mutant fixation probability . . . 19
- 1.5 Average mutant extinction time . . . 20

2 Comparison of fixation probabilities in the star and clique **20**
- 2.1 Homogeneous star versus clique . . . 20
- 2.2 Homogeneous star versus heterogeneous star . . . 21
- 2.3 Heterogeneous star versus clique . . . 21

3 Comparison of fixation probabilities in the line and clique **22**
- 3.1 Homogeneous line versus clique . . . 22
- 3.2 Homogeneous line versus heterogeneous line . . . 23
- 3.3 Heterogeneous line versus clique . . . 24

4 Spatial structures with one strong-outflow deme **27**
- 4.1 Highly symmetric structure with one special deme . . . 28
  - 4.1.1 Fixation probability . . . 28
  - 4.1.2 Condition for amplification of selection . . . 28
- 4.2 More general structures with one strong-outflow deme . . . 29

5 Circulation theorem extension and limitations **30**
- 5.1 First order in the baseline mutant fitness advantage st . . . 30
- 5.2 Second order in the baseline mutant fitness advantage st . . . 31
  - 5.2.1 Clique with heterogeneous environment . . . 32
  - 5.2.2 A particular cycle with heterogeneous environment . . . 33

6 Rare migration regime **35**
- 6.1 Star with heterogeneous environment . . . 35
  - 6.1.1 Mutant fixation probability . . . 35
  - 6.1.2 Amplification of selection . . . 37
- 6.2 Line with heterogeneous environment . . . 38
  - 6.2.1 Mutant fixation probability . . . 38
  - 6.2.2 Amplification of selection . . . 45

1 Mutant fixation in the branching process regime

1.1 Model

For completeness, we present here in more detail the model introduced in the main text section "Models and methods". Next, we use this model to calculate mutant fixation probabilities in the branching process regime.

We consider spatially structured populations with D demes, each located on each node of a graph. We assume that there are two types of individuals, mutants and wild-types. Let us denote by s the baseline relative fitness advantage of mutants with respect to wild-types. Let us further model environment heterogeneity by introducing a deme-dependent prefactor δ_i in the mutant relative fitness advantage, such that in deme i, we have a relative fitness difference of $\delta_i s$ between the two types. In other words, taking wild-type fitness as reference ($f_W = 1$), we have $f_{M,i} = 1+\delta_i s$, where $f_{M,i}$ denotes mutant fitness in deme i, while f_W denotes wild-type fitness.

We start from the serial dilution model presented in Ref. [36], and we extend it to the heterogeneous case, where mutant fitness advantage is deme-dependent. In this model, demes undergo alternations of local deterministic exponential growth for time t, and of events of simultaneous dilution and migration leading to new bottlenecks, see Figure S1A. We call m_{ij} the migration probability from deme i to deme j and assume $\sum_{k=1}^{D} m_{ki} = 1$ for all i.

We focus on the fate of a mutant that appears in deme i at a bottleneck, giving an initial mutant fraction $x_0^{(i)} = 1/K$ in that deme, where K is bottleneck size, and 0 in other demes. For this, we consider the first growth and migration-dilution events happening. The mutant fraction after exponential growth reads in deme i [36]:

$$x_0'^{(i)} = \frac{e^{\delta_i st}}{K + e^{\delta_i st} - 1} \equiv \frac{\lambda^{(i)}}{K}\,, \tag{S1}$$

where we introduced $\lambda^{(i)}$, which is a deme-specific growth factor. Then, we model the subsequent migration-dilution event through binomial sampling from each deme to each other demes. In particular, mutants are sampled from the grown deme i, of size N_i', to a destination deme j through the binomial law $\mathcal{B}\left(N_i', K m_{ij} x_0'^{(i)}/N_i'\right)$. Assuming $N_i' \gg 1$, $K m_{ij} x_0'^{(i)}/N_i' \ll 1$ and $\lambda_{ij} = K m_{ij} x_0'^{(i)} \sim 1$, we approximate the binomial law by a Poisson law with mean

$$\lambda_{ij} = K m_{ij} x_0'^{(i)} = \lambda^{(i)} m_{ij}\,. \tag{S2}$$

Compared to the homogeneous case considered in Ref. [36], the impact of heterogeneity is that the growth factor $\lambda^{(i)}$ depends on the deme i.

1.2 Expansion of the mutant fixation probability

Assuming $s > 0$, $K \gg 1$ and $1/K \ll st \ll 1$, and following a multi-type branching process description, as in Ref. [36], the probability p_i that mutants gets extinct, starting from one single mutant in deme i at the bottleneck, satisfies:

$$p_i = \exp\left[\lambda^{(i)} \sum_{j=1}^{D} m_{ij}(p_j - 1)\right]. \tag{S3}$$

Note that, while this equation regards the mutant extinction probability, the mutant fixation probability can then be obtained as $\rho_i = 1 - p_i$.

To solve the equations in Eq. S3, we perform a perturbative expansion in $st \ll 1$:

$$p_j = 1 - a_j st + \frac{b_j}{2}(st)^2 - \frac{c_j}{6}(st)^3 + o((st)^3) \qquad j = 1, \ldots, D\,, \tag{S4}$$

where a_j, b_j and c_j are coefficients to be determined. Expanding Eq. S1 yields

$$\lambda^{(j)} = 1 + \delta_j st + \frac{\delta_j^2 (st)^2}{2} + o((st)^2) \qquad j = 1, \ldots, D. \tag{S5}$$

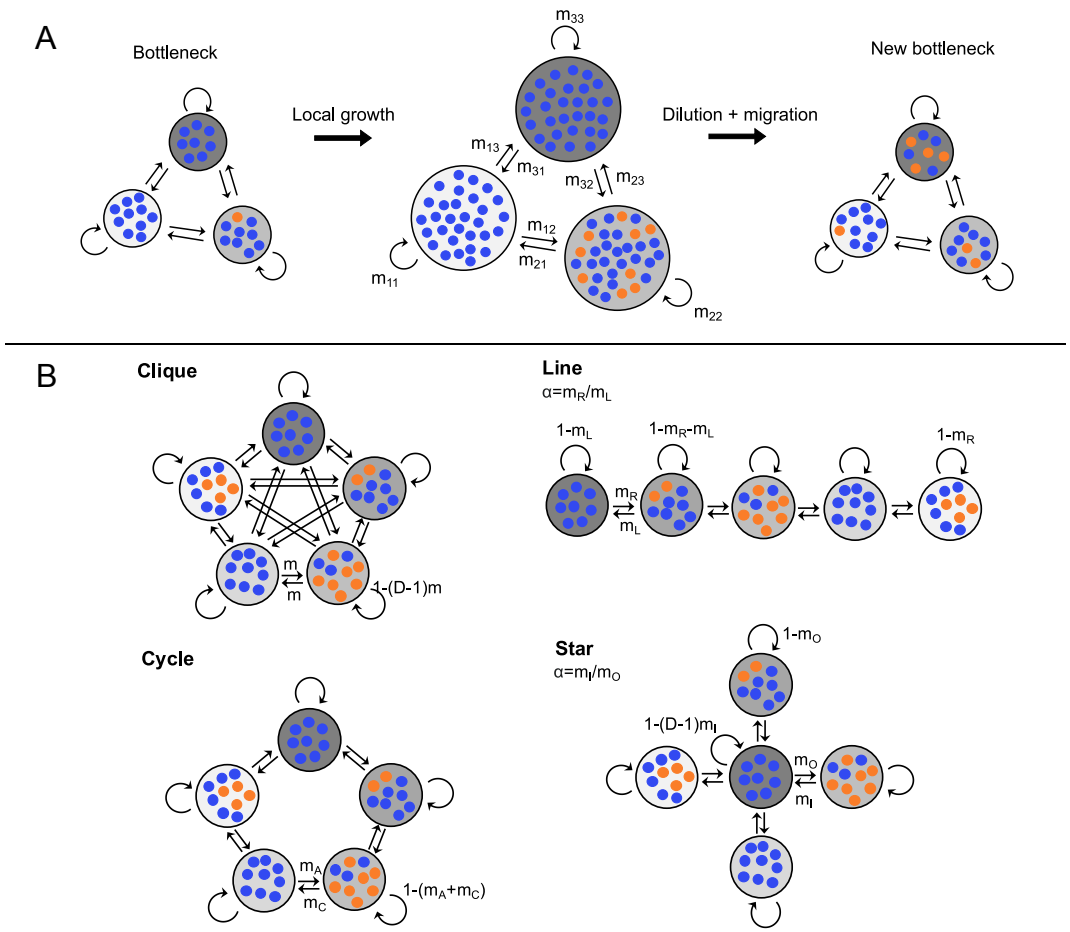

Figure S1: **Serial dilution model for spatially structured populations with environmental heterogeneities.** Panel A: An elementary step of the serial dilution model. Starting from a bottleneck, each deme undergoes a deterministic local growth step followed by a dilution and migration step. Thus, a new bottleneck is reached. The mutant fitness advantage in deme i is $\delta_i s$, with δ_i encoding environment differences between demes, and s the baseline fitness advantage of mutants relative to wild-types. Panel B: Structures considered in this study: clique with migration probability m, line with migration probability to the right m_R and to the left m_L, cycle with migration probability m_A in the anticlockwise direction and m_C in the clockwise direction, and star, with incoming migration probability m_I from each leaf to the center, and outgoing migration probability m_O from the center to each leaf.

Eq. S3 then yields, for $j = 1, \ldots, D$:

$$\begin{aligned} p_j &= \exp\left[\left(1 + \delta_j st + \delta_j^2 \frac{(st)^2}{2} + o((st)^2)\right) \sum_{k=1}^{D} m_{jk} \left(-a_k st + \frac{b_k}{2}(st)^2 - \frac{c_k}{6}(st)^3 + o((st)^3)\right)\right] \\ &= \exp\left[-st \sum_{k=1}^{D} m_{jk} a_k + (st)^2 \sum_{k=1}^{D} m_{jk} \left(\frac{b_j}{2} - a_j \delta_j\right) + (st)^3 \sum_{k=1}^{D} m_{jk} \left(\frac{b_k}{2}\delta_j - a_k \frac{\delta_j^2}{2} - \frac{c_k}{6}\right) + o((st)^3)\right]. \end{aligned} \tag{S6}$$

This gives, to third order in $st \ll 1$:

$$p_j = 1 - st \sum_k m_{jk} a_k + \frac{(st)^2}{2} \left[\left(\sum_{k=1}^{D} m_{jk} a_k \right)^2 + \sum_{k=1}^{D} m_{jk} \left(b_k - 2\delta_j a_k \right) \right]$$
$$+ (st)^3 \left[-\frac{1}{6} \left(\sum_{k=1}^{D} m_{jk} a_j \right)^3 - \sum_{k=1}^{D} m_{jk} a_k \sum_{l=1}^{D} m_{jl} \left(\frac{b_l}{2} - a_l \delta_j \right) + \sum_{k=1}^{D} m_{jk} \left(\frac{b_k}{2} \delta_j - a_k \frac{\delta_j^2}{2} - \frac{c_k}{6} \right) \right]. \tag{S7}$$

Eqs. S4 and S7 yield by identification, for $j = 1, \ldots, D$:

$$\begin{cases} a_j = \sum_{k=1}^{D} m_{jk} a_k \,, \\ b_j = \sum_{k=1}^{D} m_{jk} b_k + a_j^2 - 2\delta_j a_j \,, \\ c_j = \sum_{k=1}^{D} m_{jk} c_k - 2a_j^3 + 3a_j b_j - 3\delta_j b_j + 3\delta_j a_j^2 - 3\delta_j^2 a_j . \end{cases} \tag{S8}$$

The first line in Eq. S8 is the same in a homogeneous environment [36], but the other ones differ, as they involve δ_j.

In the following sub-sections, we use Eq. S8 to explicitly calculate the first-order coefficients a_i for different structures with strong symmetries, shown in Figure S1B.

1.3 Mutant fixation probability in strongly symmetric spatial structures

1.3.1 Clique with heterogeneous environment

In the clique (see Figure S1B), $m_{ij} = m$ for all $i \neq j$. Hence, the first line of Eq. S8 becomes $a_j = m \sum_{k=1}^{D} a_k$ for all j. This implies that all a_j coefficients are equal, say to a. To obtain the value of a, we now use the second line of Eq. S8:

$$b_j m(D-1) = m \sum_{k \neq j} b_k + a^2 - 2a\delta_j \qquad j = 1, \ldots, D \,. \tag{S9}$$

Summing Eq. S9 over j yields:

$$m(D-1) \sum_{j=1}^{D} b_j = m \sum_{j=1}^{D} \sum_{k \neq j} b_k + Da^2 - 2a \sum_{j=1}^{D} \delta_j$$
$$= m(D-1) \sum_{j=1}^{D} b_j + Da^2 - 2a \sum_{j=1}^{D} \delta_j \,. \tag{S10}$$

Thus, as $a \neq 0$, we obtain the first-order coefficient $a = 2\langle \delta \rangle$ for the clique, with $\langle \delta \rangle = \sum_{j=1}^{D} \delta_j / D$.

Therefore, the fixation probability ρ_i of a single mutant starting in deme i at a bottleneck in a clique reads to first order in st:

$$\rho_i = 1 - p_i = ast = 2\langle \delta \rangle st \,, \quad \text{for all } i \,. \tag{S11}$$

Thus, to first order, only the mean relative fitness advantage of the mutant across the structure matters for the mutant fixation probability in the clique. Moreover, this result is the same as in a well-mixed population with the same $\langle \delta \rangle$ [57]. Hence, to first order, the heterogeneity within the clique has no impact on fixation probability. This comes on top of the fact that the spatial structure of the clique has no impact on fixation probability. All heterogeneous cliques have the same fixation probability as the corresponding homogeneous well-mixed population.

Note that the clique is a circulation, i.e., a graph where at each node the sum of incoming and outgoing migrations is equal. Circulation graphs are considered in more detail in SI Section 5.

1.3.2 Cycle with heterogeneous environment

Let us now consider the cycle, with migration probabilities to nearest neighbor demes that can differ in the clockwise and anticlockwise directions, and are denoted by m_C and m_A, respectively (see Figure S1B).

For circulation graphs, which satisfy $\sum_k m_{ki} = \sum_k m_{ik} = 1$, and include the clique and the cycle, using the Perron-Frobenius theorem and the first line of Eq. S8 (which is not affected by environment heterogeneity) allows to show that all the a_i coefficients equal, see Ref. [36]. Let us briefly recall this proof for completeness. The the first line of Eq. S8 shows that the vector $(a_1, \dots, a_D)$ is an eigenvector of the matrix M of migration probabilities with eigenvalue 1. As the matrix M is non-negative and irreducible [36], the Perron-Frobenius theorem ensures that the largest real eigenvalue r of M is simple, positive, and satisfies:

$$\min_i \sum_j m_{ij} \leq r \leq \max_i \sum_j m_{ij} \,. \tag{S12}$$

As circulations satisfy $\sum_i m_{ij} = \sum_j m_{ij} = 1$, we have $r = 1$. Since $(1, \dots, 1)$ is an eigenvector of M associated to 1, it generates the eigenspace associated to the eigenvalue 1, and thus $(a_1, \dots, a_D)$ is proportional to $(1, \dots, 1)$, i.e. all the a_i coefficients equal. Let us call them a (as above for the clique).

The second line of Eq. S8 then reads:

$$b_j = \sum_{k=1}^{D} m_{jk} b_k + a^2 - 2\delta_j a = m_{jj} b_j + \sum_{k \neq j} m_{jk} b_k + a^2 - 2\delta_j a \qquad j = 1, \dots, D. \tag{S13}$$

In the cycle (see Figure S1B), we have $m_{ii} = 1 - m_A - m_C$. Hence, the previous equation becomes:

$$\begin{cases} (m_A + m_C) b_1 = m_A b_2 + m_C b_D + a^2 - 2\delta_1 a \,, \\ (m_A + m_C) b_j = m_A b_{j+1} + m_C b_{j-1} + a^2 - 2\delta_j a \qquad j = 2, \dots, D-1 \,, \\ (m_A + m_C) b_D = m_A b_1 + m_C b_{D-1} + a^2 - 2\delta_D a \,. \end{cases} \tag{S14}$$

The sum of Eqs. S14 reads:

$$\sum_{j=1}^{D} (m_A + m_C) b_j = \sum_{j=1}^{D} (m_A + m_C) b_j + D a^2 - 2a \sum_{j=1}^{D} \delta_j. \tag{S15}$$

Thus, $a = 2\langle \delta \rangle$, which entails that the mutant fixation probability ρ_i to first order in st is again

$$\rho_i = 2\langle \delta \rangle st \,, \quad \text{for all } i \,. \tag{S16}$$

1.3.3 Star with heterogeneous environment

Let us now consider the star, with incoming migration probabilities from a leaf to the center that can differ from outgoing ones from the center to a leaf, and are denoted by m_I and m_O, respectively (see Figure S1B).

As noted earlier, the first line in Eq. S8 is not impacted by environment heterogeneity. Thus, as in Ref. [36], the first-order coefficients for the fixation probability for a mutant starting in the center and in a leaf, denoted respectively by a_C and a_L, satisfy $a_L = \alpha a_C$, where $\alpha = m_I / m_O$ represents migration asymmetry. Note that environment heterogeneity across leaves does not make these first-order coefficients dependent on the leaf where the mutant start.

Let $\mathcal{L}$ be the set of the indexes labeling the leaves of the star. The second line in Eq. S8, written for the center (with second-order coefficient b_C) and for one of the leaves $j \in \mathcal{L}$ (with second-order coefficient b_j), yields:

$$\begin{cases} (D-1) m_I b_C = m_O \sum_{k \in \mathcal{L}} b_k + a_C^2 - 2\delta_C a_C \,, \\ m_O b_j = m_I b_C + a_L^2 - 2\delta_j a_L \,, \qquad j \in \mathcal{L}. \end{cases} \tag{S17}$$

Summing Eqs. S17 over all demes gives:

$$(D-1) m_I b_C + m_O \sum_{j \in \mathcal{L}} b_j = (D-1) m_I b_C + m_O \sum_{k \in \mathcal{L}} b_k + a_C^2 + (D-1) a_L^2 - 2\delta_C a_C - 2 \sum_{j \in \mathcal{L}} \delta_j a_L \,, \tag{S18}$$

i.e., after simplification, and using $a_L = \alpha a_C$:

$$a_C^2[1+\alpha^2(D-1)] = 2a_C\delta_C + 2\alpha a_C \sum_{j\in\mathcal{L}} \delta_j. \tag{S19}$$

Hence, as $a_C \neq 0$, we obtain:

$$a_C = \frac{2(\delta_C + \alpha \sum_{i\in\mathcal{L}} \delta_i)}{1+\alpha^2(D-1)} \quad \text{and} \quad a_L = \alpha a_C\,. \tag{S20}$$

Let us now consider a mutant appearing at a bottleneck in a deme chosen uniformly at random. Its fixation probability ρ reads, to first order in st:

$$\begin{aligned}\rho = st\,\frac{a_C + (D-1)a_L}{D} &= 2st\,\frac{[1+\alpha(D-1)](\delta_C + \alpha\sum_{i\in\mathcal{L}}\delta_i)}{D[1+\alpha^2(D-1)]} \\ &= 2\langle\delta\rangle st\,\frac{[1+\alpha(D-1)][\sigma_C(1-\alpha)+1+\alpha(D-1)]}{D[1+\alpha^2(D-1)]}\,,\end{aligned} \tag{S21}$$

where we introduced $\langle\delta\rangle = \sum_{i=1}^{D}\delta_i/D$, and $\sigma_C = (\delta_C - \langle\delta\rangle)/\langle\delta\rangle$. Importantly, the result in Eq. S21 only depends on selection through the mean mutant fitness effect, via $\langle\delta\rangle$, and through the relative fitness excess in the center, via σ_C. In other words, the heterogeneity of selection across leaves does not impact this fixation probability to first order. We show the first-order coefficient of the fixation probability as a function of α and σ_C in Figure 1A.

Note that for a homogeneous star, where $\sigma_C = 0$ and δ takes a unique value, say Δ, across the whole population, Eq. S21 reduces to:

$$\rho = 2\Delta st\,\frac{[1+\alpha(D-1)]^2}{D[1+\alpha^2(D-1)]}\,, \tag{S22}$$

i.e. the result from Ref. [36] for the homogeneous star. Note also that for $\alpha = 1$, when the star is a circulation, Eq. S21 yields the same result as for other circulations considered so far, namely $\rho = 2\langle\delta\rangle st$ (see Eqs. S11 and S16).

1.3.4 Line with heterogeneous environment

Let us now consider the line, with migration probabilities to the left that can differ from those to the right, and are denoted by m_L and m_R, respectively (see Figure S1B). Contrary to other structures discussed so far, the line was not considered in Ref. [36] in the homogeneous case. Hence, the results below are new even in the homogeneous case.

The first line in Eq. S8, written for each node of the line, yields:

$$\begin{cases} a_1 = (1-m_L)a_1 + m_R a_2\,, \\ a_j = (1-m_L-m_R)a_j + m_R a_{j+1} + m_L a_{j-1} \qquad j = 2,\dots,D-1\,, \\ a_D = (1-m_R)a_D + m_L a_{D-1}\,. \end{cases} \tag{S23}$$

Introducing migration asymmetry $\alpha = m_R/m_L$, we get to:

$$\begin{cases} a_1 = \alpha a_2\,, \\ a_j(1+\alpha) = \alpha a_{j+1} + a_{j-1} \qquad j = 2,\dots,D-1\,, \\ a_D = a_{D-1}/\alpha\,. \end{cases} \tag{S24}$$

It can be shown by induction that

$$a_j = \frac{B}{\alpha^{j-1}}\,, \tag{S25}$$

where B is a constant, is a solution of Eq. S24.

Let us now use the equations corresponding to the second line of Eq. S8, written for each node of the line, to determine the values of the constant B:

$$\begin{cases} b_1 m_L = m_R b_2 + a_1^2 - 2\delta_1 a_1\,, \\ b_j(m_L+m_R) = m_R b_{j+1} + m_L b_{j-1} + a_j^2 - 2\delta_j a_j \qquad j = 2,\dots,D-1\,, \\ b_D m_R = m_L b_{D-1} + a_D^2 - 2\delta_D a_D\,. \end{cases} \tag{S26}$$

Summing Eqs. S26 over all nodes of the line yields:

$$m_L b_1 + \sum_{j=2}^{D-1} b_j(m_L+m_R) + b_D m_R = m_R b_2 + m_L b_{D-1} + \sum_{j=2}^{D-1} b_{j+1} m_R + \sum_{j=2}^{D-1} b_{j-1} m_L + \sum_{j=1}^{D} a_j^2 - 2\sum_{j=1}^{D} \delta_j a_j \,, \tag{S27}$$

which simplifies into

$$\sum_{j=1}^{D} a_j^2 = 2\sum_{j=1}^{D} \delta_j a_j \,. \tag{S28}$$

Using Eqs. S25 and S28 then gives:

$$B = 2\frac{\sum_{j=1}^{D} \delta_j \alpha^{-j+1}}{\sum_{j=1}^{D} \alpha^{-2j+2}} = 2\frac{\alpha^2-1}{\alpha^2-\alpha^{2(1-D)}} \sum_{j=1}^{D} \delta_j \alpha^{-j+1}, \tag{S29}$$

The first-order coefficient a_k of the fixation probability for a mutant starting in deme k, thus reads:

$$a_k = \frac{B}{\alpha^{k-1}} = 2\alpha^{-k}\frac{\alpha^2-1}{1-\alpha^{-2D}} \sum_{j=1}^{D} \delta_j \alpha^{-j}. \tag{S30}$$

Let us now consider a mutant appearing at a bottleneck in a deme chosen uniformly at random. Its fixation probability ρ reads, to first order in st:

$$\rho = st\frac{1}{D}\sum_{k=1}^{D} a_k = \frac{2st}{D}\frac{1+\alpha}{1+\alpha^{-D}} \sum_{j=1}^{D} \delta_j \alpha^{-j}. \tag{S31}$$

In particular, for a homogeneous line where all δ_i are equal, say to Δ, this reduces to:

$$\rho = \frac{2\Delta st}{D}\frac{1+\alpha}{1+\alpha^{-D}} \sum_{j=1}^{D} \alpha^{-j} = \frac{2\Delta st}{D}\frac{(1+\alpha)(1-\alpha^D)}{(1-\alpha)(1+\alpha^D)} \,. \tag{S32}$$

Note that if $\alpha = 1$, when the line is a circulation, Eq. S25 reduces to $a_j = C$, with C a constant. Then, Eq. S28 yields $C = 2\langle\delta\rangle$, and hence $\rho = 2\langle\delta\rangle st$, which is the same result as for the other circulation graphs we considered so far.

1.4 General determination of the mutant fixation probability

To go beyond strongly symmetric structures, let us present a method to obtain the first-order coefficient in st of the fixation probability in any strongly connected graph (meaning that there is a path between each pair of vertices of the graph, in both directions). To this end, we first consider the first line in Eq. S8, which can be rewritten in vector form as:

$$M\boldsymbol{a} = \boldsymbol{a} \,, \tag{S33}$$

with $\boldsymbol{a} = (a_1, \ldots, a_D)$. Thus, we are looking for an eigenvector of M for eigenvalue 1. As the graph is strongly connected, its migration matrix M is irreducible. Since M is an irreducible, non-negative matrix, and satisfies $\sum_i m_{ij} = 1$ for all j, the Perron–Frobenius theorem guarantees that 1 is an eigenvalue of M, and is simple.

To determine the norm of the corresponding eigenvector $\boldsymbol{a}$, we use the second line in Eq. S8, thereby generalizing the strategy we used above for symmetric structures. We isolate b_j, use $\sum_{k=1}^{D} m_{kj} = 1$, and sum over all possible j:

$$\begin{aligned} b_j &= m_{jj} b_j + \sum_{k\neq j} m_{jk} b_k + a_j^2 - 2\delta_j a_j \,, \text{ i.e.} \\ b_j - \left(1 - \sum_{k\neq j} m_{kj}\right) b_j &= \sum_{k\neq j} m_{jk} b_k + a_j^2 - 2\delta_j a_j \,, \text{ thus} \\ \sum_j \sum_{k\neq j} m_{kj} b_j &= \sum_j \sum_{k\neq j} m_{jk} b_k + \sum_j a_j^2 - \sum_j 2\delta_j a_j \,, \text{ i.e.} \\ 0 &= \sum_j a_j^2 - 2\sum_j \delta_j a_j \,. \end{aligned} \tag{S34}$$

For given δ_j values, this equation provides a constraint on the a_i, which allows to determine the norm of $\boldsymbol{a}$. Indeed, considering an eigenvector $\boldsymbol{a}'$ of M with eigenvalue 1, the vector $\boldsymbol{a}$ we are looking for can be written as $\boldsymbol{a} = C\boldsymbol{a}'$, where C is a constant, which should satisfy:

$$C^2 \sum_j (a'_j)^2 = 2C \sum_j a'_j \delta_j \,. \tag{S35}$$

With $C \neq 0$, this finally yields $\boldsymbol{a} = C\boldsymbol{a}'$ with

$$C = \frac{2\sum_j a'_j \delta_j}{\sum_j (a'_j)^2} \,. \tag{S36}$$

1.5 Average mutant extinction time

The average extinction time $t_i^{(\mathrm{ex})}$ of the lineage of a single mutant introduced in deme i at a bottleneck can be calculated in the branching process approximation from the probability generating function [36, 80]. Specifically, in a multi-type branching process, the vector of extinction times, expressed in number of generations, $\boldsymbol{t}^{(\mathrm{ex})} = \left(t_1^{(\mathrm{ex})}, t_2^{(\mathrm{ex})}, \ldots, t_D^{(\mathrm{ex})}\right)$, is given by:

$$\boldsymbol{t}^{(\mathrm{ex})} = \boldsymbol{f}(0) + \sum_{n=1}^{\infty} n \left[\boldsymbol{f}^{(n)}(0) - \boldsymbol{f}^{(n-1)}(0)\right] , \tag{S37}$$

with $\boldsymbol{f}$ the generating function, whose component i satisfies:

$$f_i : \boldsymbol{x} \mapsto \exp\left[\lambda^{(i)} \sum_j m_{ij}(x_j - 1)\right] , \tag{S38}$$

with $\lambda^{(i)}$ given by Eq. S5.

2 Comparison of fixation probabilities in the star and clique

Let us focus on the heterogeneous star structure, and on its impact on mutant fixation probability. First, for reference, in Section 2.1, we briefly compare a homogeneous star to a clique. Next, in Section 2.2, we determine under what conditions heterogeneity can increase the fixation probability in the star, compared to a homogeneous star. Finally, in Section 2.3, we compare a heterogeneous star to a clique, to determine if a heterogeneous star can suppress or amplify selection.

In all cases, when we compare a structure with heterogeneous environment to another one with homogeneous environment, we match their average mutant fitness advantage, i.e. in our notations, we match their $\langle\delta\rangle$. Our comparisons all rely on the first-order fixation probabilities derived in Section 1 in the branching process approximation.

2.1 Homogeneous star versus clique

We first consider a homogeneous star with relative mutant fitness advantage $s\Delta$ in all demes. We compare it to a heterogeneous clique with relative mutant fitness advantage $s\delta_i$ in deme i, satisfying $\langle\delta\rangle = \Delta$. Using the fixation probabilities in Eqs. S22 and S11, we find that the homogeneous star has a first-order fixation probability lower than the heterogeneous clique if and only if:

$$\frac{1}{D}\frac{[1+(D-1)\alpha]^2}{[1+\alpha^2(D-1)]} < 1 \,. \tag{S39}$$

Note that the heterogeneity of the clique does not impact its fixation probability to first order (see Eq. (S11)), and thus, this condition is the same as that found in Ref. [36], when comparing the homogeneous star and the homogeneous clique. As shown in Ref. [36], this condition is always satisfied, except for $\alpha = 1$, when the two fixation probabilities are equal. Thus, the homogeneous star suppresses natural selection under frequent asymmetric migrations.

2.2 Homogeneous star versus heterogeneous star

Let us compare the fixation probabilities in a heterogeneous star and in a homogeneous star, given respectively in Eqs. S21 and S22 to first order in st. Our homogeneous star has relative mutant fitness advantage $s\Delta$ in all demes, while our heterogeneous star has relative mutant fitness advantage $s\delta_i$ in deme i, satisfying $\langle\delta\rangle = \Delta$. The first-order fixation probability is larger in the heterogeneous star than in the homogeneous star if and only if:

$$\frac{[1+\alpha(D-1)][\sigma_C(1-\alpha)+1+\alpha(D-1)]}{D[1+\alpha^2(D-1)]} > \frac{[1+\alpha(D-1)]^2}{D[1+\alpha^2(D-1)]}\,, \tag{S40}$$

As the denominator and the term $1+\alpha(D-1)$ are positive, this is equivalent to

$$\sigma_C(1-\alpha) > 0\,. \tag{S41}$$

Thus, the relative fitness excess in the center should have the same sign as $1-\alpha$ for heterogeneity to enhance mutant fixation probability. This means that if $\alpha < 1$ (i.e. $m_I < m_O$, more outflow from the center than inflow), heterogeneity benefits mutant fixation if the center features a larger mutant fitness advantage than the leaves. Conversely, if $\alpha > 1$ (i.e. $m_I > m_O$, more inflow to the center than outflow), heterogeneity benefits mutant fixation if the center features a smaller mutant fitness advantage than the leaves.

2.3 Heterogeneous star versus clique

We have shown that a homogeneous star has a smaller mutant fixation probability than a clique, but that a heterogeneous star can have a larger mutant fixation probability than a homogeneous one. What is the overall effect of a heterogeneous star structure compared to a clique? In particular, can environment heterogeneity allow the star to overcome the suppression of selection effect it has under homogeneous environments? To address this question, we compare a heterogeneous star to a clique. Recall that only average fitness matters to first order for the mutant fixation probability in the clique. Hence, we consider a clique which can be homogeneous or heterogeneous, but which has the same average fitness as our heterogeneous star.

The fixation probabilities in a heterogeneous star and in a clique are given respectively in Eqs. S21 and S11 to first order in st. The first-order fixation probability is larger in the heterogeneous star than in a clique if and only if:

$$\frac{[1+\alpha(D-1)][\sigma_C(1-\alpha)+1+\alpha(D-1)]}{D[1+\alpha^2(D-1)]} > 1\,. \tag{S42}$$

This condition is equivalent to:

$$\begin{aligned}&\sigma_C(1-\alpha)[1+\alpha(D-1)] > D[1+\alpha^2(D-1)] - [1+\alpha(D-1)]^2\,, \text{ i.e.}\\ &\sigma_C(1-\alpha)[1+\alpha(D-1)] > (D-1)(1-\alpha)^2\,.\end{aligned} \tag{S43}$$

The condition in Eq. S43 can be expressed as:

- $\sigma_C > f_{\text{star}}(\alpha, D)$ if $\alpha < 1$,
- $\sigma_C < f_{\text{star}}(\alpha, D)$ if $\alpha > 1$,

where we introduced

$$f_{\text{star}}(\alpha, D) = \frac{(D-1)(1-\alpha)}{1+\alpha(D-1)}\,. \tag{S44}$$

We show $f_{\text{star}}(\alpha, D)$ versus α in Figure S2A, and highlight in pink the regions of the plane (α, σ_C) where amplification of selection exists (see also Figure 1). We further present an example of amplification of selection in Figure S2B. The associated fixation and extinction times are shown in Figure S2C-D. As observed with the line in the main text (see Figure 2), we simultaneously obtain amplification and acceleration of selection, albeit to a smaller extent.

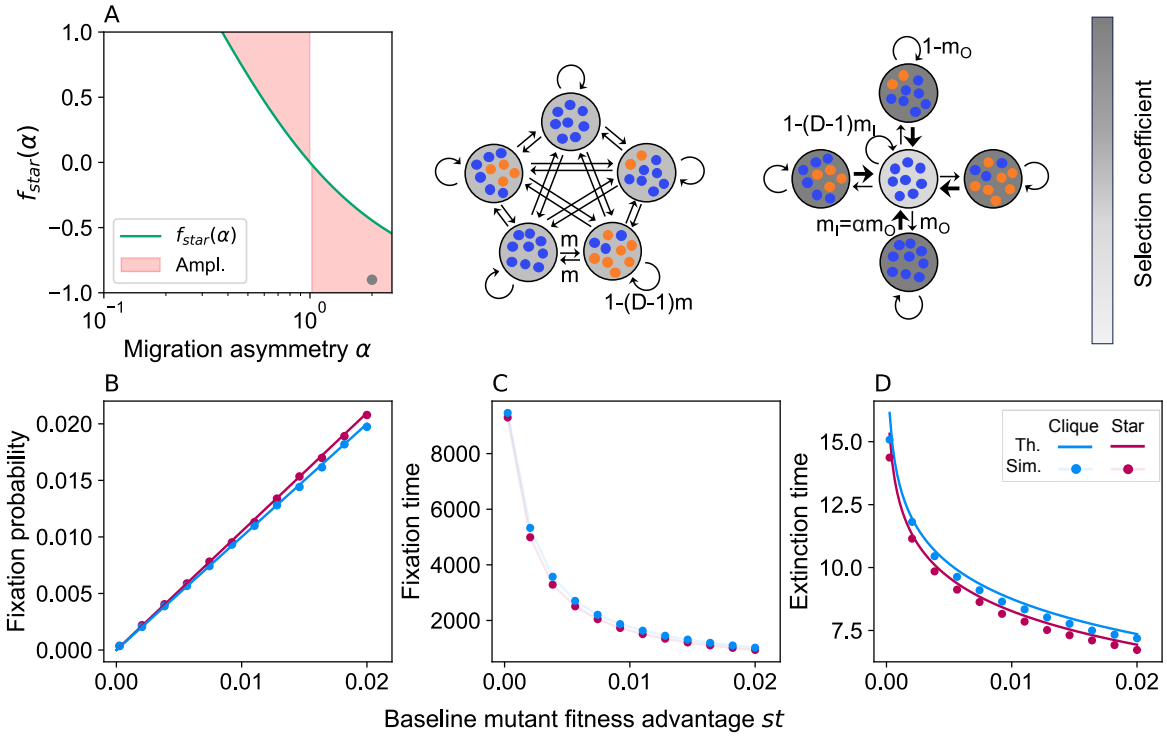

Figure S2: **Amplification of natural selection by the heterogeneous star with frequent migrations.** Panel A: $f_{\text{star}}(\alpha, D = 5)$ defined in Eq. S44 is plotted as a function of α. The pink region highlights the parameter range where Eq. S43 predicts that a heterogeneous star amplifies selection relative to a clique. The gray marker indicates the parameter set used in the other panels. Panel B: Fixation probability for a heterogeneous star and a clique with the same $\langle\delta\rangle$ as a function of the baseline mutant fitness advantage st. Panels C-D: Mutant fixation and extinction time, respectively, expressed in numbers of bottlenecks, as a function of the baseline mutant fitness st. Results from the branching process theory ("Th.") are shown in panels B (Eq. S21) and D (Eq. S37). Stochastic simulation results ("Sim.") are shown in panels B-D. Parameters: $D = 5$, $K = 1000$; for the star: $\alpha = 2$; $\delta_C = 0.05$ in the center; $\delta_L = 0.6125$ in all leaves, yielding $\langle\delta\rangle = 0.5$ and $\sigma_C = -0.9$; for the clique: $\delta = 0.5$ in all demes. Each marker comes from 5×10^5 stochastic simulation realizations.

3 Comparison of fixation probabilities in the line and clique

In this section, we focus on the line structure, and on its impact on mutant fixation probability. First, in Section 3.1, we compare a homogeneous line to a clique, to assess the baseline impact of the line spatial structure. Then, in Section 3.2 we compare a homogeneous line to a heterogeneous line, to assess the impact of environment heterogeneity in a line. Finally, in Section 3.3, we compare a heterogeneous line to a clique, to determine if a heterogeneous line can suppress or amplify selection.

As done above for the star, in all cases, when we compare a structure with heterogeneous environment to another one with homogeneous environment, we match their average mutant fitness advantage, i.e. in our notations, we match their $\langle\delta\rangle$. Besides, our comparisons again rely on the first-order fixation probabilities derived in Section 1.3 in the branching process approximation.

3.1 Homogeneous line versus clique

Let us consider a homogeneous line with relative mutant fitness advantage $s\Delta$ in all demes. Let us compare it to a heterogeneous clique with relative mutant fitness advantage $s\delta_i$ in deme i, satisfying $\langle\delta\rangle = \Delta$. We derived their fixation probabilities in Eqs. S32 and S11, respectively. Recall that the result for the clique was unaffected by environment heterogeneity – thus, our comparison will hold for homogeneous and heterogeneous cliques. A homogeneous line has a first-order mutant fixation

probability lower than a heterogeneous clique if and only if:

$$\frac{1}{D}\frac{(1+\alpha)(1-\alpha^D)}{(1-\alpha)(1+\alpha^D)} < 1\,. \tag{S45}$$

This condition is always satisfied, except if $\alpha = 1$, when the two fixation probabilities are equal. It is illustrated in Figure S3. Hence, the homogeneous line suppresses selection, as long as it features migration asymmetry. This is consistent with our general result on homogeneous spatially structured populations from Ref. [36].

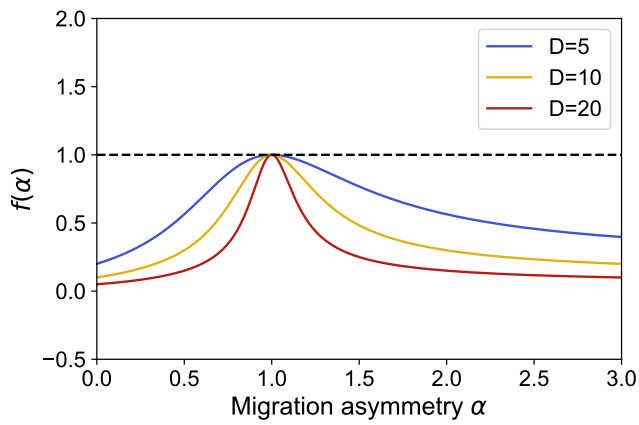

Figure S3: **Suppression of selection in the homogeneous line with migration asymmetry.** The function $f(\alpha) = (1+\alpha)(1-\alpha^D)/[D(1-\alpha)(1+\alpha^D)]$ involved in Eq. S45 is plotted versus the migration asymmetry α in the line for $D = 5, 10, 20$.

3.2 Homogeneous line versus heterogeneous line

Let us compare the fixation probabilities in a heterogeneous line and in a homogeneous line, given respectively in Eqs. S31 and S32 to first order in st. Our homogeneous line has relative mutant fitness advantage $s\Delta$ in all demes, while our heterogeneous line has relative mutant fitness advantage $s\delta_i$ in deme i, satisfying $\langle\delta\rangle = \Delta$. The first-order fixation probability is larger in the heterogeneous star than in the homogeneous star if and only if:

$$\frac{1}{1+\alpha^{-D}}\sum_{j=1}^{D}\delta_j\alpha^{-j} > \Delta\frac{(1-\alpha^D)}{(1-\alpha)(1+\alpha^D)}\,, \quad \text{i.e.}$$
$$\sum_{j=1}^{D}\frac{\delta_j}{\Delta}\alpha^{-j} > \frac{1-\alpha^{-D}}{\alpha-1}\,. \tag{S46}$$

Let us now introduce the relative mutant fitness excess σ_j in deme j such that for all j: $\delta_j = \langle\delta\rangle(1+\sigma_j) = \Delta(1+\sigma_j)$. Note that the σ_j satisfy $\sum_{j=1}^{D}\sigma_j = 0$. Eq. S46 then becomes:

$$\sum_{j=1}^{D}\alpha^{-j} + \sum_{j=1}^{D}\sigma_j\alpha^{-j} > \frac{1-\alpha^{-D}}{\alpha-1}\,, \quad \text{i.e.}$$
$$S(\alpha) \equiv \sum_{j=1}^{D}\sigma_j\alpha^{-j} > 0\,. \tag{S47}$$

Monotonic mutant fitness advantage variation along the line. Let us consider the case where the mutant fitness advantage varies monotonically along the line. Without loss of generality, let us assume that it monotonically decreases left to right, from deme 1 to deme D. Since the σ_j satisfy $\sum_{j=1}^{D}\sigma_j = 0$, there exists $k \in [1, D]$ such that

$$\sigma_1 > \ldots \sigma_k \geq 0 > \sigma_{k+1} > \cdots > \sigma_D. \tag{S48}$$

If $\alpha > 1$, then for all $j > k \geq 1$, we have $\alpha^{-j} < \alpha^{-k}$, while for all j satisfying $1 \leq j \leq k$, we have $\alpha^{-j} \geq \alpha^{-k}$. Combining this with Eq. S48 yields:

$$S(\alpha) = \sum_{j=1}^{k} \sigma_j \alpha^{-j} + \sum_{j=k+1}^{D} \sigma_j \alpha^{-j} > \alpha^{-k} \sum_{j=1}^{k} \sigma_j + \alpha^{-k} \sum_{j=k+1}^{D} \sigma_j = \alpha^{-k} \sum_{j=1}^{D} \sigma_j = 0\,, \tag{S49}$$

which gives $S(\alpha) > 0$. Hence, Eq. S47 holds for all $\alpha > 1$ in our line with monotonically decreasing fitness advantage from left to right.

If $\alpha < 1$, a similar reasoning leads to $S(\alpha) < 0$. Hence, Eq. S47 never holds for $\alpha < 1$ in our line with monotonically decreasing fitness advantage from left to right.

Thus, the heterogeneous line with monotonically decreasing mutant fitness advantage from left to right features a larger mutant fixation probability than the homogeneous line for $\alpha > 1$, but a smaller one for $\alpha < 1$, and the same one for $\alpha = 1$. When $\alpha > 1$, most migrations are from left to right, i.e. demes where mutants are most advantaged are upstream of the overall migration flow. This favors mutant spread and fixation.

3.3 Heterogeneous line versus clique

Let us now compare a heterogeneous line to a clique. Recall that only average fitness matters to first order for the mutant fixation probability in the clique. Hence, we consider a clique which can be homogeneous or heterogeneous, but which has the same average fitness as our heterogeneous line. The fixation probabilities in a heterogeneous line and in a clique are given respectively in Eqs. S31 and S11 to first order in st. The first-order fixation probability is larger in the heterogeneous line than in a clique if and only if:

$$\frac{1}{D} \frac{1+\alpha}{1+\alpha^{-D}} \sum_{j=1}^{D} \delta_j \alpha^{-j} > \langle \delta \rangle\,. \tag{S50}$$

Let us now introduce, as above, σ_j such that $\delta_j = \langle \delta \rangle (1 + \sigma_j)$. Recall that $\sum_{j=1}^{D} \sigma_j = 0$. Eq. S50 becomes:

$$\begin{aligned} \frac{1}{D} \frac{1+\alpha}{1+\alpha^{-D}} \left(\sum_{j=1}^{D} \alpha^{-j} + S(\alpha) \right) > 1\,, \text{ i.e.} \\ S(\alpha) > D \frac{1+\alpha^{-D}}{1+\alpha} - \frac{1-\alpha^{-D}}{\alpha - 1}\,, \text{ i.e.} \\ S(\alpha) > \frac{(D-1)\alpha - (D+1) + (D+1)\alpha^{1-D} - (D-1)\alpha^{-D}}{\alpha^2 - 1} \equiv g(\alpha)\,. \end{aligned} \tag{S51}$$

If a heterogeneous line satisfies Eq. S51, it features a higher mutant fixation probability than a homogeneous clique, to first order in st. This means that environment heterogeneity then allows the line to overcome the suppression of selection that the homogeneous line features when compared to the clique.

No amplification is possible if the mutant fitness advantage monotonically decreases left to right and $\alpha < 1$. We showed in the previous section that if the mutant fitness advantage monotonically decreases left to right and $\alpha < 1$, the mutant fixation probability in the heterogeneous line is smaller than in the homogeneous line. Because the homogeneous line itself suppresses selection, we conclude that no amplification is possible if the mutant fitness advantage monotonically decreases left to right and $\alpha < 1$.

Another way to see this, which connects more directly to Figure 2A, is that if $\alpha < 1$, $S(\alpha) < 0$ (see previous section), while we then have $g(\alpha) > 0$ (see below), which entails $S(\alpha) < g(\alpha)$. To show that $g(\alpha) > 0$ if $\alpha < 1$, we notice that the denominator of $g(\alpha)$ is then negative, and thus we aim to show that the numerator is negative too. Denoting the numerator as

$$g_N(\alpha) = (D-1)\alpha - (D+1) + (D+1)\alpha^{1-D} - (D-1)\alpha^{-D}, \tag{S52}$$

its derivative with respect to α reads:

$$g'_N(\alpha) = (D-1)\left[1 + \alpha^{-D}(-D-1+D\alpha^{-1})\right], \tag{S53}$$

and its second derivative with respect to α is:

$$g''_N(\alpha) = D(D-1)(D+1)\,(\alpha-1)\,\alpha^{-D-2}. \tag{S54}$$

When $\alpha < 1$, $g''_N(\alpha) < 0$. Thus, g'_N is a decreasing function on $(0,1)$. As $\lim_{\alpha\to 1^-} g'_N(\alpha) = 0^+$, we have $g'_N(\alpha) > 0$ on $(0,1)$, which entails that g_N is an increasing function on $(0,1)$. As $g_N(1) = 0$, we conclude that $g_N(\alpha) < 0$ on $(0,1)$. Hence, $g(\alpha) > 0$ if $\alpha < 1$ as announced, and there cannot be amplification of selection for $\alpha < 1$.

Step environmental profile with one special upstream deme. Let us consider the case where the mutant is advantaged only in the leftmost deme ($\delta_1 = 1$, $\delta_i = 0$ for $i > 1$). We plot $S(\alpha)$ together with $g(\alpha)$ in such a case in Figure 2A in the main text. This Figure suggests that Eq. S51 is valid for all $\alpha > 1$, and that the difference between $S(\alpha)$ and $g(\alpha)$ becomes smaller and smaller when α increases. To better understand this, let us investigate asymptotics for $\alpha \to \infty$. In the simple case considered here, we have:

$$S(\alpha) = (D-1)\alpha^{-1} - \sum_{i=2}^{D} \alpha^{-i} \sim (D-1)\alpha^{-1} - \alpha^{-2}, \tag{S55}$$

where we have retained the two leading terms in powers of α when $\alpha \to \infty$. Doing the same for $g(\alpha)$, Eq. S51 gives:

$$g(\alpha) \sim (D-1)\alpha^{-1} - (D+1)\alpha^{-2}. \tag{S56}$$

Thus, in this case, $S(\alpha) > g(\alpha)$ in terms of asymptotic behavior for $\alpha \to \infty$. Note however that for other choices of σ_i that monotonically decrease from left to right, the curves representing $S(\alpha)$ and $g(\alpha)$ often cross again for some $\alpha > 1$, meaning that amplification then exists in a finite range of α.

Examples of other environmental profiles. Let us first continue our analysis of the simple step environmental gradient. In Figure 2B in the main text, we considered the case where mutants had an advantage only in the deme upstream of the main migration flow (special deme on the left and $\alpha > 1$). Figure 2A also shows that Eq. S51 does not hold with the same environment profile when $\alpha < 1$. In Figure S4A, we further show the case where the mutant is advantaged in the rightmost deme with $\alpha > 1$ (by symmetry, this is equivalent to having a special leftmost deme with asymmetry $1/\alpha$, giving $\alpha < 1$), and as predicted above, we obtain suppression of selection. This suppression is even stronger than in a homogeneous line. These results show that in the line, when the environmental profile has the same orientation as the overall migration flow, selection can be amplified. Meanwhile, when the environmental profile is homogeneous or opposes the overall migration flow, selection is suppressed.

Figure S4B-C (see also Figure 2C-D) also shows that while the line with similarly-oriented migration flow and environmental profile can accelerate fixation or extinction compared to the homogeneous clique and to the homogeneous line with the same migration asymmetry. Conversely, Figure S4B-C shows that the line with opposite migration flow and environmental profile tends to feature slower fixation or extinction than the homogeneous clique and to the homogeneous line with the same migration asymmetry.

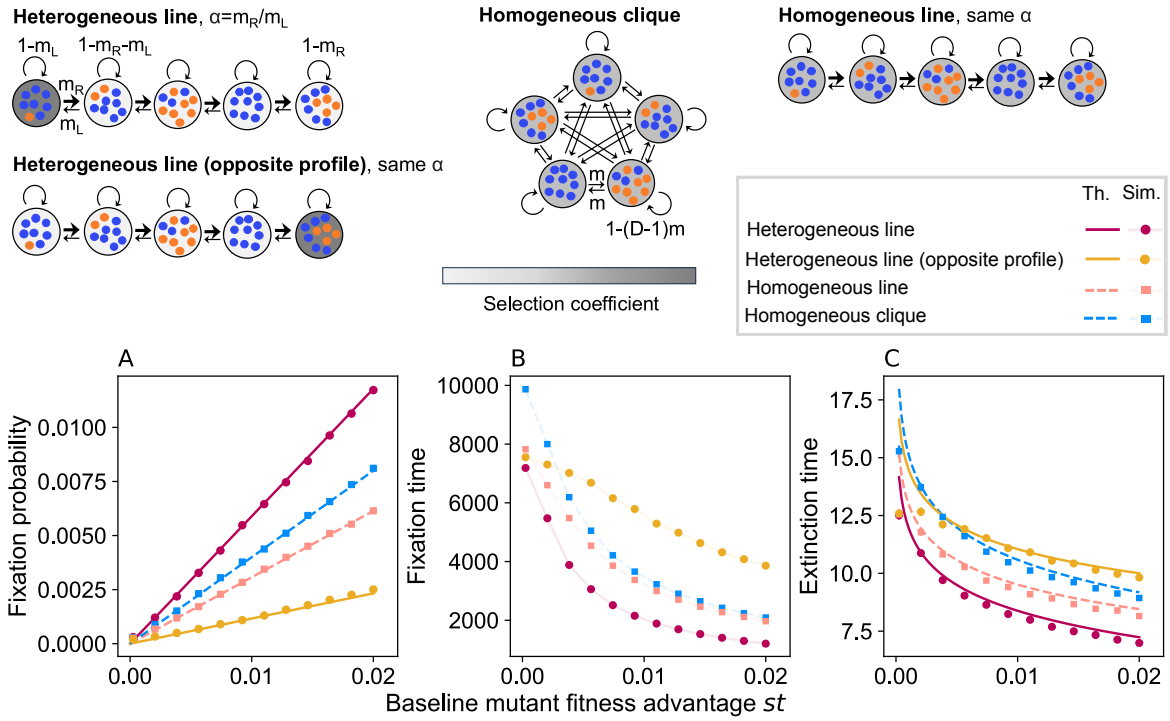

Figure S4: **Impact of the direction of the environmental profile in the line.** Top: Schematic of all spatial structures considered in this Figure: heterogeneous lines with overall migration flow and environmental profile that are either similarly oriented or opposite (left); homogeneous clique (middle), and homogeneous line with the same migration probabilities (right). All spatial structures have the same average mutant fitness advantage (same $\langle\delta\rangle$). Panel A: Mutant fixation probability in the different spatial structures considered, versus baseline mutant fitness advantage st. Panel B: Mutant fixation time, in number of bottlenecks, in the different spatial structures considered, versus baseline mutant fitness advantage st. Panel C: Same as in B, but for mutant extinction time. Results from the branching process theory ("Th.") are shown in panels A (Eq. S31) and C (Eq. S37). Stochastic simulation results ("Sim.") are shown in panels A-C. Parameter values for all structures: $D = 5$, $K = 1000$; for all lines: $\alpha = 1.5$, $m_L = 0.3$; for the clique: $m = 0.15$; for heterogeneous lines: $\delta = 1$ in the special deme, $\delta = 0$ in other ones. Each marker comes from 5×10^5 stochastic simulation realizations.

In Figure S5, we further investigate the effect of different environmental profiles in a line with $\alpha > 1$. We consider a linear and a Gaussian profile, both with the same orientation as the overall migration flow (i.e., the demes where the mutants are most advantaged are upstream). These profiles are intermediate cases between the step environmental profile and the homogeneous environment. We chose them so that the average mutant fitness advantage is the line is the same in all cases (same $\langle\delta\rangle$), see Figure S5A for a depiction of the spatial profiles considered. We observe in Figure S5B that these various cases yield some amplification of selection, and that larger environmental contrast between demes is associated to more amplification of selection. Figure S5C-D further suggest that larger environmental contrast between demes leads to more acceleration of mutant fixation and extinction.

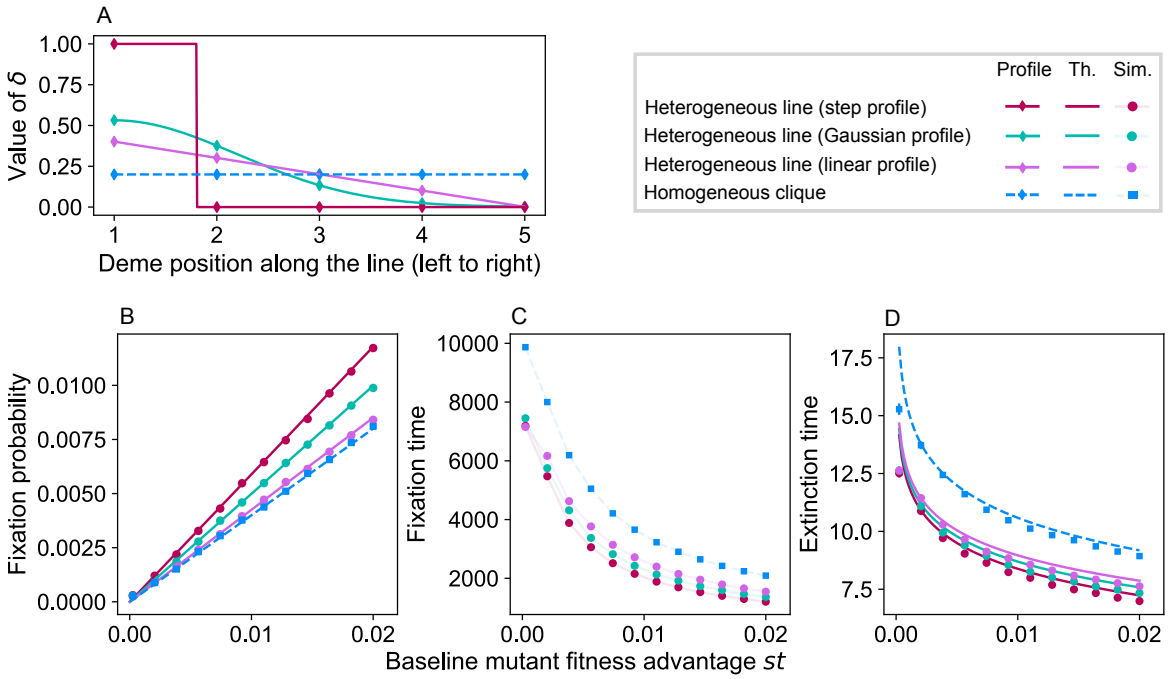

Figure S5: **Impact of different environmental profiles in the line.** Panel A: Different environmental profiles considered: step, Gaussian, linear, and homogeneous. For each of them, the mutant fitness advantage prefactor δ is shown versus position along the line. In what follows, we consider lines with $\alpha = 1.5$ and values δ_i taken in each of these profiles at regular intervals for $i \in \{1, \ldots, 5\}$ (markers) for each of the 5 demes of the graph. The profiles are chosen so that all lines have the same $\langle \delta \rangle$. Panel B: Mutant fixation probability in the different structures considered, versus baseline mutant fitness advantage st. Panel C: Mutant fixation time, in number of bottlenecks, in the different structures considered, versus baseline mutant fitness advantage st. Panel D: Same as in C, but for mutant extinction time. Results from the branching process theory ("Th.") are shown in panels B (Eq. S11) and D (Eq. S37). Stochastic simulation results ("Sim.") are shown in panels B-D. Parameter values for all structures: $D = 5$, $K = 1000$; for all lines: $\alpha = 1.5$, $m_L = 0.3$; for the clique: $m = 0.15$. Each marker comes from 5×10^5 stochastic simulation realizations.

4 Spatial structures with one strong-outflow deme

Our results for the heterogeneous star and of the heterogeneous line show that environment heterogeneity can allow spatially structured populations with frequent asymmetric migrations to amplify natural selection. They also suggest that this happens when the overall migration flow goes from a region where mutants are most beneficial to a region where they are less beneficial. To further explore this, we now consider a more general spatial structure, where all pairs of demes are connected by migrations, but where one deme has a strong outflow, i.e. it sends out more individuals than others. We assess the impact of having a different environment in that special deme.

First, in Section 4.1, we consider the simplest version of this structure with a special deme where the environment and the outflow both differ from those of other demes, assuming a highly symmetric migration matrix. We determine mutant fixation probability to first order in st, and obtain a condition on the asymmetry in migrations and the environment heterogeneity to obtain amplification of selection. Next, in Section 4.2, we consider more general and less symmetric migration matrices, with coefficients drawn in Dirichlet distributions (see Ref. [36] for the homogeneous environment case), with one strong-outflow deme where the environment differs from that of other demes.

4.1 Highly symmetric structure with one special deme

4.1.1 Fixation probability

Let us consider a simple structure where the first deme has a different migration outflow, i.e. it sends out more (or fewer) individuals than others. Specifically, we assume that all outgoing migrations from deme 1 happen with probability m_1, while all other migrations across the structure occur with probability m_2. Figure 3 illustrates the case $m_2 < m_1$. In addition to having a different outflow, the first deme is such that the relative mutant fitness advantage is $\delta_1 s$, while in all other demes it is $\delta_2 s$. Under these assumptions, only the first deme is different from others, and all other ones are equivalent to each other: this structure is highly symmetric.

Since $\sum_{k=1}^{D} m_{kj} = 1$ for all j, we have the following constraint on migration probabilities:

$$m_1 + (D-1)m_2 = 1\,. \tag{S57}$$

The first line of Eq. S8, written for the first node and for another one, yields:

$$a_1 = m_1 a_1 + (D-1)m_1 a_2\,, \tag{S58}$$
$$a_2 = m_2 a_1 + (D-1)m_2 a_2\,, \tag{S59}$$

Note that we have used the symmetry of the structure to write that $a_i = a_2$ for all $i \geq 2$. Using Eqs. S57, both Eq. S58 and Eq. S59 reduce to:

$$a_2 = \alpha\, a_1\,, \quad \text{with} \quad \alpha = \frac{m_2}{m_1}\,. \tag{S60}$$

The second line of Eq. S8, written for the first node and for another one, yields:

$$b_1 = m_1 b_1 + (D-1)m_1 b_2 + a_1^2 - 2a_1\delta_1\,, \tag{S61}$$
$$b_2 = m_2 b_1 + (D-1)m_2 b_2 + a_2^2 - 2a_2\delta_2\,, \tag{S62}$$

Summing Eq. S61 with $(D-1)$ times Eq. S62, and using Eq. S57, we obtain:

$$a_1^2 + (D-1)a_2^2 - 2a_1\delta_1 + 2(D-1)a_2\delta_2 = 0\,, \tag{S63}$$

which yields

$$a_1 = 2\frac{\delta_1 + (D-1)\delta_2\alpha}{1+(D-1)\alpha^2}\,. \tag{S64}$$

Eqs. S60 and S64 then provide the fixation probability ρ, to first order in st, of a mutant appearing at a bottleneck in a deme chosen uniformly at random in the structure:

$$\rho = st\,\frac{a_1 + (D-1)a_2}{D} = 2st\,\frac{[1+\alpha(D-1)][\delta_1 + (D-1)\delta_2\alpha]}{D\,[1+(D-1)\alpha^2]}. \tag{S65}$$

Note that, for $\alpha = 1$, this reduces to $\rho = 2\langle\delta\rangle st$, as in all other structures considered so far.

4.1.2 Condition for amplification of selection

The fixation probabilities in our structure and in a clique are given respectively in Eqs. S65 and S11 to first order in st. The first-order fixation probability is larger in our structure than in a clique with the same average relative mutant fitness advantage if and only if

$$\begin{gathered}\frac{[1+\alpha(D-1)][\delta_1 + (D-1)\delta_2\alpha]}{1+(D-1)\alpha^2} > \delta_1 + (D-1)\delta_2\,, \quad \text{i.e.} \\ \delta_1\alpha(1-\alpha) > \delta_2(1-\alpha)\,.\end{gathered} \tag{S66}$$

Let us introduce

$$\beta = \frac{\delta_2}{\delta_1}\,, \tag{S67}$$

which characterizes environment heterogeneity in this structure. If $\alpha < 1$, i.e. if the special deme has a stronger outflow than others, Eq. S66 reduces to:

$$\beta < \alpha \,. \tag{S68}$$

Since here $\alpha < 1$, we find that the mutant should have a sufficiently stronger advantage in the special deme than in the other demes for the structure to amplify selection (δ_1 should be sufficiently larger than δ_2).

If $\alpha > 1$, i.e. if the special deme has a weaker outflow than others, Eq. S66 reduces to:

$$\beta > \alpha \,. \tag{S69}$$

Since here $\alpha > 1$, we find that the mutant should have a sufficiently stronger advantage in the other demes than in the special deme for the structure to amplify selection (δ_2 should be sufficiently larger than δ_1).

These results generalize our previous observations in the star and line that environment heterogeneity can allow spatially structured populations with frequent asymmetric migrations to amplify natural selection when the overall migration flow goes from a region where mutants are most beneficial to a region where they are less beneficial.

4.2 More general structures with one strong-outflow deme

Let us now consider more general structures with one special deme. Specifically, let us consider Dirichlet cliques with one special deme. Dirichlet cliques are spatial structures with tunable migration asymmetries on each edge of a clique, which were introduced, and studied with a homogeneous environment, in Ref. [36]. They have migration probabilities $(m_{1j}, m_{2j}, \ldots, m_{Dj})$ sampled from a Dirichlet distribution with parameters $\eta_1, \ldots, \eta_D$ for each j. The Dirichlet distribution has probability distribution function:

$$\Phi_{(\eta_1,\ldots,\eta_D)}(x_1, \ldots, x_D) = \frac{1}{B(\eta_1, \ldots, \eta_D)} \prod_{i=1}^{D} x_i^{\eta_i - 1}, \tag{S70}$$

with $B(\eta_1, \ldots, \eta_D) = \prod_{i=1}^{D} \Gamma(\eta_k)/\Gamma(\sum_{i=1}^{D} \eta_k)$ and where Γ denotes the gamma function. Random variables $(X_1, \ldots, X_D)$ sampled from this distribution have respective expectation values $\mathbb{E}(X_i) = \eta_i / \sum_j \eta_j$. Considering $(\eta_1, \eta_2, \ldots, \eta_D) = (\eta, 1, \ldots, 1)$ allows us to make deme 1 special in terms of migration outflow. In fact, the expectation values are such that $\mathbb{E}(m_{i1})/\mathbb{E}(m_{1i}) = 1/\eta$ for all i, which entails that, ignoring the variability of these migration probabilities, $1/\eta$ maps to $\alpha = m_2/m_1$ in the highly-symmetric structure considered in the previous sections.

Construction of Figure 3. In Figure 3, we consider values of η both greater than and less than 1, in order to produce cases with either strong outflow or weak outflow from deme 1. For each value of η, we generate several (in practice, 5×10^3) Dirichlet cliques, and we associate all of them to $\alpha = 1/\eta$. Note that despite this mapping to the highly-symmetric structure considered above, the migration probabilities are variable across various edges in a given Dirichlet clique, and across different Dirichlet cliques. As an illustration, Figure S6 shows example histograms for two different values of η of m_{1i} for all i, with expectation value m_1, and of m_{ij} for all $i \neq 1$ and all j, with expectation value m_2.

In Figure 3, we also vary environment heterogeneity, via the ratio $\beta = \delta_1/\delta_2$, while keeping fixed the average mutant fitness advantage $\langle \delta \rangle$ in each of the structures we consider. This leads to:

$$\delta_2 = \frac{D\langle \delta \rangle}{\beta + D - 1}\,, \qquad \text{and} \qquad \delta_1 = \beta \delta_2 \,. \tag{S71}$$

We finally use the general method presented in Section 1.4 to obtain mutant fixation probability to first order in st for the Dirichlet cliques associated to a given α. Comparing to the first-order mutant fixation probability for a standard clique then gives the regions of amplification of selection shown in Figure 3.

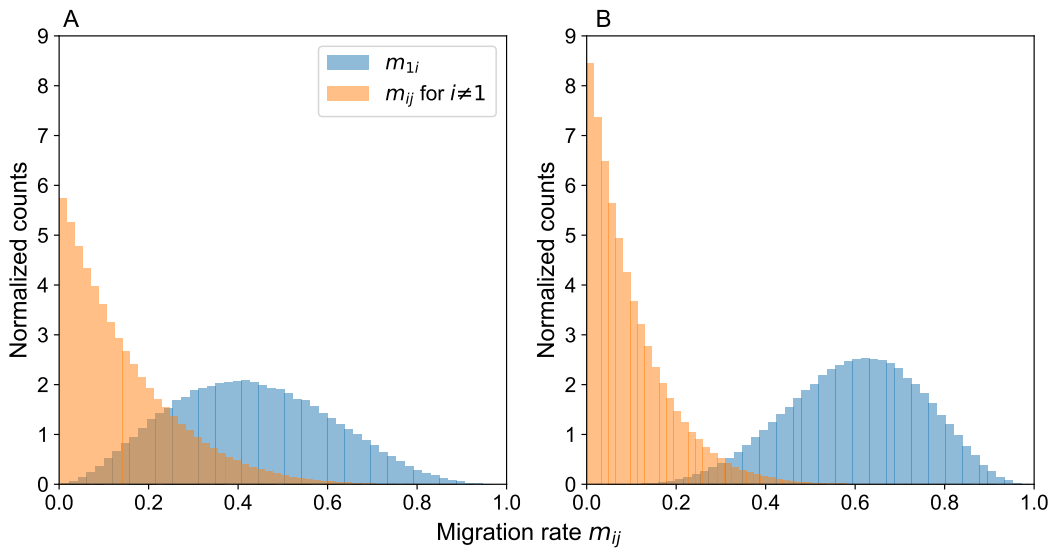

Figure S6: **Distribution of migration probabilities in Dirichlet cliques with one strong-outflow deme.** Histograms of m_{1i} for all i, whose expectation value is m_1, are shown in blue, and histograms of m_{ij} for all $i \neq 1$ and all j, whose expectation value is m_2, are shown in orange. Parameter values: Panel A: $\eta = 3$, yielding $m_1 = 0.43$, $m_2 = 0.14$, $\alpha = 0.33$; Panel B: $\eta = 6$, yielding $m_1 = 0.60$, $m_2 = 0.10$ and $\alpha = 0.17$. For each panel, 5×10^4 Dirichlet clique migration matrices were generated.

5 Circulation theorem extension and limitations

Circulations are graphs such that for all demes i, $\sum_j m_{ji} = \sum_j m_{ij}$. In other words, the total incoming migration flow to deme i is equal to the total outgoing migration flow from deme i. The circulation theorem was derived for graphs with a homogeneous environment, first in the framework of evolutionary graph theory with one individual per node of the graph [19], and then for graphs with a deme on each node in the rare migration regime [35] and with frequent migrations in the branching process approximation [36]. It states that all circulation graphs have the same mutant fixation probability, which does not depend on the deme where the mutant appears. In addition, this fixation probability is the same as in a well-mixed population of the same size, either exactly under the assumptions used [19, 56] or up to a finite-size effect correction [35]. Thus, circulations are a class of graphs where spatial structure has (essentially) no effect on mutant fixation probability for homogeneous environments. In this Section, we investigate whether the circulation theorem still holds with environment heterogeneity.

5.1 First order in the baseline mutant fitness advantage st

As previously shown in SI Section 1.3.2, for circulation graphs, combining the Perron–Frobenius theorem to the first line of Eq. S8 implies that all the first-order coefficients a_i coefficients are equal for all demes, say to a. Moreover, the second line of Eq. S8 then provides $a = 2\langle\delta\rangle$ (see Eq. S34 in Section 1.4, written in the specific case where all a_i are equal). Hence, to first order in st, the probability of fixation of a mutant starting from any deme in a circulation is:

$$\rho = 2\langle\delta\rangle st\,, \tag{S72}$$

which is the same as in a well-mixed population. Thus, to first order in the branching process regime, the circulation theorem extends to structures with heterogeneous fitness differences across demes.

We show in Figure S7A our analytical prediction for the first-order fixation probabilities, given by Eq. S72, together with simulation results for four different circulations with heterogeneous environments: a clique, a cycle, a star with migration asymmetry $\alpha = 1$, and a line with migration asymmetry $\alpha = 1$. We also report results for the well-mixed population with mutant fitness advantage $\langle\delta\rangle s$. Our simulation results agree with our analytical prediction. We also show the mutant extinction time in

Figure S7B, both from simulations and from a numerical calculation (see SI Section 1.5), for the four circulation graphs and the corresponding well-mixed population. We again observe good agreement between results from simulations and calculations.

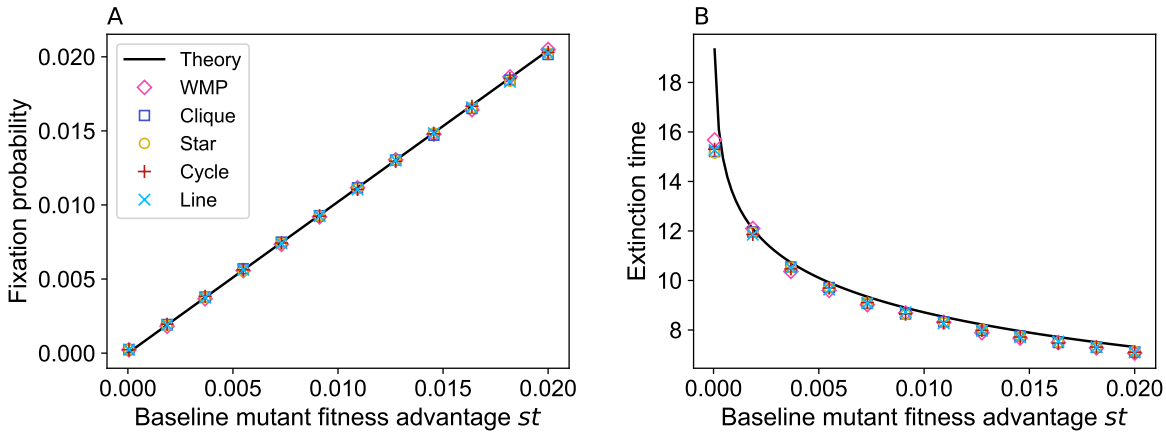

Figure S7: **Fixation probability and extinction time for structured populations on circulation graphs with environmental heterogeneity across demes.** Panel A: Fixation probability for four different graph structures: cycle, clique, line, and star, under the condition $\sum_i m_{ij} = \sum_i m_{ji}$ for all nodes j, is shown as a function of the baseline mutant fitness advantage st. Panel B: Mutant extinction time, expressed in number of bottlenecks, as a function of the baseline mutant fitness advantage st, for the same structures. Solid lines represents results from the branching process theory (Eq. S11 in panel A, Eq. S37 in panel B), while markers represent results from stochastic simulations. The well-mixed population simulation result for the same $\langle\delta\rangle$ is included in both panels for reference. Parameter values: $D = 5$; $K = 1000$; δ_i values: $0.49, 0.32, 0.70, 0.41, 0.62$ (independently sampled from a uniform distribution on the interval $[0, 1]$), resulting in $\langle\delta\rangle = 0.51$; $m = m_I = m_O = 0.15$; $m_L = m_R = m_A = m_C = 0.3$; each marker comes from 5×10^5 simulation realizations.

5.2 Second order in the baseline mutant fitness advantage st

To assess whether the circulation theorem extends beyond first order, let us consider second-order terms. We start from the second line of Eq. S8, written in matrix form as:

$$\boldsymbol{b} = M\boldsymbol{b} + a^2\mathbf{1} - 2a\boldsymbol{\delta}\,. \tag{S73}$$

Here, we introduced the vector of second-order coefficients $\boldsymbol{b} = (b_1, \ldots, b_D)$, as well as the vectors $\boldsymbol{\delta} = (\delta_1, \ldots, \delta_D)$, and $\mathbf{1} = (1, \ldots, 1)$. Meanwhile, M is the migration matrix with coefficients m_{ij}, and $a = 2\langle\delta\rangle$ is the first-order coefficient (see Section 5.1). Recall that the first line of Eq. S8 implies that $\mathbf{1}$ is an eigenvector of M with eigenvalue 1.

To determine $\boldsymbol{b}$, we generalize the approach developed for homogeneous environments in Ref. [36], and use a Jordan decomposition of the migration matrix M. It allows us to complete $\mathbf{1}$ into a complex basis such that the complementary space $\mathcal{E}_\perp$ of the space $\mathcal{E}$ generated by $\mathbf{1}$ is stable under the action of M. We decompose $\boldsymbol{b}$ as follows: $\boldsymbol{b} = \boldsymbol{b}_\perp + \boldsymbol{b}_\parallel$, with $\boldsymbol{b}_\parallel = b_\parallel\mathbf{1} \in \mathcal{E}$ and $\boldsymbol{b}_\perp \in \mathcal{E}_\perp$. Similarly, we write $\boldsymbol{\delta} = \boldsymbol{\delta}_\perp + \boldsymbol{\delta}_\parallel$, with $\boldsymbol{\delta}_\parallel = \delta_\parallel\mathbf{1}$. We can then rewrite Eq. S73 as:

$$\boldsymbol{b}_\parallel + \boldsymbol{b}_\perp = M\boldsymbol{b}_\parallel + M\boldsymbol{b}_\perp + a^2\mathbf{1} - 2a\boldsymbol{\delta}_\parallel - 2a\boldsymbol{\delta}_\perp. \tag{S74}$$

Thus, in $\mathcal{E}$, since $M\boldsymbol{b}_\parallel = \boldsymbol{b}_\parallel$:

$$\begin{aligned} &\boldsymbol{b}_\parallel = \boldsymbol{b}_\parallel + a^2\mathbf{1} - 2a\boldsymbol{\delta}_\parallel\,, \quad \text{i.e.} \\ &a^2 = 2a\delta_\parallel, \end{aligned} \tag{S75}$$

and in $\mathcal{E}_\perp$:

$$\boldsymbol{b}_\perp = M\boldsymbol{b}_\perp - 2a\boldsymbol{\delta}_\perp. \tag{S76}$$

Since $a = 2\langle\delta\rangle$ (see Section 5.1), Eq. S75 ensures that $\delta_\parallel = \langle\delta\rangle$. Thus, we have:

$$\boldsymbol{\delta}_\perp = \boldsymbol{\delta} - \boldsymbol{\delta}_\parallel = (\delta_1 - \langle\delta\rangle, \delta_2 - \langle\delta\rangle, \ldots, \delta_D - \langle\delta\rangle)\,. \tag{S77}$$

As shown in Section 1.3.2, the largest eigenvalue of M is 1 and is associated to the eigenspace $\mathcal{E}_\parallel$, and all other eigenvalues have a strictly smaller modulus. Thus, $(\mathbb{I} - M)$ restricted to $\mathcal{E}_\perp$, where $\mathbb{I}$ denotes the identity matrix, has no zero eigenvalue, and is invertible. Hence, Eq. S76 yields:

$$\boldsymbol{b}_\perp = -4\langle\delta\rangle(\mathbb{I} - M)^{-1}\boldsymbol{\delta}_\perp\,, \tag{S78}$$

with $\boldsymbol{\delta}_\perp$ given in Eq. S77.

Next, to find $b_\parallel$, we use the third line of Eq. S8. Using $\sum_k m_{kj} = 1$, and $a_j = a$ for all j, the third line of Eq. S8 becomes, for all $j \in [1, D]$,

$$\sum_{k=1}^{D} m_{kj}c_j = \sum_{k=1}^{D} m_{jk}c_k - 2a^3 + 3ab_j - 3\delta_j b_j + 3\delta_j a^2 - 3\delta_j^2 a\,. \tag{S79}$$

Summing this equation over all $j \in [1, D]$ yields:

$$\sum_{j=1}^{D}\sum_{k=1}^{D} m_{kj}c_j = \sum_{j=1}^{D}\sum_{k=1}^{D} m_{jk}c_k - 2Da^3 + 3a\sum_{j=1}^{D} b_j - 3\sum_{j=1}^{D}\delta_j b_j + 3a^2\sum_{j=1}^{D}\delta_j - 3a\sum_{j=1}^{D}\delta_j^2\,, \tag{S80}$$

which reduces to

$$3\sum_{j=1}^{D} b_j(a - \delta_j) = 2Da^3 - 3a^2 D\langle\delta\rangle + 3a\sum_{j=1}^{D}\delta_j^2\,. \tag{S81}$$

Writing $b_j = b_\parallel + b'_j$ for all j, where b'_j is the j-th component of $\boldsymbol{b}_\perp$, and recalling that for circulations $a = 2\langle\delta\rangle$ (see Section 5.1), we obtain:

$$b_\parallel = \frac{4}{3}\langle\delta\rangle^2 + 2\langle\delta^2\rangle - \frac{1}{D}\sum_j b'_j\left(2 - \frac{\delta_j}{\langle\delta\rangle}\right) = \frac{4}{3}\langle\delta\rangle^2 + 2\langle\delta^2\rangle - 2\langle b'\rangle + \frac{\langle b'\delta\rangle}{\langle\delta\rangle}\,, \tag{S82}$$

where b'_j can be obtained from Eq. S78.

5.2.1 Clique with heterogeneous environment

Recall that in the clique (see Figure S1B), $m_{ij} = m$ for all $i \neq j$. For a heterogeneous clique, $\boldsymbol{b}_\perp$ with components

$$b'_i = 4\langle\delta\rangle\frac{\langle\delta\rangle - \delta_i}{Dm} \tag{S83}$$

satisfies Eq. S78.

Let us now calculate $b_\parallel$ for a heterogeneous clique, using Eq. S82. Eq. S83 entails that $\langle b'\rangle = 0$, and allows us to write:

$$\langle b'\delta\rangle = \frac{1}{D}\sum_j b'_j\delta_j = \frac{4\langle\delta\rangle}{D^2 m}\sum_j\left(\langle\delta\rangle - \delta_j\right)\delta_j = \frac{4\langle\delta\rangle}{Dm}\left(\langle\delta\rangle^2 - \langle\delta^2\rangle\right)\,, \tag{S84}$$

so Eq. S82 yields:

$$b_\parallel = \frac{4}{3}\langle\delta\rangle^2 + 2\langle\delta^2\rangle + \frac{4}{Dm}\left(\langle\delta\rangle^2 - \langle\delta^2\rangle\right)\,. \tag{S85}$$

Eq. S83 and Eq. S85 show that, to second order in st, the mutant fixation probability in a heterogeneous clique generically depends on the deme i where the mutant starts, and on migration intensity m. Therefore, the circulation theorem does not hold to second order in st for heterogeneous structures.

In the particular case of the homogeneous clique with $\delta_i = \Delta$ for all i, Eq. S83 reduces to $b'_i = 0$ for all i, and Eq. S85 reduces to $b_\parallel = 10\Delta^2/3$, yielding a mutant fixation probability $\rho_i = 2\Delta st - 5(\Delta st)^2/3 + o((st)^2)$ for all i. This is in agreement with the result of Ref. [36] for homogeneous

circulations (see Eq. S16 in the Supplementary Material of that paper, written for a mutant with effective fitness advantage Δst). Recall that the circulation theorem holds for homogeneous environments in the branching process approximation [36].

Note that the mutant fixation probability averaged over starting demes reads:

$$\rho = 2\langle\delta\rangle st - \frac{b_\parallel + \langle b'\rangle}{2}(st)^2 + o((st)^2) = 2\langle\delta\rangle st - \frac{b_\parallel}{2}(st)^2 + o((st)^2)\,, \tag{S86}$$

where $b_\parallel$ is given by Eq. S85. Thus, to second order, this fixation probability does not involve $\boldsymbol{b}_\perp$, and only depends on environment heterogeneity through $\langle\delta\rangle$ and $\langle\delta^2\rangle$.

Let us compare the mutant fixation probability, averaged over starting demes, in a heterogeneous clique and in a homogeneous clique with the same $\langle\delta\rangle$. Calling ρ and ρ^{homo} these two fixation probabilities, Eq. S86 yields:

$$\begin{aligned}\rho - \rho^{\text{homo}} &= \frac{(st)^2}{2}\left(b_\parallel^{\text{homo}} - b_\parallel\right) = \frac{(st)^2}{2}\left[\frac{10}{3}\langle\delta\rangle^2 - \frac{4}{3}\langle\delta\rangle^2 - 2\langle\delta^2\rangle - \frac{4}{Dm}\left(\langle\delta\rangle^2 - \langle\delta^2\rangle\right)\right] \\ &= \frac{2-Dm}{Dm}(st)^2\left(\langle\delta^2\rangle - \langle\delta\rangle^2\right)\,.\end{aligned} \tag{S87}$$

In the clique, $\sum_i m_{ij} = 1$ entails that $m_{ii} = 1-(D-1)m$, and as all migration probabilities are between 0 and 1, we have $(D-1)m \leq 1$ and, and thus $Dm \leq 1+m \leq 2$. This entails that $\rho \geq \rho^{\text{homo}}$.

Thus, in the clique, environment heterogeneity generically amplifies natural selection to second order in st. Furthermore, the larger the variance of the δ_i is, and the smaller m is, the stronger this effect is.

5.2.2 A particular cycle with heterogeneous environment

Recall that in the cycle, migration probabilities are nonzero only to nearest neighbor demes (and to the original deme itself). Migrations to nearest neighbor demes can differ in the clockwise and anticlockwise directions, and are denoted by m_C and m_A, respectively (see Figure S1B). Here, we present explicit calculations in the specific case of a heterogeneous cycle with $D = 5$ and $m_A = m_C = m$. Solving Eq. S78 in this case leads to:

$$\boldsymbol{b}_\perp = \begin{pmatrix} b'_1 \\ b'_2 \\ b'_3 \\ b'_4 \\ b'_5 \end{pmatrix} = \frac{4\langle\delta\rangle}{5m}\begin{pmatrix} \delta_3+\delta_4-2\delta_1 \\ \delta_4+\delta_5-2\delta_2 \\ \delta_5+\delta_1-2\delta_3 \\ \delta_1+\delta_2-2\delta_4 \\ \delta_2+\delta_3-2\delta_5 \end{pmatrix}. \tag{S88}$$

Let us now calculate $b_\parallel$ in this case, using Eq. S82. Eq. S88 entails that $\langle b'\rangle = 0$, and allows us to write:

$$\langle b'\delta\rangle = \frac{1}{5}\sum_{j=1}^{5} b'_j\delta_j = -\frac{8\langle\delta\rangle}{25m}\left(5\langle\delta^2\rangle - \sum_{j=1}^{5}\delta_j\delta_{(j+2)\bmod 5}\right), \tag{S89}$$

so Eq. S82 yields:

$$b_\parallel = \frac{4}{3}\langle\delta\rangle^2 + 2\langle\delta^2\rangle - \frac{8}{25m}\left(5\langle\delta^2\rangle - \sum_{j=1}^{5}\delta_j\delta_{(j+2)\bmod 5}\right). \tag{S90}$$

Note that in a homogeneous cycle with $D = 5$ and $m_A = m_C = m$, where $\delta_i = \Delta$ for all i, Eq. S88 reduces to $\boldsymbol{b}_\perp = \boldsymbol{0}$, and Eq. S90 reduces to $b_\parallel = 10\Delta^2/3$, which is the same as above for the homogeneous clique. This is consistent with the fact that the circulation theorem holds for homogeneous environments in the branching process approximation [36].

The mutant fixation probability averaged over starting demes reads:

$$\rho = 2\langle\delta\rangle st - \frac{b_\parallel + \langle b'\rangle}{2}(st)^2 + o((st)^2) = 2\langle\delta\rangle st - \frac{b_\parallel}{2}(st)^2 + o((st)^2)\,, \tag{S91}$$

where $b_\parallel$ is given by Eq. S89. As for the clique, to second order, this fixation probability does not involve $\boldsymbol{b}_\perp$.

Let us compare the mutant fixation probability, averaged over starting demes, in a heterogeneous cycle and in a homogeneous cycle with the same $\langle\delta\rangle$, still in the particular case where $D = 5$ and $m_A = m_C = m$. Calling ρ and ρ^{homo} these two fixation probabilities, Eq. S91 yields:

$$\begin{aligned}\rho - \rho^{\text{homo}} &= \frac{(st)^2}{2}\left(b_{\parallel}^{\text{homo}} - b_{\parallel}\right) = \frac{(st)^2}{2}\left[\frac{10}{3}\langle\delta\rangle^2 - \frac{4}{3}\langle\delta\rangle^2 - 2\langle\delta^2\rangle + \frac{8}{25m}\left(5\langle\delta^2\rangle - \sum_{j=1}^{5}\delta_j\delta_{(j+2)\bmod 5}\right)\right] \\ &= (st)^2\left[\langle\delta\rangle^2 - \langle\delta^2\rangle + \frac{4}{25m}\left(5\langle\delta^2\rangle - \sum_{j=1}^{5}\delta_j\delta_{(j+2)\bmod 5}\right)\right]. \end{aligned} \tag{S92}$$

Let us now investigate the sign of $\rho - \rho^{\text{homo}}$. Noticing that

$$\left(\sum_{i=1}^{5}\delta_i\right)^2 = \sum_{i=1}^{5}\delta_i^2 + 2\sum_{i=1}^{5}\delta_i\delta_{(i+1)\bmod 5} + 2\sum_{i=1}^{5}\delta_i\delta_{(i+2)\bmod 5}\,, \tag{S93}$$

we can write, in terms of rough orders of magnitude,

$$\sum_{i=1}^{5}\delta_i\delta_{(i+2)\bmod 5} \simeq \sum_{i=1}^{5}\delta_i\delta_{(i+1)\bmod 5} \simeq \frac{1}{4}\left[\left(\sum_{i=1}^{5}\delta_i\right)^2 - \sum_{i=1}^{5}\delta_i^2\right] = \frac{25}{4}\langle\delta\rangle^2 - \frac{5}{4}\langle\delta^2\rangle\,. \tag{S94}$$

Eq. S92 then yields:

$$\rho - \rho^{\text{homo}} \simeq (st)^2\left[\langle\delta\rangle^2 - \langle\delta^2\rangle + \frac{4}{25m}\left(5\langle\delta^2\rangle - \frac{25}{4}\langle\delta\rangle^2 + \frac{5}{4}\langle\delta^2\rangle\right)\right] \simeq \frac{1-m}{m}(st)^2\left(\langle\delta^2\rangle - \langle\delta\rangle^2\right). \tag{S95}$$

In our particular cycle with $m_A = m_C = m$, the condition $\sum_i m_{ij} = 1$ for all j gives $2m + m_{ii} = 1$, i.e. $m_{ii} = 1 - 2m$. Since all migration probabilities are between 0 and 1, we have $m \leq 1/2$. Hence, under the rough assumption of Eq. S94, Eq. S95 indicates that $\rho \gtrsim \rho^{\text{homo}}$ and that the smaller m is, and the larger the variance of the δ_i is, the larger $\rho - \rho^{\text{homo}}$ is expected to become. These approximate results are reminiscent of the exact results obtained for the clique in Eq. S87.

Figure S8A shows the exact value of the deviation with respect to the homogeneous case of $b_{\parallel}$, from Eq. S92, for multiple heterogeneous cycles, differing by their environmental heterogeneity, via $\boldsymbol{\delta}$. We observe that the approximate second-order coefficient, from Eq. S95, yields the correct trend of its dependence in $\text{Var}(\delta) = \langle\delta^2\rangle - \langle\delta\rangle^2$ (in agreement with a linear fit), but that there is substantial spread around that trend. We also observe that the discrepancy between the exact and the approximate formulas is small (resp. large) when $\left|\sum_{i=1}^{5}\delta_i\delta_{(i+2)\bmod 5} - \sum_{i=1}^{5}\delta_i\delta_{(i+1)\bmod 5}\right|$ is small (resp. large), as expected given the approximation made.

Since for the cycle the variance does not fully capture the impact of environment heterogeneity, we further explore the role of the spatial placement of heterogeneity in the cycle. A metric to quantify local variation between neighboring demes compared to the global variation is:

$$V = \frac{\left(\sum_{i=1}^{5}|\delta_i - \delta_{(i+1)\bmod 5}|\right)^2}{5\text{Var}(\delta)}, \tag{S96}$$

where δ_i denotes the deme-specific mutant fitness advantage prefactor, and $\text{Var}(\delta)$ is the variance of these prefactors across demes. The numerator of V quantifies local environment variation, and the denominator overall environment heterogeneity. At a fixed value of the variance, a gradual local variation results in a small numerator, resulting in a small value of V. Meanwhile, repeated abrupt alternations in δ_i for nearby demes result in a large numerator and hence a large value of V. In Figure S8B, we color the excess fixation probability in the cycle due to the second order term (i.e. $-b_{\parallel}$) based on the value of V in Eq. S96. We observe that when similar values of δ_i are clustered together (i.e. for small V), the excess fixation probability tends to be higher.

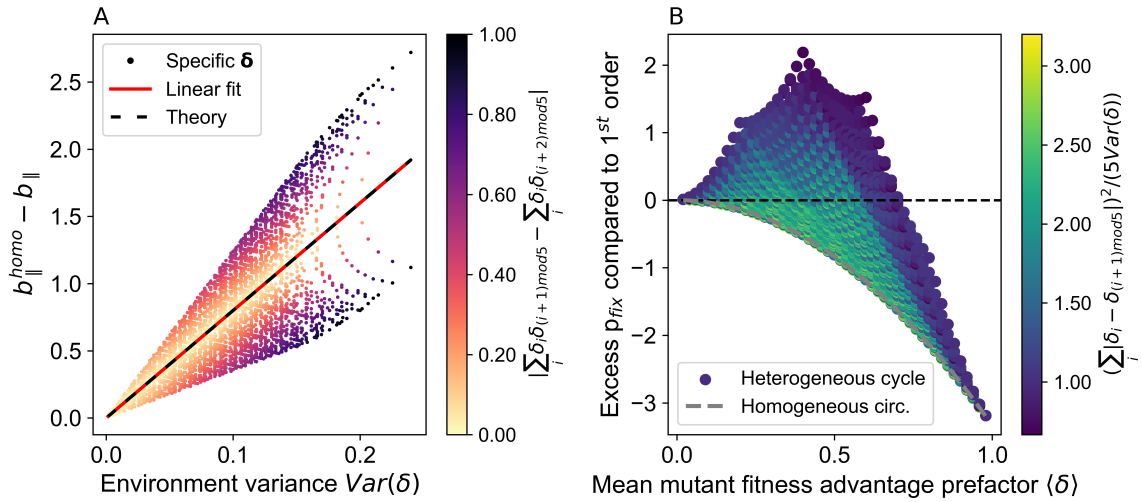

Figure S8: **Impact of environment heterogeneity on the second-order coefficient of the fixation probability in the cycle.** Panel A: Difference $b_{\|}^{\text{homo}} - b_{\|}$ between the second-order coefficients for a cycle with heterogeneous and homogeneous environment (see Eq. S92), plotted against the environment variance $\text{Var}(\delta)$. Markers are colored according to $\left|\sum_{i=1}^{5} \delta_i \delta_{(i+2)\text{mod}\,5} - \sum_{i=1}^{5} \delta_i \delta_{(i+1)\text{mod}\,5}\right|$. Solid red line: linear fit of the data. Dashed black line: approximate theoretical prediction from Eq. S95. Panel B: The excess fixation probability ("p_{fix}") provided by the second order term, i.e. concretely, $-b_{\|}$, is shown versus the mean mutant fitness advantage prefactor $\langle\delta\rangle$ across the structure, for various heterogeneous cliques, as in Figure 4, but colored according to the ratio of local to global environmental variation, defined in Eq. S96. Dashed gray line: homogeneous environment case (Eq. S85). Parameter values for both panels: $D = 5$, $m_A = m_C = m = 0.2$ for the cycle. Numbers in $\{0, 0.1, \ldots, 0.9, 1\}$ are employed for each δ_i, and all combinations of them are considered.

6 Rare migration regime

In this Section, we turn to the rare migration regime, that is to the case where fixation or extinction of a type within a deme happens on faster timescales than any migrations between demes. Recall that so far, all analytical calculations were made assuming frequent migrations, in the branching process framework. However, with rare migrations, another approach allows to obtain analytical results. Indeed, given the separation of timescales that exists in this regime, one can consider that each deme is either fully mutant or fully wild-type when migrations happen. One can then study mutant fixation using a Markov chain in a coarse-grained description, where migrations can result into a change of state of demes from fully mutant to fully wild-type, and vice-versa [35, 44]. Below, we consider the star and the line with rare migrations. We calculate their mutant fixation probabilities for heterogeneous environments, and we show that amplification of selection can be observed in this regime. Importantly, in this regime, we can address deleterious mutants as well as beneficial ones, and consider a broad range of fitness differences, while the branching process approach is restricted to beneficial mutants ($s > 0$) satisfying $st \ll 1$ and $st \gg 1/K$.

6.1 Star with heterogeneous environment

6.1.1 Mutant fixation probability

Let us consider a star with D demes, where migrations from each leaf to the center (resp. from the center to each leaf) occur with a rate per individual m_I (resp. m_O). In the rare migration regime, the state of the system can be fully described by two numbers: (1) a binary number indicating whether the center is wild-type or mutant, and (2) the number i of mutant leaves.

Below, we determine the probability of fixation of a mutant in the star in the rare migration regime, starting from a fully mutant deme chosen uniformly at random. For this, we generalize the calculation of Ref. [35], which assumed the same environment in each deme (see the Supplementary Material

of that paper), to the case of heterogeneous environments. We focus on the case where the center has a different environment from the leaves. We assume that all leaves have the same environment, thereby preserving the symmetry of the star, where all leaves are equivalent. Thus, the key difference compared to the homogeneous case [35] is that here, the probability of fixation of a given type (mutant or wild-type) in the center is different from that in a leaf. In practice, here, for simplicity, we will assume that this arises from the fact that the mutant has a different fitness advantage in the center and in leaves.

Note that, compared to Ref. [35], we do not take into account the fact that the equilibrium deme size (or bottleneck size) of a deme can differ depending on whether the deme is mutant or wild type. Indeed, here, we consider serial dilution models, which are similar to Wright-Fisher models, and where this bottleneck size is set by a regulation, assumed to be independent from composition. (In models with individual-level birth and death probabilities and logistic regulation, such as that of Ref. [35], the steady-state deme size depends on fitness, and thus differs between mutants and wild-types, but this difference is small when fitnesses f satisfy $f \gg g$, where g represents death rate. The calculation below can easily be extended to take this difference into account if necessary [35].)

Upon a given migration event, the probability that the mutant type fixes in the center, if the center is initially wild-type and i leaves are mutant, reads

$$T_{(0,i)\to(1,i)} = \frac{m_I i}{m_I i + m_I(D-1-i) + m_O N_W (D-1)} \rho_M^C \,, \tag{S97}$$

where ρ_M^C is the probability of fixation of one mutant in a wild-type center. Indeed, this scenario happens if there is a migration from a mutant leaf to the center, and the mutant then fixes in the center. Similarly, the probability that the wild-type fixes in the center, if the center is initially mutant and i leaves are mutant, reads

$$T_{(1,i)\to(0,i)} = \frac{m_I (D-1-i)}{m_I i + m_I(D-1-i) + m_O (D-1)} \rho_W^C \,, \tag{S98}$$

where ρ_W^C is the probability of fixation of one wild-type individual in a mutant center. Then, the probability that the number of mutant leaves increases by 1 if the center is mutant is

$$T_{(1,i)\to(1,i+1)} = \frac{m_O (D-1-i)}{m_I i + m_I(D-1-i) + m_O (D-1)} \rho_M^L \,, \tag{S99}$$

where ρ_M^L is the probability of fixation of one mutant in a wild-type leaf. Finally, the probability that the number of mutant leaves decreases by 1 if the center is wild-type is

$$T_{(0,i)\to(0,i-1)} = \frac{m_O i}{m_I i + m_I(D-1-i) + m_O (D-1)} \rho_W^L \,, \tag{S100}$$

where ρ_W^L is the probability of fixation of one wild-type individual in a mutant leaf.

As in Ref. [35], we call $\Phi_{0,i}^{\text{star}}$ (resp. $\Phi_{1,i}^{\text{star}}$) the fixation probability of the mutant type starting from i fully mutant leaves and a wild-type center (resp. a mutant center). The fixation probabilities $\Phi_{0,i}^{\text{star}}$ and $\Phi_{1,i}^{\text{star}}$ satisfy the following recurrence relationship (see Refs. [35, 82]):

$$\begin{cases} \Phi_{0,0}^{\text{star}} = 0 \,, \\ \Phi_{1,i}^{\text{star}} = T_{(1,i)\to(0,i)} \Phi_{0,i}^{\text{star}} + T_{(1,i)\to(1,i+1)} \Phi_{1,i+1}^{\text{star}} \\ \qquad\qquad + \left[1 - T_{(1,i)\to(0,i)} - T_{(1,i)\to(1,i+1)}\right] \Phi_{1,i}^{\text{star}} \text{ for } 0 \le i \le D-2 \,, \\ \Phi_{0,i}^{\text{star}} = T_{(0,i)\to(1,i)} \Phi_{1,i}^{\text{star}} + T_{(0,i)\to(0,i-1)} \Phi_{0,i-1}^{\text{star}} \\ \qquad\qquad + \left[1 - T_{(0,i)\to(1,i)} - T_{(0,i)\to(0,i-1)}\right] \Phi_{0,i}^{\text{star}} \text{ for } 1 \le i \le D-1 \,, \\ \Phi_{1,D-1}^{\text{star}} = 1 \,, \end{cases} \tag{S101}$$

which yields:

$$\begin{cases} \Phi_{0,0}^{\text{star}} = 0\,, \\ \Phi_{1,i}^{\text{star}} = \dfrac{-1+\Gamma_1\left[-1+(1+\Gamma_0)\left(\frac{\Gamma_0(1+\Gamma_1)}{1+\Gamma_0}\right)^i\right]}{-1+\Gamma_1\left[-1+(1+\Gamma_0)\left(\frac{\Gamma_0(1+\Gamma_1)}{1+\Gamma_0}\right)^{D-1}\right]} \text{ for } 0 \leq i \leq D-2\,, \\ \Phi_{0,i}^{\text{star}} = \dfrac{(1+\Gamma_1)\left[-1+\left(\frac{\Gamma_0(1+\Gamma_1)}{1+\Gamma_0}\right)^i\right]}{-1+\Gamma_1\left[-1+(1+\Gamma_0)\left(\frac{\Gamma_0(1+\Gamma_1)}{1+\Gamma_0}\right)^{D-1}\right]} \text{ for } 1 \leq i \leq D-1\,, \\ \Phi_{1,D-1}^{\text{star}} = 1\,, \end{cases} \tag{S102}$$

with

$$\Gamma_1 = \alpha \frac{\rho_W^C}{\rho_M^L}\,, \tag{S103}$$

$$\Gamma_0 = \frac{1}{\alpha}\frac{\rho_W^L}{\rho_M^C}\,, \tag{S104}$$

where we have used migration asymmetry

$$\alpha = \frac{m_I}{m_O}\,. \tag{S105}$$

Let us now consider the probability ρ_1^{star} that a single mutant, appearing uniformly at random in the population, fixes in the whole population. In the rare migration regime, it first fixes in the deme where it appeared, and then it spreads. Let us denote by ρ_M^C and ρ_M^L, respectively, the fixation probability of a single mutant in the center and in a leaf. Note that they depend on whether we consider a Moran-like model (as in Ref. [35]) or a Wright-Fisher-like model (as our dilution model introduced in [36] and used here). For consistency with the rest of the paper, we employ the serial dilution model, yielding, for a single mutant placed in the center at a bottleneck:

$$\rho_M^C = \frac{1-e^{-2\delta_C st}}{1-e^{-2K\delta_C st}} \text{ and } \rho_W^C = \frac{1-e^{2\delta_C st}}{1-e^{2K\delta_C st}}\,, \tag{S106}$$

and similarly for ρ_M^L, but with δ_L taking the place of δ_C, if the mutant starts in a leaf. Here, we have denoted by $\delta_C st$ and $\delta_L st$ the mutant effective relative fitness advantages in the center and in a leaf, respectively.

Then, we have:

$$\rho_1^{\text{star}} = \frac{1}{D}\rho_M^C \Phi_{1,0}^{\text{star}} + \frac{D-1}{D}\rho_M^L \Phi_{0,1}^{\text{star}}\,, \tag{S107}$$

with $\Phi_{1,0}^{\text{star}}$ and $\Phi_{0,1}^{\text{star}}$ given in Eq. S102.

6.1.2 Amplification of selection

Figure 5 shows that the heterogeneous star in the rare migration regime is an amplifier of selection compared to a homogeneous circulation with the same mean mutant fitness when δ_C is substantially larger than δ_L, i.e. when beneficial (resp. deleterious) mutants are substantially more advantaged (resp. disadvantaged) in the center than in leaves. We observe this amplification for negative and for small absolute baseline mutant fitness advantages, corresponding to weakly deleterious and weakly beneficial mutants, in a broad range of migration asymmetries $\alpha = m_I/m_O$. Recall that the homogeneous star is a suppressor of selection for $\alpha < 1$ and an amplifier of selection for $\alpha > 1$ [35], and that the amplification effect is observed under rare migrations for $\alpha > 1$ when $st \lesssim 1/K$ [36]. To better understand these results, let us consider different selection regimes, under rare migrations, and assuming $s > 0$.

First, if $1/K \ll 2\delta_C st \ll 1$ and $1/K \ll 2\delta_L st \ll 1$, then the fixation probabilities in a single deme (see Eq. S106) reduce to

$$\rho_M^C \approx 1 - e^{-2\delta_C st} \approx 2\delta_C st - 2\delta_C^2 s^2 t^2 \text{ and } \rho_W^C \approx 0\,, \tag{S108}$$

and similarly in the leaf (note that ρ_W^C is in fact exponentially suppressed). In this regime, once a mutant has fixed in a deme, the wild type is unable to retake over that deme, and fixation in the whole population always ensues. Thus, the mutant fixation probability in the star, averaged over the deme where the mutant starts, reads:

$$\rho \approx \frac{1}{D}\rho_M^C + \frac{D-1}{D}\rho_M^L \approx 2\langle\delta\rangle st - 2\langle\delta^2\rangle s^2 t^2\,. \tag{S109}$$

Under our assumptions, we have $1/K \ll 2\langle\delta\rangle st \ll 1$, and hence, we can express the difference of fixation probability between a heterogeneous and a homogeneous structure with the same $\langle\delta\rangle$ as:

$$\rho - \rho^{\text{homo}} \approx -2(st)^2\left(\langle\delta^2\rangle - \langle\delta\rangle^2\right) < 0\,, \tag{S110}$$

which demonstrates that in this regime, environment heterogeneity leads to suppression of selection, and explains the observations of Figure 5B for larger st.

Second, if $\delta_C > \delta_L$, there may be a regime where $1/K \ll 2\delta_C st \ll 1$ but $2\delta_L st \lesssim 1/K$. In this case, the situation is the same as before for a mutant starting in the center: if it fixes there, it should ultimately take over the whole population. Indeed, wild-type individuals migrating to the center cannot take over due to their substantial fitness disadvantage (their fixation probability is exponentially suppressed). However, the situation is different for a mutant starting in a leaf: once it has fixed there, it may be re-invaded by wild-type individuals from the center, before the mutant can fix in the center. In a homogeneous circulation with the same $\langle\delta\rangle$, if D is large enough, we will have $2\langle\delta\rangle st \lesssim 1/K$, as in a leaf, and thus the homogeneous circulation will not benefit from a "safe" deme for mutants: this leads to amplification in this regime. Moreover, the heterogeneous star structure with $\delta_C > \delta_L$ means that a mutant starting in a leaf will take over the whole structure if it just takes over the center, making this structure quite favorable to mutant fixation in this regime. Takeover of the center starting from a leaf is more likely if α is large, leading to more amplification in that case.

6.2 Line with heterogeneous environment

6.2.1 Mutant fixation probability

Here, we extend our derivation of mutant fixation probability in a line with rare migrations, made in the homogeneous case in Ref. [58], to heterogeneous case.

Equation on the fixation probability. Let us consider a line graph made of D demes in the rare migration regime. We denote by m_L (respectively m_R) the migration rate to the left (respectively to the right). We introduce environment heterogeneity by considering D_L demes on the left-hand side of the line where the mutant relative fitness advantage is $\delta_L s$, and $D_R = D - D_L$ demes on the right-hand side where the mutant relative fitness advantage is $\delta_R s$. Considering the serial dilution model, the fixation probability of one mutant (resp. wild-type) in a wild-type (resp. mutant) deme is

$$\rho_M^b = \frac{1 - e^{-2\delta_b st}}{1 - e^{-2K\delta_b st}} \qquad \text{and} \qquad \rho_W^b = \frac{1 - e^{2\delta_b st}}{1 - e^{2K\delta_b st}}, \tag{S111}$$

with $b \in \{L, R\}$.

As pointed out in Ref. [58], in the rare migration regime, the fact that mutants have to spread from the deme where the mutant appeared to other ones in order to fix entails that, at all times, there is one contiguous cluster of demes of mutants. Let us denote by $\phi_{i,j}$ the probability that mutants fix in the line starting from a cluster of $j-i$ adjacent fully mutant demes. Here, $i \in [0, D]$ indicates the position of the first mutant deme along the line, while $j \in [0, D]$ is the position of the first wild-type deme along the line, with the constraint that $i \leq j$ (the case $j = D$ corresponds to a situation where there are no wild-type demes to the right of the mutant cluster). Note that exceptionally, in this derivation, demes are numbered from 0 to $D - 1$.

The equation satisfied by the fixation probability $\phi_{i,j}$ is

$$\phi_{i,j} = p_1\phi_{i,j+1} + p_2\phi_{i-1,j} + p_3\phi_{i,j-1} + p_4\phi_{i+1,j}\,, \tag{S112}$$

where the indices i, j correspond respectively to the position of the first mutant (type M) deme and the position of the next first wild type (type W). Here, in contrast with the homogeneous case addressed in Ref. [58], the transition probabilities p_1, p_2, p_3, p_4 depend on where the cluster of mutant demes is located, because of the environment heterogeneity. Specifically, they depend on the zones where the indices i, j are located, represented in Fig. S9.

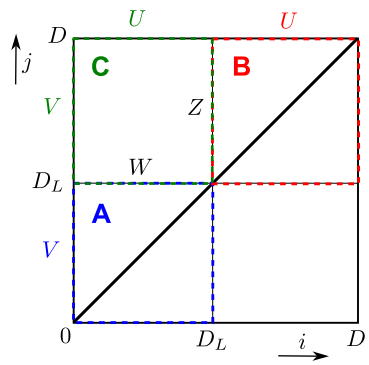

Figure S9: **Schematic of the zones where the indices i and j can vary.** Each zone (A, B, C) is associated with specific values of the transition probabilities p_1, p_2, p_3, and p_4. Boundary conditions (U, V, W, Z) are shown. The black diagonal corresponds to mutant extinction, where $\phi_{i,i} = 0$ for all $i \in [0, D]$, while the upper-left corner corresponds to mutant fixation on the graph, with $\phi_{0,D} = 1$.

Their expressions in these different zones, illustrated in Fig. S10, are the following:

- Zone A ($0 < i < j < D_L$):

$$p_1^A = \frac{\alpha}{(1+\alpha)(1+\gamma_L)}, p_2^A = \frac{1}{(1+\alpha)(1+\gamma_L)}, \tag{S113}$$

$$p_3^A = \frac{\gamma_L}{(1+\alpha)(1+\gamma_L)}, p_4^A = \frac{\alpha\gamma_L}{(1+\alpha)(1+\gamma_L)}, \tag{S114}$$

- Zone B ($D_L < i < j < D$):

$$p_1^B = \frac{\alpha}{(1+\alpha)(1+\gamma_R)}, p_2^B = \frac{1}{(1+\alpha)(1+\gamma_R)}, \tag{S115}$$

$$p_3^B = \frac{\gamma_R}{(1+\alpha)(1+\gamma_R)}, p_4^B = \frac{\alpha\gamma_R}{(1+\alpha)(1+\gamma_R)}, \tag{S116}$$

- Zone C ($i < D_L, j > D_L$):

$$p_1^C = \frac{\alpha\beta_M}{1+\gamma_R\beta_M+\alpha(\gamma_L+\beta_M)}, p_2^C = \frac{1}{1+\gamma_R\beta_M+\alpha(\gamma_L+\beta_M)}, \tag{S117}$$

$$p_3^C = \frac{\gamma_R\beta_M}{1+\gamma_R\beta_M+\alpha(\gamma_L+\beta_M)}, p_4^C = \frac{\alpha\gamma_L}{1+\gamma_R\beta_M+\alpha(\gamma_L+\beta_M)}, \tag{S118}$$

with migration asymmetry $\alpha = m_R/m_L$, and introducing $\beta_a = \rho_a^R/\rho_a^L$ ($a \in (W, M)$), and $\gamma_b = \rho_W^b/\rho_M^b$, ($b \in (L, R)$). The boundary conditions are denoted by $\phi_{i,i} = 0$, $\phi_{0,j} = V_j$, $\phi_{i,D} = U_i$, see Fig. S9, where U_i and V_j are expressed below.

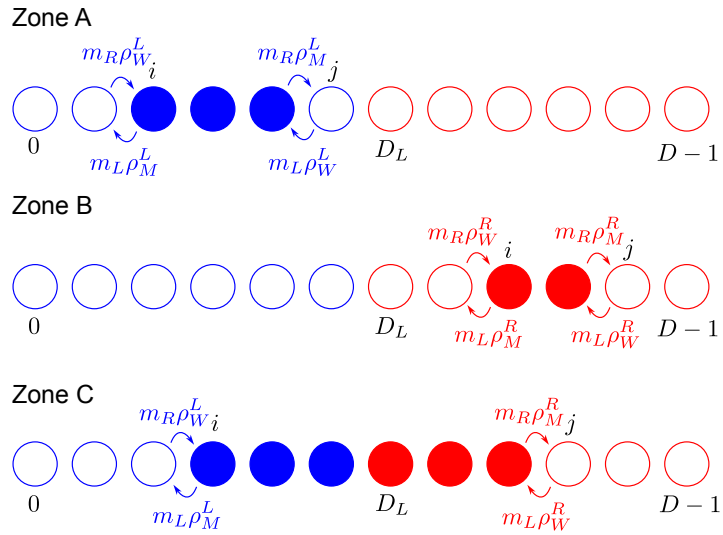

Figure S10: Example configurations for each region A, B and C.

Boundary conditions.

- Expression of $V_j = \phi_{0,j}$:

$$\begin{cases} (\alpha+\gamma_L)V_j = \alpha V_{j+1} + \gamma_L V_{j-1} \text{ , if } j < D_L, \\ (\alpha+\gamma_R)V_j = \alpha V_{j+1} + \gamma_R V_{j-1} \text{ , if } j > D_L, \end{cases} \tag{S119}$$

and for $j = D_L$,

$$(\alpha\beta_M + \gamma_L)V_{D_L} = \alpha\beta_M V_{D_L+1} + \gamma_L V_{D_L-1}. \tag{S120}$$

The solution is

$$V_j = \begin{cases} A_L + B_L \left(\frac{\gamma_L}{\alpha}\right)^j \text{ , if } j < D_L, \\ A_R + B_R \left(\frac{\gamma_R}{\alpha}\right)^j \text{ , if } j > D_L. \end{cases} \tag{S121}$$

The boundary conditions are $A_L + B_L = 0$ and $A_R + B_R \left(\frac{\gamma_R}{\alpha}\right)^D = 1$. Branching left and right solutions imposes that $A_L + B_L \left(\frac{\gamma_L}{\alpha}\right)^{D_L} = A_R + B_R \left(\frac{\gamma_R}{\alpha}\right)^{D_L}$. It yields

$$A_L = \frac{1}{Z_V}\beta_M \left(\frac{\gamma_R}{\gamma_L}\right)^{D_L} \left(1 - \frac{\gamma_R}{\alpha}\right), \tag{S122}$$

$$B_L = -\frac{1}{Z_V}\beta_M \left(\frac{\gamma_R}{\gamma_L}\right)^{D_L} \left(1 - \frac{\gamma_R}{\alpha}\right), \tag{S123}$$

$$A_R = \frac{1}{Z_V}\left[\beta_M \left(\frac{\gamma_R}{\gamma_L}\right)^{D_L} \left(1 - \frac{\gamma_R}{\alpha}\right)\left(1 - \left(\frac{\gamma_L}{\alpha}\right)^{D_L}\right) + \left(1 - \frac{\gamma_L}{\alpha}\right)\left(\frac{\gamma_R}{\alpha}\right)^{D_L}\right], \tag{S124}$$

$$B_R = \frac{1}{Z_V}\left(1 - \frac{\gamma_L}{\alpha}\right), \tag{S125}$$

with

$$Z_V = \beta_M \left(\frac{\gamma_R}{\gamma_L}\right)^{D_L} \left(1 - \frac{\gamma_R}{\alpha}\right)\left(1 - \left(\frac{\gamma_L}{\alpha}\right)^{D_L}\right) + \left(1 - \frac{\gamma_L}{\alpha}\right)\left(\left(\frac{\gamma_R}{\alpha}\right)^{D_L} - \left(\frac{\gamma_R}{\alpha}\right)^{D}\right). \tag{S126}$$

- Expression of $U_i = \phi_{i,D}$:

$$\begin{cases} (1+\alpha\gamma_L)U_i = \alpha\gamma_L U_{i+1} + U_{i-1} \text{ , if } i < D_L, \\ (1+\alpha\gamma_R)U_i = \alpha\gamma_R U_{i+1} + U_{i-1} \text{ , if } i > D_L, \end{cases} \tag{S127}$$

and for $i = D_L$

$$(1+\alpha\beta_M\gamma_R)\,U_{D_L} = \alpha\beta_M\gamma_R U_{D_L+1} + U_{D_L-1}. \tag{S128}$$

The general solution is

$$U_i = \begin{cases} E_L + \frac{F_L}{(\alpha\gamma_L)^i}\ , \text{ if } i < D_L, \\ E_R + \frac{F_R}{(\alpha\gamma_R)^i}\ , \text{ if } i > D_L. \end{cases} \tag{S129}$$

The boundary conditions are $E_L + F_L = 1$ and $E_R + \dfrac{F_R}{(\alpha\gamma_R)^D} = 0$. Branching both solutions imposes that $E_L + \dfrac{F_L}{(\alpha\gamma_L)^{D_L}} = E_R + \dfrac{F_R}{(\alpha\gamma_R)^{D_L}}$. It yields

$$E_L = \frac{1}{Z_U}\left[-\frac{\beta_M}{(\alpha\gamma_L)^{D_L}}\left(1-\frac{1}{\alpha\gamma_R}\right) + \left(\frac{\gamma_R}{\gamma_L}\right)^{D_L-1}\left(1-\frac{1}{\alpha\gamma_L}\right)\left(\frac{1}{(\alpha\gamma_R)^{D_L}} - \frac{1}{(\alpha\gamma_R)^{D}}\right)\right], \tag{S130}$$

$$F_L = \frac{1}{Z_U}\beta_M\left(1-\frac{1}{\alpha\gamma_R}\right), \tag{S131}$$

$$E_R = -\frac{1}{Z_U}\left(\frac{\gamma_R}{\gamma_L}\right)^{D_L-1}\left(1-\frac{1}{\alpha\gamma_L}\right)\frac{1}{(\alpha\gamma_R)^{D}}, \tag{S132}$$

$$F_R = \frac{1}{Z_U}\left(\frac{\gamma_R}{\gamma_L}\right)^{D_L-1}\left(1-\frac{1}{\alpha\gamma_L}\right), \tag{S133}$$

with

$$Z_U = \beta_M\left(1-\frac{1}{\alpha\gamma_R}\right)\left(1-\frac{1}{(\alpha\gamma_L)^{D_L}}\right) + \left(\frac{\gamma_R}{\gamma_L}\right)^{D_L-1}\left(1-\frac{1}{\alpha\gamma_L}\right)\left(\frac{1}{(\alpha\gamma_R)^{D_L}} - \frac{1}{(\alpha\gamma_R)^{D}}\right). \tag{S134}$$

Expression of $\phi_{i,j}$ in the different zones. In each zone, the fixation probability is given by [83]

$$\phi^k_{i,j} = \sum_{a=1}^{L^k_x-1}\left[p^k_1\phi_{a,L^k_y}T^k_{(a,L^k_y-1)i,j} + p^k_3\phi_{a,0}T^k_{(a,1)i,j}\right] + \sum_{b=1}^{L^k_y-1}\left[p^k_2\phi_{0,b}T^k_{(1,b)i,j} + p^k_4\phi_{L^k_x,a}T^k_{(L^k_x-1,b)i,j}\right] \tag{S135}$$

with

$$T^k_{(a,b)i,j} = \frac{4}{L^k_xL^k_y}\left(\frac{p^k_2}{p^k_4}\right)^{\frac{i-a}{2}}\left(\frac{p^k_3}{p^k_1}\right)^{\frac{j-b}{2}}\sum_{r=1}^{L^k_x-1}\sum_{s=1}^{L^k_y-1}\frac{\sin\left(\frac{ir\pi}{L^k_x}\right)\sin\left(\frac{ar\pi}{L^k_x}\right)\sin\left(\frac{bs\pi}{L^k_y}\right)\sin\left(\frac{js\pi}{L^k_y}\right)}{1-2\sqrt{p^k_2p^k_4}\cos\left(\frac{r\pi}{L^k_x}\right)-2\sqrt{p^k_1p^k_3}\cos\left(\frac{s\pi}{L^k_y}\right)}, \tag{S136}$$

with $k \in (A, B, C)$, $i \in [1, ..., L^k_x - 1]$ and $j \in [1, ..., L^k_y - 1]$.

- Zone A ($0 < i, j < D_L$): $L^A_x = L^A_y = D_L$

$$\begin{aligned}\phi^A_{i,j} &= \sum_{a=1}^{D_L-1}\left[p^A_1\phi_{a,D_L}T^A_{(a,D_L-1)i,j} + p^A_2\phi_{0,a}T^A_{(1,a)i,j} + p^A_3\phi_{a,0}T^A_{(a,1)i,j} + p^A_4\phi_{D_L,a}T^A_{(D_L-1,a)i,j}\right] \\ &= \sum_{a=1}^{D_L-1}\left[p^A_1W_aT^A_{(a,D_L-1)i,j} + p^A_2V_aT^A_{(1,a)i,j} + p^A_3\phi_{a,0}T^A_{(a,1)i,j} + p^A_4\phi_{D_L,a}T^A_{(D_L-1,a)i,j}\right],\end{aligned} \tag{S137}$$

where $V_a = \phi_{0,a}$ was computed previously, but $W_a = \phi_{a,D_L}$ is unknown for now. We determine $\phi_{a,0}$ and $\phi_{D_L,a}$ using the constraint

$$\phi^A_{i,i} = 0 = \sum_{a=1}^{D_L-1}\left[p^A_1W_aT^A_{(a,D_L-1)i,i} + p^A_2V_aT^A_{(1,a)i,i} + p^A_3\phi_{a,0}T^A_{(a,1)i,i} + p^A_4\phi_{D_L,a}T^A_{(D_L-1,a)i,i}\right], \tag{S138}$$

and the property $T_{(a,b)i,i} = \gamma_L^{a-b} T_{(b,a)i,i}$, which yields

$$0 = \sum_{a=1}^{D_L-1} \left[T^A_{(a,D_L-1)i,i} \left(p_1^A W_a + p_4^A \phi_{D_L,a} \gamma_L^{D_L-1-a} \right) + T^A_{(a,1)i,i} \left(p_3^A \phi_{a,0} + p_2^A V_a \gamma_L^{1-a} \right) \right]. \quad \text{(S139)}$$

Building on Ref. [82], one can determine the solution:

$$\phi_{D_L,a} = -\gamma_L^{a-D_L} W_a, \quad \text{(S140)}$$

$$\phi_{a,0} = -\gamma_L^{-a} V_a. \quad \text{(S141)}$$

Finally,

$$\phi^A_{i,j} = \sum_{a=1}^{D_L-1} p_1^A W_a \left[T^A_{(a,D_L-1)i,j} - \gamma_L^{a-D_L+1} T^A_{(D_L-1,a)i,j} \right] + p_2^A V_a \left[T^A_{(1,a)i,j} - \gamma_L^{1-a} T^A_{(a,1)i,j} \right]. \quad \text{(S142)}$$

- Zone B ($D_L < i, j < D$): $L_x^B = L_y^B = D - D_L = D_R$

$$\begin{aligned} \phi^B_{i+D_L,j+D_L} &= \sum_{a=1}^{D_R-1} \Big[p_1^B \phi_{a+D_L,D} T^B_{(a,D_R-1)i,j} + p_2^B \phi_{D_L,a+D_L} T^B_{(1,a)i,j} \\ &\qquad + p_3^B \phi_{a+D_L,D_L} T^B_{(a,1)i,j} + p_4^B \phi_{D,a+D_L} T^B_{(D_R-1,a)i,j} \Big] \\ &= \sum_{a=1}^{D_R-1} \Big[p_1^B U_{a+D_L} T^B_{(a,D_R-1)i,j} + p_2^B Z_{a+D_L} T^B_{(1,a)i,j} \\ &\qquad + p_3^B \phi_{a+D_L,D_L} T^B_{(a,1)i,j} + p_4^B \phi_{D,a+D_L} T^B_{(D_R-1,a)i,j} \Big], \end{aligned} \quad \text{(S143)}$$

where $Z_{a+D_L} = \phi_{D_L,a+D_L}$, which is unknown. Using the same technique as for Zone A, we find

$$\phi_{D,a+D_L} = -\gamma_R^{a-D_R} U_{a+D_L}, \quad \text{(S144)}$$

$$\phi_{a+D_L,D_L} = -\gamma_R^{-a} Z_{a+D_L}. \quad \text{(S145)}$$

Finally,

$$\begin{aligned} \phi^B_{i+D_L,j+D_L} = \sum_{a=1}^{D_R-1} & p_1^B U_{a+D_L} \left[T^B_{(a,D_R-1)i,j} - \gamma_R^{a-D_R+1} T^B_{(D_R-1,a)i,j} \right] \\ & + p_2^B Z_{a+D_L} \left[T^B_{(1,a)i,j} - \gamma_R^{1-a} T^B_{(a,1)i,j} \right]. \end{aligned} \quad \text{(S146)}$$

- Zone C ($0 < i < D_L$, $D_L < j < D$): $L_x^C = D_L$, $L_y^C = D_R$

$$\begin{aligned} \phi^C_{i,j+D_L} &= \sum_{a=1}^{D_L-1} \left[p_1^C \phi_{a,D} T^C_{(a,D_R-1)i,j} + p_3^C \phi_{a,D_L} T^C_{(a,1)i,j} \right] \\ &\quad + \sum_{b=1}^{D_R-1} \left[p_2^C \phi_{0,b+D_L} T^C_{(1,b)i,j} + p_4^C \phi_{D_L,b+D_L} T^C_{(D_L-1,b)i,j} \right] \\ &= \sum_{a=1}^{D_L-1} \left[p_1^C U_a T^C_{(a,D_R-1)i,j} + p_3^C W_a T^C_{(a,1)i,j} \right] \\ &\quad + \sum_{b=1}^{D_R-1} \left[p_2^C V_{b+D_L} T^C_{(1,b)i,j} + p_4^C Z_{b+D_L} T^C_{(D_L-1,b)i,j} \right]. \end{aligned} \quad \text{(S147)}$$

Equations on W and Z. We would like to determine the remaining unknown boundary conditions W and Z. First, the equation on W (see Fig. S11) is, for all $i \in [1, D_L - 1]$:

$$W_i = \phi_{i,D_L} = p_1^W \phi_{i,D_L+1} + p_2^W \phi_{i-1,D_L} + p_3^W \phi_{i,D_L-1} + p_4^W \phi_{i+1,D_L}, \tag{S148}$$

with

$$p_1^W = \frac{\alpha\beta_M}{1+\gamma_L+\alpha(\beta_M+\gamma_L)}, p_2^W = \frac{1}{1+\gamma_L+\alpha(\beta_M+\gamma_L)}, \tag{S149}$$

$$p_3^W = \frac{\gamma_L}{1+\gamma_L+\alpha(\beta_M+\gamma_L)}, p_4^W = \frac{\alpha\gamma_L}{1+\gamma_L+\alpha(\beta_M+\gamma_L)}, \tag{S150}$$

where $W_0 = V_{D_L}$ and $W_{D_L} = 0$.

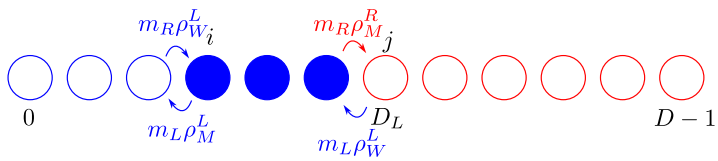

Figure S11: Example configuration in the specific case where $j = D_L$.

Eq. S148 can be rewritten as:

$$\begin{aligned}
W_i &= p_1^W \phi^C_{i,D_L+1} + p_2^W W_{i-1} + p_3^W \phi^A_{i,D_L-1} + p_4^W W_{i+1} \\
&= p_1^W \Bigg\{ \sum_{a=1}^{D_L-1} \left[p_1^C U_a T^C_{(a,D_R-1)i,1} + p_3^C W_a T^C_{(a,1)i,1} \right] \\
&\quad + \sum_{b=1}^{D_R-1} \left[p_2^C V_{b+D_L} T^C_{(1,b)i,1} + p_4^C Z_{b+D_L} T^C_{(D_L-1,b)i,1} \right] \Bigg\} \\
&\quad + p_3^W \Bigg\{ \sum_{a=1}^{D_L-1} p_1^A W_a \left[T^A_{(a,D_L-1)i,D_L-1} - \gamma_L^{a-D_L+1} T^A_{(D_L-1,a)i,D_L-1} \right] \\
&\quad + p_2^A V_a \left[T^A_{(1,a)i,D_L-1} - \gamma_L^{1-a} T^A_{(a,1)i,D_L-1} \right] \Bigg\} \\
&\quad + p_2^W W_{i-1} + p_4^W W_{i+1}.
\end{aligned} \tag{S151}$$

Similarly, the equation on Z (see Fig. S12) is, for all $j \in [1, D_R - 1]$:

$$Z_{j+D_L} = \phi_{D_L,j+D_L} = p_1^Z \phi_{D_L,j+D_L+1} + p_2^Z \phi_{D_L-1,j+D_L} + p_3^Z \phi_{D_L,j+D_L-1} + p_4^Z \phi_{D_L+1,j+D_L}, \tag{S152}$$

with

$$p_1^Z = \frac{\alpha}{\gamma_R + 1/\beta_M + \alpha(1+\gamma_R)}, \qquad p_2^Z = \frac{1/\beta_M}{\gamma_R + 1/\beta_M + \alpha(1+\gamma_R)}, \tag{S153}$$

$$p_3^Z = \frac{\gamma_R}{\gamma_R + 1/\beta_M + \alpha(1+\gamma_R)}, \qquad p_4^Z = \frac{\alpha\gamma_R}{\gamma_R + 1/\beta_M + \alpha(1+\gamma_R)}. \tag{S154}$$

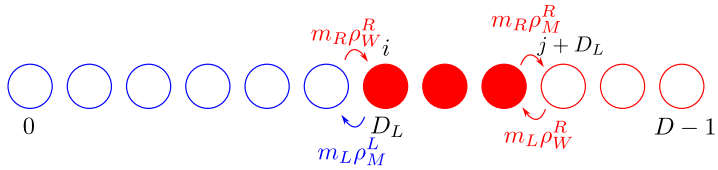

Figure S12: Example configuration in the specific case where $i = D_L$.

Again, we find

$$
\begin{aligned}
Z_{j+D_L} &= p_1^Z Z_{j+D_L+1} + p_2^Z \phi^C_{D_L-1,j+D_L} + p_3^Z Z_{j+D_L-1} + p_4^Z \phi^B_{D_L+1,j+D_L} \\
&= p_2^Z \Bigg\{ \sum_{a=1}^{D_L-1} \left[p_1^C U_a T^C_{(a,D_R-1)D_L-1,j} + p_3^C W_a T^C_{(a,1)D_L-1,j} \right] \\
&\quad + \sum_{b=1}^{D_R-1} \left[p_2^C V_{b+D_L} T^C_{(1,b)D_L-1,j} + p_4^C Z_{b+D_L} T^C_{(D_L-1,b)D_L-1,j} \right] \Bigg\} \\
&\quad + p_4^Z \Bigg\{ \sum_{a=1}^{D_R-1} p_1^B U_{a+D_L} \left[T^B_{(a,D_R-1)1,j} - \gamma_R^{a-D_R+1} T^B_{(D_R-1,a)1,j} \right] \\
&\quad + p_2^B Z_{a+D_L} \left[T^B_{(1,a)1,j} - \gamma_R^{1-a} T^B_{(a,1)1,j} \right] \Bigg\} \\
&\quad + p_1^Z Z_{j+D_L+1} + p_3^Z Z_{j+D_L-1}. \qquad \text{(S155)}
\end{aligned}
$$

It is convenient to rewrite Eqs. S151 and S155 in the form of a linear system:

$$
\sum_{k=0}^{D_L} A_{i,k} W_k + \sum_{\ell=0}^{D_R} B_{i,\ell} Z_{\ell+D_L} = E_i \qquad (0 \le i \le D_L), \qquad \text{(S156)}
$$

$$
\sum_{k=0}^{D_L} C_{j,k} W_k + \sum_{\ell=0}^{D_R} D_{j,\ell} Z_{\ell+D_L} = F_j \qquad (0 \le j \le D_R). \qquad \text{(S157)}
$$

where for all $0 < i < D_L$ and $0 < j < D_R$:

$$
\begin{aligned}
A_{i,k} &= p_3^W p_1^A \left[T^A_{(k,D_L-1)i,D_L-1} - \gamma_L^{k-D_L+1} T^A_{(D_L-1,k)i,D_L-1} \right] \\
&\quad + p_1^W p_3^C T^C_{(k,1)i,1} + p_2^W \delta_{k,i-1} + p_4^W \delta_{k,i+1} - \delta_{k,i}, \qquad \text{(S158)} \\
B_{i,\ell} &= p_1^W p_4^C T^C_{(D_L-1,\ell)i,1}, \qquad \text{(S159)} \\
C_{j,k} &= p_2^Z p_3^C T^C_{(k,1)D_L-1,j}, \qquad \text{(S160)} \\
D_{j,\ell} &= p_4^Z p_2^B \left[T^B_{(1,\ell)1,j} - \gamma_R^{1-\ell} T^B_{(\ell,1)1,j} \right] \\
&\quad + p_2^Z p_4^C T^C_{(D_L-1,\ell)D_L-1,j} + p_1^Z \delta_{\ell,j+1} + p_3^Z \delta_{\ell,j-1} - \delta_{\ell,j}, \qquad \text{(S161)} \\
E_i &= -p_1^W p_1^C \sum_{a=1}^{D_L-1} U_a T^C_{(a,D_R-1)i,1} - p_1^W p_2^C \sum_{b=1}^{D_R-1} V_{b+D_L} T^C_{(1,b)i,1} \\
&\quad - p_3^W p_2^A \sum_{a=1}^{D_L-1} V_a \left[T^A_{(1,a)i,D_L-1} - \gamma_L^{1-a} T^A_{(a,1)i,D_L-1} \right], \qquad \text{(S162)} \\
F_j &= -p_2^Z p_1^C \sum_{a=1}^{D_L-1} U_a T^C_{(a,D_R-1)D_L-1,j} - p_2^Z p_2^C \sum_{b=1}^{D_R-1} V_{b+D_L} T^C_{(1,b)D_L-1,j} \\
&\quad - p_4^Z p_1^B \sum_{a=1}^{D_R-1} U_{a+D_L} \left[T^B_{(a,D_R-1)1,j} - \gamma_R^{a-D_R+1} T^B_{(D_R-1,a)1,j} \right], \qquad \text{(S163)}
\end{aligned}
$$

and

$$
\begin{aligned}
&A_{0,k} = \delta_{0,k}, && A_{D_L,k} = \delta_{D_L,k}, && D_{0,\ell} = \delta_{0,\ell}, && D_{D_R,\ell} = \delta_{D_R,\ell}, && \text{(S164)} \\
&B_{0,\ell} = 0, && B_{D_L,\ell} = 0, && C_{0,k} = 0, && C_{D_R,k} = 0, && \text{(S165)} \\
&E_0 = V_{D_L}, && E_{D_L} = 0, && F_0 = 0, && F_{D_R} = U_{D_L}. && \text{(S166)}
\end{aligned}
$$

Conclusion. Numerically solving the linear system in Eqs. S156 and S157 (using matrix inversion) provides the values of W and Z. Then, the fixation probability of mutants, starting from one mutant

placed uniformly at random in the line graph is

$$\rho_1^{\text{line}} = \frac{1}{D}\left\{\rho_M^L\left[V_1 + \sum_{i=1}^{D_L-2}\phi_{i,i+1}^A + W_{D_L-1}\right] + \rho_M^R\left[Z_{D_L+1} + \sum_{i=D_L+1}^{D-2}\phi_{i,i+1}^B + U_{D-1}\right]\right\}, \tag{S167}$$

with

$$\begin{aligned}\phi_{i,i+1}^A = &\sum_{a=1}^{D_L-1} p_1^A W_a\left[T^A_{(a,D_L-1)i,i+1} - \gamma_L^{a-D_L+1}T^A_{(D_L-1,a)i,i+1}\right]\\ &+ \sum_{a=1}^{D_L-1} p_2^A V_a\left[T^A_{(1,a)i,i+1} - \gamma_L^{1-a}T^A_{(a,1)i,i+1}\right],\end{aligned} \tag{S168}$$

$$\begin{aligned}\phi_{i+D_L,i+D_L+1}^B = &\sum_{a=1}^{D_R-1} p_1^B U_{a+D_L}\left[T^B_{(a,D_R-1)i,i+1} - \gamma_R^{a-D_R+1}T^B_{(D_R-1,a)i,i+1}\right]\\ &+ \sum_{a=1}^{D_R-1} p_2^B Z_{a+D_L}\left[T^B_{(1,a)i,i+1} - \gamma_R^{1-a}T^B_{(a,1)i,i+1}\right].\end{aligned} \tag{S169}$$

6.2.2 Amplification of selection

In Fig. S13, the fixation probability obtained in Eq. S167, for a mutant in the heterogeneous line with rare migrations, is plotted as a function of the baseline relative mutant fitness advantage st. Several distinct regimes emerge as st is increased while $st \ll 1$. First, for very small st, selection is suppressed compared to the homogeneous circulation. Then, for slightly larger st, we observe a small amplification of selection, provided the migration asymmetry is less than 1. Next, suppression is again observed. While these results are complex, due to the interplay of migration and environment heterogeneity and to different regimes of selection, they show that the line can amplify selection in the rare migration regime when the environment is heterogeneous.

A qualitative analysis can be made along the lines of Section 6.1.2. Here, for simplicity, and as in Figure S13, we assume that only one deme on the left has δ_L and the other ones have δ_R.

First, if $1/K \ll 2\delta_L st \ll 1$ and $1/K \ll 2\delta_R st \ll 1$, the difference of fixation probability between a heterogeneous and a homogeneous structure with the same $\langle\delta\rangle$ can be expressed as for the star, see Eq. S110, and thus, environment heterogeneity leads to suppression of selection, explaining the observations of Figure S13 for larger st.

Second, if $\delta_L > \delta_R$, there may be a regime where $1/K \ll 2\delta_L st \ll 1$ but $2\delta_R st \lesssim 1/K$. Following the same reasoning as for the star, we conclude that a mutant starting in the left-most deme will take over in the whole population if it fixes there. Meanwhile, a mutant starting elsewhere that fixes in its original deme may be re-invaded by wild-type individuals. This is more likely in the line than in our heterogeneous star, because there are more ways to get re-invaded before full fixation. Nevertheless, the benefit of having one deme where the mutant is substantially advantaged and safe from re-invasions makes the heterogeneous line slightly amplify selection in this regime, compared to a homogeneous circulation.

Finally, when both δ_L and δ_R are very small, the benefit from having a deme where the mutant is fitter is minimal, and the heterogeneous line behaves as a suppressor of selection, as the homogeneous line [58].

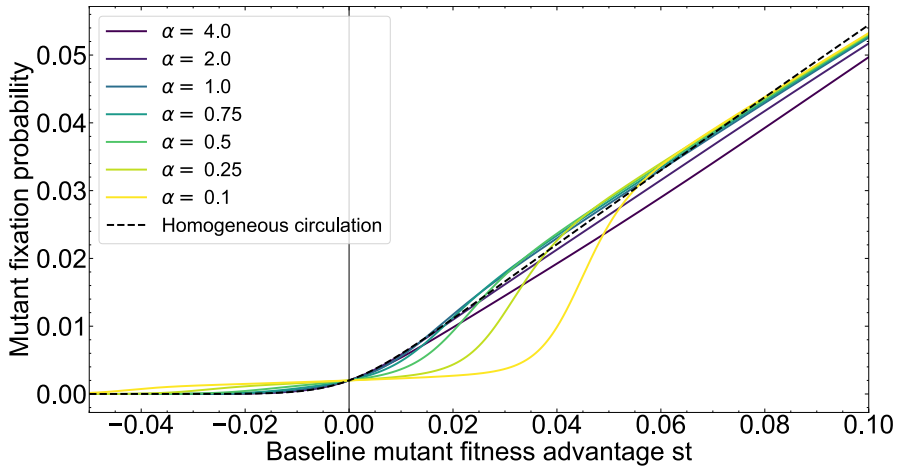

Figure S13: **Fixation probability in the heterogeneous line with rare migrations.** We plot the fixation probability starting from one mutant appearing uniformly at random in the line graph, given by Eq. (S167), as a function of the baseline mutant fitness advantage st. Parameters: $D = 5$, $D_L = 1$, $\delta_L = 1$, $\delta_R = 0.1$, $K = 100$. The case of a homogeneous circulation with the same average mutant relative fitness advantage is shown for reference.

References

[1] Noah Fierer. Embracing the unknown: disentangling the complexities of the soil microbiome. *Nature Reviews Microbiology*, 15:579–590, 2017.

[2] Gregory P. Donaldson, S. Melanie Lee, and Sarkis K. Mazmanian. Gut biogeography of the bacterial microbiota. *Nature Reviews Microbiology*, 14(1):20–32, 2016.

[3] Feilun Wu, Yuanchi Ha, Andrea Weiss, Meidi Wang, Jeffrey Letourneau, Shangying Wang, Nan Luo, Shuquan Huang, Charlotte T. Lee, Lawrence A. David, and Lingchong You. Modulation of microbial community dynamics by spatial partitioning. *Nature Chemical Biology*, 18(4):394–402, 2022.

[4] Joseph Edwards, Cameron Johnson, Christian Santos-Medellín, and Venkatesan Sundaresan. Structure, variation, and assembly of the root-associated microbiomes of rice. *Proceedings of the National Academy of Sciences*, 112(8):E911–E920, 2015.

[5] Samuel Bickel and Dani Or. Soil bacterial diversity mediated by microscale aqueous-phase processes across biomes. *Nature Communications*, 11(116):1–9, 2020.

[6] Esteban G. Jobbágy and Robert B. Jackson. The distribution of soil nutrients with depth: Global patterns and the imprint of plants. *Biogeochemistry*, 53(1):51–77, 2001.

[7] D. Naylor, R. McClure, and J. Jansson J. Trends in microbial community composition and function by soil depth. *Microorganism*, 10(3):540, 2022.

[8] Vigdis Torsvik, Lise Øvreås, and Tron Frede Thingstad. Prokaryotic diversity–magnitude, dynamics, and controlling factors. *Science*, 296(5570):1064–1066, 2002.

[9] Roman Stocker. Marine microbes see a sea of gradients. *Science*, 338(6107):628–633, 2012.

[10] Tom Fenchel and Bland Finlay. Oxygen and the spatial structure of microbial communities. *Biological reviews of the Cambridge Philosophical Society*, 83(4):553–569, 2008.

[11] Elizabeth K. Costello, Christian L. Lauber, Micah Hamady, Noah Fierer, Jeffrey I. Gordon, and Rob Knight. Bacterial community variation in human body habitats across space and time. *Science*, 326(5960):1694–1697, 2009.

[12] Giselle McCallum and Carolina Tropini. The gut microbiota and its biogeography. *Nature Reviews Microbiology*, 22(2):105–118, 2023.

[13] Nia Verdon, Ofelia Popescu, Simon Titmuss, and Rosalind J. Allen. Habitat fragmentation enhances microbial collective defence. *Journal of The Royal Society Interface*, 22(223):20240611, 2025.

[14] S. Wright. Evolution in Mendelian populations. *Genetics*, 16(2):97–159, 1931.

[15] M. Kimura and G. H. Weiss. The Stepping Stone Model of Population Structure and the Decrease of Genetic Correlation with Distance. *Genetics*, 49(4):561–576, 1964.

[16] T. Maruyama. On the fixation probability of mutant genes in a subdivided population. *Genetics Research*, 15(2):221–225, 1970.

[17] T. Maruyama. A simple proof that certain quantities are independent of the geographical structure of population. *Theoretical Population Biology*, 5(2):148–154, 1974.

[18] N. Barton. The probability of fixation of a favoured allele in a subdivided population. *Genetical Research*, 62:149–157, 1993.

[19] Erez Lieberman, Christoph Hauert, and Martin A Nowak. Evolutionary dynamics on graphs. *Nature*, 433:312–315, 2005.

[20] K. Kaveh, N. L. Komarova, and M. Kohandel. The duality of spatial death-birth and birth-death processes and limitations of the isothermal theorem. *Royal Society Open Science*, 2(4):140465, 2015.

[21] L. Hindersin and A. Traulsen. Most undirected random graphs are amplifiers of selection for birth-death dynamics, but suppressors of selection for death-birth dynamics. *PLOS Computational Biology*, 11(11):1–14, 2015.

[22] K. Pattni, M. Broom, J. Rychtář, and L. J. Silvers. Evolutionary graph theory revisited: when is an evolutionary process equivalent to the Moran process? *Proceedings of the Royal Society A: Mathematical, Physical and Engineering Sciences*, 471(2182):20150334, 2015.

[23] Josef Tkadlec, Andreas Pavlogiannis, Krishnendu Chatterjee, and Martin A Nowak. Limits on amplifiers of natural selection under death-birth updating. *PLOS Computational Biology*, 16(1):e1007494, 2020.

[24] B. Adlam, K. Chatterjee, and M. A. Nowak. Amplifiers of selection. *Proceedings of the Royal Society A: Mathematical, Physical and Engineering Sciences*, 471(2181):20150114, 2015.

[25] Andreas Pavlogiannis, Josef Tkadlec, Krishnendu Chatterjee, and Martin A. Nowak. Amplification on Undirected Population Structures: Comets Beat Stars. *Scientific Reports*, 7(1):82, 2017.

[26] Marcus Frean, Paul B Rainey, and Arne Traulsen. The effect of population structure on the rate of evolution. *Proceedings of the Royal Society B: Biological Sciences*, 280(1762):20130211, 2013.

[27] Laura Hindersin, Marius Möller, Arne Traulsen, and Benedikt Bauer. Exact numerical calculation of fixation probability and time on graphs. *Biosystems*, 150:87–91, 2016.

[28] Josef Tkadlec, Andreas Pavlogiannis, Krishnendu Chatterjee, and Martin A Nowak. Population structure determines the tradeoff between fixation probability and fixation time. *Communications biology*, 2(1):138, 2019.

[29] Josef Tkadlec, Andreas Pavlogiannis, Krishnendu Chatterjee, and Martin A. Nowak. Fast and strong amplifiers of natural selection. *Nature Communications*, 12:4009, 2021.

[30] B. Houchmandzadeh and M. Vallade. The fixation probability of a beneficial mutation in a geographically structured population. *New Journal of Physics*, 13(7):073020, 2011.

[31] B. Houchmandzadeh and M. Vallade. Exact results for fixation probability of bithermal evolutionary graphs. *Biosystems*, 112(1):49–54, 2013.

[32] G. W. Constable and A. J. McKane. Population genetics on islands connected by an arbitrary network: an analytic approach. *Journal of theoretical biology*, 358:149–165, 2014.

[33] S. Yagoobi and A. Traulsen. Fixation probabilities in network structured meta-populations. *Scientific Reports*, 11(1):17979, 2021.

[34] S. Yagoobi, N. Sharma, and A. Traulsen. Categorizing update mechanisms for graph-structured metapopulations. *Journal of the Royal Society Interface*, 20(200):20220769, 2023.

[35] Loïc Marrec, Irene Lamberti, and Anne-Florence Bitbol. Toward a Universal Model for Spatially Structured Populations. *Physical Review Letters*, 127(21):218102, 2021.

[36] Alia Abbara and Anne-Florence Bitbol. Frequent asymmetric migrations suppress natural selection in spatially structured populations. *PNAS Nexus*, 2:pgad392, 2023.

[37] Wes Maciejewski and Gregory J. Puleo. Environmental evolutionary graph theory. *Journal of Theoretical Biology*, 360:117–128, 2014.

[38] Kamran Kaveh, Alex McAvoy, and Martin A. Nowak. Environmental fitness heterogeneity in the moran process. *Royal Society Open Science*, 6(1):181661, 2019.

[39] Kamran Kaveh, Alex McAvoy, Krishnendu Chatterjee, and Martin A. Nowak. The moran process on 2-chromatic graphs. *PLOS Computational Biology*, 16(11):1–18, 2020.

[40] Joachim Brendborg, Panagiotis Karras, Andreas Pavlogiannis, Asger Ullersted Rasmussen, and Josef Tkadlec. Fixation maximization in the positional moran process. *Proceedings of the AAAI Conference on Artificial Intelligence*, 36(9):9304–9312, 2022.

[41] Jakub Svoboda, Josef Tkadlec, Kamran Kaveh, and Krishnendu Chatterjee. Coexistence times in the moran process with environmental heterogeneity. *Proceedings of the Royal Society A: Mathematical, Physical and Engineering Sciences*, 479(2271):20220685, 2023.

[42] Hossein Nemati, Kamran Kaveh, and Mohammad Reza Ejtehadi. Counterintuitive properties of evolutionary measures: A stochastic process study in cyclic population structures with periodic environments. *Journal of Theoretical Biology*, 564:111436, 2023.

[43] T. Nagylaki. The strong-migration limit in geographically structured populations. *J Math Biol*, 9(2):101–114, 1980.

[44] M. Slatkin. Fixation probabilities and fixation times in a subdivided population. *Evolution*, 35(3):477–488, 1981.

[45] M. C. Whitlock and N. H. Barton. The effective size of a subdivided population. *Genetics*, 146(1):427–441, 1997.

[46] M. Nordborg and S. M. Krone. Separation of time scales and convergence to the coalescent in structured populations. In *Modern Developments in Theoretical Population Genetics: The Legacy of Gustave Malécot*, pages 194—-232. Oxford University Press, Oxford, 2002.

[47] M. C. Whitlock. Fixation Probability and Time in Subdivided Populations. *Genetics*, 164(2):767–779, 2003.

[48] P. Sjödin, I. Kaj, S. Krone, M. Lascoux, and M. Nordborg. On the meaning and existence of an effective population size. *Genetics*, 169(2):1061–1070, 2005.

[49] Christoph Hauert, Yu-Ting Chen, and Lorens A. Imhof. Fixation times in deme structured, finite populations with rare migration. *Journal of Statistical Physics*, 156:739–759, 2014.

[50] Benjamin Allen, Gabor Lippner, Yu-Ting Chen, Babak Fotouhi, Naghmeh Momeni, Shing-Tung Yau, and Martin A. Nowak. Evolutionary dynamics on any population structure. *Nature*, 544(7649):227–230, 2017.

[51] Jesse Kreger, Donovan Brown, Natalia L. Komarova, Dominik Wodarz, and Justin Pritchard. The role of migration in mutant dynamics in fragmented populations. *Journal of Evolutionary Biology*, 36(2):444–460, 2023.

[52] S. Kryazhimskiy, D. P. Rice, and M. M. Desai. Population subdivision and adaptation in asexual populations of Saccharomyces cerevisiae. *Evolution*, 66(6):1931–1941, 2012.

[53] J. R. Nahum, P. Godfrey-Smith, B. N. Harding, J. H. Marcus, J. Carlson-Stevermer, and B. Kerr. A tortoise-hare pattern seen in adapting structured and unstructured populations suggests a rugged fitness landscape in bacteria. *Proc Natl Acad Sci U S A*, 112(24):7530–7535, 2015.

[54] Michael T. France and Larry J. Forney. The Relationship between Spatial Structure and the Maintenance of Diversity in Microbial Populations. *The American Naturalist*, 193(4):503–513, 2019.

[55] P. P. Chakraborty, L. R. Nemzer, and R. Kassen. Experimental evidence that network topology can accelerate the spread of beneficial mutations. *Evolution letters*, 7:447–456, 2023.

[56] Alia Abbara, Lisa Pagani, Celia García-Pareja, and Anne-Florence Bitbol. Mutant fate in spatially structured populations on graphs: connecting models to experiments. *PLOS Computational Biology*, 20:e1012424, 2024.

[57] J. B. S. Haldane. A mathematical theory of natural and artificial selection, part v: Selection and mutation. *Mathematical Proceedings of the Cambridge Philosophical Society*, 23(7):838–844, 1927.

[58] Richard Servajean, Arthur Alexandre, and Anne-Florence Bitbol. Impact of complex spatial population structure on early and long-term adaptation in rugged fitness landscapes. *Evolution*, 79:935–950, 2025.

[59] L. Hindersin and A. Traulsen. Counterintuitive properties of the fixation time in network-structured populations. *Journal of the Royal Society Interface*, 11:20140606, 2014.

[60] Jonas Cremer, Igor Segota, Chih-Yu Yang, Markus Arnoldini, John T. Sauls, Zhongge Zhang, Edgar Gutierrez, Alex Groisman, and Terence Hwa. Effect of flow and peristaltic mixing on bacterial growth in a gut-like channel. *Proceedings of the National Academy of Sciences of the United States of America*, 113(41):11414–11419, 2016.

[61] Jonas Cremer, Markus Arnoldini, and Terence Hwa. Effect of water flow and chemical environment on microbiota growth and composition in the human colon. *Proceedings of the National Academy of Sciences of the United States of America*, 114(25):6438–6443, 2017.

[62] Alinaghi Salari and Jonas Cremer. Diurnal variations in digestion and flow drive microbial dynamics in the gut. *PRX Life*, 3:023012, 2025.

[63] Darka Labavić, Claude Loverdo, and Anne-Florence Bitbol. Hydrodynamic flow and concentration gradients in the gut enhance neutral bacterial diversity. *Proceedings of the National Academy of Sciences of the United States of America*, 119(1):e2108671119, 2022.

[64] Olivia M. Ghosh and Benjamin H. Good. Emergent evolutionary forces in spatial models of luminal growth and their application to the human gut microbiota. *Proceedings of the National Academy of Sciences of the United States of America*, 119(28):e2114931119, 2022.

[65] Qiucen Zhang, Guillaume Lambert, David Liao, Hyunsung Kim, Kristelle Robin, Chih-kuan Tung, Nader Pourmand, and Robert H. Austin. Acceleration of Emergence of Bacterial Antibiotic Resistance in Connected Microenvironments. *Science*, 333(6050):1764–1767, 2011.

[66] Philip Greulich, Bartłomiej Waclaw, and Rosalind J. Allen. Mutational Pathway Determines Whether Drug Gradients Accelerate Evolution of Drug-Resistant Cells. *Physical Review Letters*, 109(8):088101, 2012.

[67] Rutger Hermsen, J. Barrett Deris, and Terence Hwa. On the rapidity of antibiotic resistance evolution facilitated by a concentration gradient. *Proceedings of the National Academy of Sciences of the United States of America*, 109(27):10775–10780, 2012.

[68] Michael Baym, Tami D. Lieberman, Eric D. Kelsic, Remy Chait, Rotem Gross, Idan Yelin, and Roy Kishony. Spatiotemporal microbial evolution on antibiotic landscapes. *Science*, 353(6304):1147–1151, 2016.

[69] Lluís Hernández-Navarro, Matthew Asker, Alastair M. Rucklidge, and Mauro Mobilia. Coupled environmental and demographic fluctuations shape the evolution of cooperative antimicrobial resistance. *Journal of The Royal Society Interface*, 20(208):20230393, 2023.

[70] Lluís Hernández-Navarro, Matthew Asker, and Mauro Mobilia. Eco-evolutionary dynamics of cooperative antimicrobial resistance in a population of fluctuating volume and size. *Journal of Physics A: Mathematical and Theoretical*, 57:265003, 2024.

[71] J. A. G. M. de Visser and J. Krug. Empirical fitness landscapes and the predictability of evolution. *Nature Reviews Genetics*, 15(7):480–490, 2014.

[72] Suman G. Das, Muhittin Mungan, and Joachim Krug. Epistasis-mediated compensatory evolution in a fitness landscape with adaptational tradeoffs. *Proceedings of the National Academy of Sciences*, 122(15):e2422520122, 2025.

[73] N. Sharma and A. Traulsen. Suppressors of fixation can increase average fitness beyond amplifiers of selection. *Proc Natl Acad Sci U S A*, 119(37):e2205424119, Sep 2022.

[74] Nikhil Sharma, Suman G. Das, Joachim Krug, and Arne Traulsen. Graph-structured populations elucidate the role of deleterious mutations in long-term evolution. *Nature Communications*, 16(1):2355, 2025.

[75] M. M. Desai and D. S. Fisher. Beneficial Mutation–Selection Balance and the Effect of Linkage on Positive Selection. *Genetics*, 176(3):1759–1798, 2007.

[76] B. H. Good, M. J. McDonald, J. E. Barrick, R. E. Lenski, and M. M. Desai. The dynamics of molecular evolution over 60,000 generations. *Nature*, 551(7678):45–50, 2017.

[77] J. R. Blundell, K. Schwartz, D. Francois, D. S. Fisher, G. Sherlock, and S. F. Levy. The dynamics of adaptive genetic diversity during the early stages of clonal evolution. *Nat Ecol Evol*, 3(2):293–301, Feb 2019.

[78] S. Lessard. An exact sampling formula for the Wright-Fisher model and a solution to a conjecture about the finite-island model. *Genetics*, 177:1249–54, 11 2007.

[79] C. Burden and R. Griffiths. Stationary distribution of a 2-island 2-allele Wright-Fisher diffusion model with slow mutation and migration rates. *Theoretical Population Biology*, 124:70–80, 2018.

[80] T. E. Harris. *The Theory of Branching Processes*. Springer, 1963.

[81] F. Boenkost, A. Gonzalez-Casanova, C. Pokalyuk, and A. Wakolbinger. Haldane's formula in Cannings models: the case of moderately strong selection. *Journal of Mathematical Biology*, 83:70, 2021.

[82] Mark Broom and Jan Rychtář. An analysis of the fixation probability of a mutant on special classes of non-directed graphs. *Proceedings of the Royal Society A: Mathematical, Physical and Engineering Sciences*, 464(2098):2609–2627, 2008.

[83] James W Miller. A matrix equation approach to solving recurrence relations in two-dimensional random walks. *Journal of applied probability*, 31(3):646–659, 1994.